PLASMON EXCHANGE MECHANISM OF HIGH-TEMPERATURE SUPERCONDUCTIVITY AT FINITE TEMPERATURES

Mr. Nouphy Hompanya

A Thesis submitted in Partial Fulfillment of the Requirements for the

Degree of Doctor of Philosophy in Physics

Suranaree University of Technology

Academic Year 2004

กลไกการแลกเปลี่ยนพลาสมอนของสภาพนำยวดยิ่ง
อุณหภูมิสูงที่อุณหภูมิอันตะ
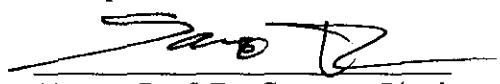

นายหนูพี โฮมปัญญา

PLASMON EXCHANGE MECHANISM OF HIGH-

TEMPERATURE SUPERCONDUCTIVITY AT

FINITE TEMPERATURES

Suranaree University of Technology has approved this thesis submitted in partial fulfillment of the requirement for the Degree of Doctor of Philosophy.
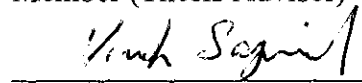
Thesis Examining Committee

_____

(Asst. Prof. Dr. Prapun Manyum)

Chairperson

_____
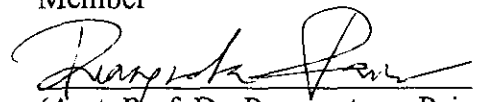
(Assoc. Prof. Dr. Samnao Phatisena)

Member (Thesis Advisor)

_____

(Prof. Dr. Virulh Sa-yakanit)
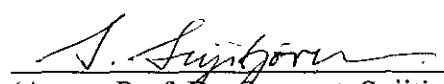
Member

_____

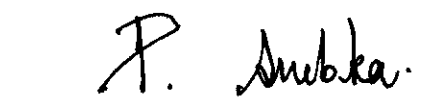(Assoc. Prof. Dr. Prasart Suebka)

Member

_____

(Asst. Prof. Dr. Puangratana Pairor)

Member

_____

(Assoc. Prof. Dr. Sarawut Sujitjorn)

Vice Rector for Academic Affairs

_____

(Assoc. Prof. Dr. Prasart Suebka)

Dean of Institute of Science
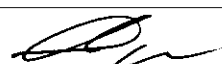
โมดรวมของชั้นบางแก๊สอิเล็กตรอนแสดงลักษณะเฉพาะ   โดยการปรากฏพลาสมอนเชิงเสียงเพิ่มเติมจากพลาสมอนเชิงแสง   ผลของพลาสมอนเชิงเสียงที่มีต่อสมบัติการนำยวดยิ่งทำการศึกษาโดยวิธีการคู่ควบอย่างแรงด้วยโฟนอนและพลาสมอน   สมการความถี่ของพลาสมอนในตัวนำยวดยิ่งแบบชั้นบางจะรวมทั้งผลของอุณหภูมิ   และเวกเตอร์คลื่นขนาดอันตะเข้าไปในการคำนวณด้วย พบว่าผลของอุณหภูมิมีค่าน้อยกว่าผลจากอันดับสูงของเวกเตอร์คลื่น q ที่อุณหภูมิต่ำ การกั้นของอันตรกิริยาคูลอมบ์ในระบบของชั้นบางจะไม่สมบูรณ์   และพลวัตของอันตรกิริยาจะเริ่มมีความสำคัญโพลาไรเซชันที่ปรากฏในสมการของค่าคงตัวไดอิเล็กทริก จะต้องมีการคำนวณทั้งเชิงตัวเลข   และเชิงวิเคราะห์แล้วนำไปใช้หาค่าผกผันของฟังก์ชันไดอิเล็กทริกที่เป็นฟังก์ชันของเวกเตอร์คลื่น ความถี่ และอุณหภูมิ โดยการใช้แบบจำลอง การแลกเปลี่ยนพลาสมอน ในทฤษฎีที่ดัดแปลงจากทฤษฎีของ Eliashberg สำหรับตัวนำยวดยิ่งที่มีการคู่ควบอย่างแรงเพื่อคำนวณหาค่าอุณหภูมิวิกฤตของสาร $La_{1.85}Sr_{0.15}CuO_4$ พบว่า ผลที่เกิดจากการแลกเปลี่ยนด้วยพลาสมอน มีนัยสำคัญแต่ไม่มากเท่ากรณีการแลกเปลี่ยนด้วย โฟนอน

สาขาวิชาฟิสิกส์   ลายมือชื่อนักศึกษา_____
ปีการศึกษา 2547   ลายมือชื่ออาจารย์ที่ปรึกษา_____
                                       ลายมือชื่ออาจารย์ที่ปรึกษาร่วม_____

NOUPHY HOMPANYA : PLASMON EXCHANGE MECHANISM OF HIGH-TEMPERATURE SUPERCONDUCTIVITY AT FINITTEMPERATURES. THESIS ADVISOR : ASSOC. PROF. SAMNAO PHATISENA, Ph.D. 119 PP. ISBN 974-533-421-9
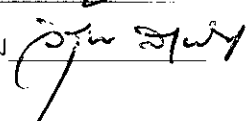
ACOUSTIC PLASMON/LAYERED SUPERCONDUCTORS/INVERSE DIELECTRIC FUNCTION/PLASMON DISPERSION/INCOMPLETE SCREENING/PLASMON EXCHANGE MODEL

Collective modes of a layered electron gas are characterized by the presence of acoustic branches in addition to the usual optical plasmon branch. The influence of such acoustic plasmons on superconducting properties is studied within the strong-coupling phonon-plasmon scheme. Plasmon dispersion relation in the layered super-conductors including temperature and finite-wave vector effects has been calculated. The temperature effect is shown to have a smaller effect compare to the effect by higher order in q in the low temperature limit. The screening of the Coulomb interaction in layered systems is incomplete and the dynamic nature of the interaction becomes important. The polarization that appears in the equation of dielectric constant has been evaluated and analyzed and the full wave-vector, frequency and temperature dependence of the inverse dielectric function has been reported. Using a plasmon exchange model in the modified Eliashberg theory for strong coupling superconductors, the plasmon contribution to the critical temperature of $La_{1.85}Sr_{0.15}CuO_4$ has been evaluated. The contribution of low-energy plasmons is significant but not dominant.

School of Physics

Academic Year 2004

Student's Signature _____

Advisor's Signature _____

Co-advisor's Signature _____

ACKNOWLEDGEMENTS

It is a great satisfaction for me that after about five years of studying here, in the Thailand, at the Suranaree University of Technology, I am able to receive and apply for the title of Doctor in Physics. This event, which I consider my great personal achievement, is not only due to my own efforts. It is a result and consequence of various circumstances, which were driven by the good will of many people. It is an honour, pleasure and duty to express my thanks to all those who have contributed to my success.

First of all, I have a high esteem for my thesis advisor Assoc. Prof. Dr. Samnao Phatisena, School of Physics, Institute of Science, Suranaree University of Technology, who is as grand brother and as friend at the same time. I would like to express my sincere gratitude to him for his kind guidance and support throughout the course of this research. I have had working under his invaluable supervision for about five years and learned a lot of unique experience for research which I will cherish throughout my life.

I am also very grateful to thank my thesis co-advisor, Prof. Dr. Virulh Sa-yakanit at Chulalongkorn University, Bangkok Thailand for his help, advice, good support when I was there for reading and searching papers, and for his good care and permanent interests for my thesis as well as for the knowledge he conveyed to me the gratitude that I have towards him cannot be expressed in a few words. I remember well all the help and advice which I got from him.

CONTENTS

CONTENTS (Continued)

CONTENTS (Continued)

LIST OF TABLES

LIST OF FIGURES

LIST OF FIGURES (Continued)

LIST OF ABBREVIATIONS

HTS   High temperature superconductivity

BCS   Bardeen-Cooper-Schrieffer

CRB   Charge reservoir block

LTS   Low temperature superconductivity

EPI   Electron-phonon interaction

2DEG   Two-dimensional electron gas

2D   Two-dimensional

3D   Three-dimensional

LEG   Layered electron gas

CHAPTER I

INTRODUCTION

1.1 A brief history of high-temperature superconductivity

After superconductivity was discovered by H. K. Onnes in 1911, many conductors were discovered and the critical temperature rose year by year. More than 2000 superconducting materials had been discovered by 1975, and the critical temperature, T_c, had reached 22.3K with the discovery of Nb_3Ge in 1973. After that, however, no higher critical temperature was obtained for more than 10 years.

A new era in superconductivity opened when J. G. Bednorz and K. A. Müller discovered a sharp drop in the resistance of $La_{2-x}Ba_xCuO_4$ at a temperature of approximately 30 K (Bednorz and Müller , 1986). They continued their study of this novel material in order to be certain that the resistivity change they had observed reflected a transition to the superconducting state. By October in the same year they had obser - ved the Meissner effect, and so established that the new material was indeed a superconductors. A month later, Jorgensen and his colleagues (Jorgensen *et al.*, 1987) confirmed the Bednorz-Müller results while their work was further supported by experiments by Zhou and his colleagues (Zhou *et al.*, 1989). In the following month, in a collaborative effort led by Chu (Chu *et al.*, 1987), a new member of this high temperature superconductor (HTS) was discovered, $YBa_2Cu_3O_7$, which possessed a T_c of over 90K. Thus within a year of the original discovery the superconducting transition

temperature had increase by a factor of three, and it was clear that a revolution in superconductivity had begun.

Within the next six years a number of additional families of high temperature superconductors were discovered. These included Tl- and Hg- based systems which had maximum T_c's of 120K and 160K respectively. All shared the feature which appeared responsible for the occurrence of HTS, the presence of planes containing Cu and O atoms, which are separated by bridging materials which act as charge reservoirs for the planes. The physical properties of these compounds were also investigated very intensively, and it was confirmed that in all cuprate superconductors the superconductivity occurred in very thin layers including Cu-O planes. Some of various isolation planes between the Cu-O planes are shown in Figure 1.1.
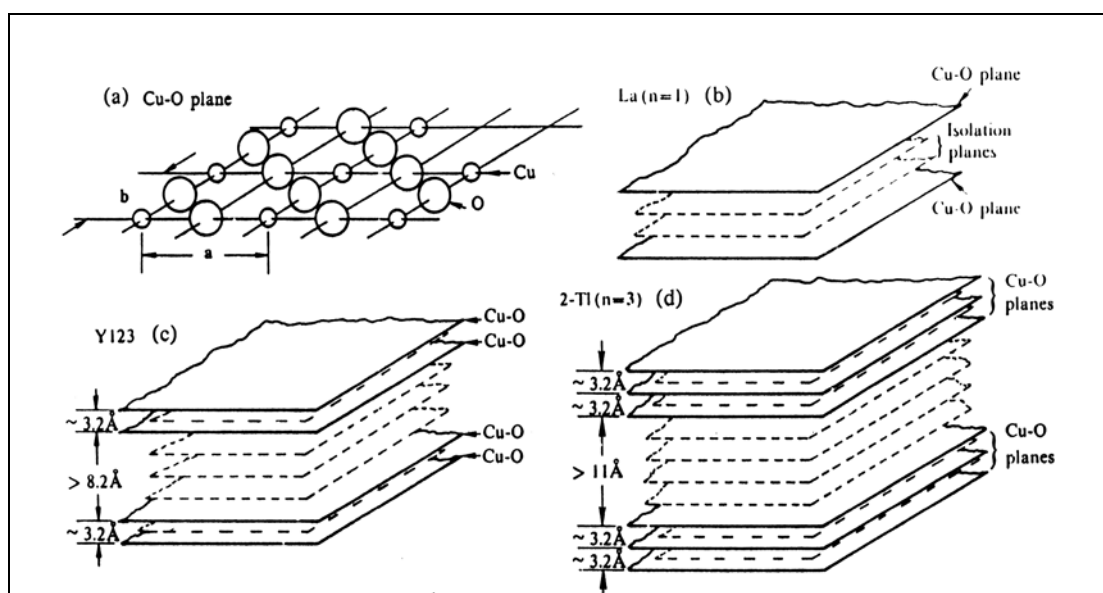
Figure 1.1 Diagram of Cu-O planes with various isolation planes between the Cu-O planes (Burns, 1992).

There have in the past ten years been many attempts to obtain high-temperature superconductivity in materials other than cuprates. Superconductivity was observed in alkali-ion doped C_{60} at 33K (Haddon *et al.*, 1991), and in MgB_2 at 39K (Nagamatsu *et al.*, 2000). But the superconductivity in both these materials is explained by the BCS theory, so it can be said at present that all the non-BCS superconductors belong to cuprate family. We therefore need to find new non-BCS superconductors outside the cuprate family if we raise the critical temperature beyond room temperature. Room temperature superconductivity is still a dream of many scientists, but there is no guideline to reach it at present. Nowadays, La-based ($T_c = 30K$), Y-based ($T_c = 90K$), Bi-based ($T_c = 120K$), and Hg-based ($T_c = 134K$) cuprates are the high temperature superconductors most frequently studied.

The theory of low temperature superconductivity has been well understood since the so-called BCS theory was put forward in 1957 (Bardeen *et al.*, 1957). It is based on a peculiarity of the interaction between 2 electrons in a crystal lattice. However BCS theory does not explain successfully the high temperature superconductivity and its precise mechanism is still a mystery. What is known is that the composition of the copper-oxide materials has to be precisely controlled if superconductivity is to occur. $YBa_2Cu_3O_7$ can be regarded as being derived from semiconducting $YBa_2Cu_3O_6$ by doping with O_2 charge carriers formed by oxidation. However the crystal is not completely saturated with oxygen atoms, and there are a number of vacancies in the lattice. Thus the actual superconducting material is often written as $YBa_2Cu_3O_{7-\delta}$, where δ must be less than 0.7 if the material is to be superconducting. The reason for this is still not clear, but it is known that the vacancies occur only in certain places in the

crystal, the copper oxide planes and chains, giving rise to a peculiar oxidation state of the copper atoms, which somehow leads to the superconducting behaviour.

Recent research trends to high temperature superconductivity are divided into three categories.The first is revealing the fundamental principles in superconductivity, the second is investigating the properties of the superconductors, and the third is applying them to practical uses. First, to explain the cause of high temperature super-conductivity, there are promising theories such as marginal Fermi liquid, spin-bag, electron's valence bond fluctuation theory, and antiferromagnetic fluctuation theory. These theories are continuously varied, changed, and developed by other theorists.

Amongst theories above, Anderson's theory (Anderson, 1987) which is based on the separation between spin and charge brought up some doubts when applied to two dimensional case although it is plausible in one dimension. Meanwhile, the antiferro-magnetic fluctuation theory led by Pines (Pines, 1990) cannot deal microscopic phe - nomena since it is based on macroscopic phenomenology. It is still in question if the theory of Scalapino (Scalapino, 1987) which form d-wave symmetry would explain high-temperature superconductivity. Since the discovery in 1911, classical supercon-ductivity has been understood in the BCS theory proposed by Bardeen, Cooper, and Schrieffer in 1957. But fundamental understanding of high temperature superconduc-tivity is still not clear after its discovery.

Second, the comprehension about its properties is continuously being deepened. Mean field of the Ginzburg-Landau theory could be applied to ideal clean type A superconductors. However, it is also significant to understand double mixture state for this state is applied to high temperature superconductivity which forms a vortex glass state because of its strong thermal fluctuation under impurity or disorder. It is essen −

tial to comprehend phase transition of this state for its physical consequence.

There has been great effort to synthesize a new HTS such as that having an infinite number of CuO_2 planes, or that based on Bi, Y, Hg and its modified forms. Recently, the study on properties of Ag-based superconductors which were manufactured under high temperature and high pressure, and the study on K_xC_{60} which were obtained by putting impurity in Fullerin C_{60} are going on.

Third, applications of superconductivity are remarkable. One of the most prospective applications is on microwave communication. The reason is that electric current consuming using superconductor is much smaller than that by other materials, beside it could be applied directly to microwave generator, filter, resonator, low noise oscillator, etc.

This period of rapid discovery may well continue for some time. While it is certainly early to review any aspect of these novel materials, intense effort has been turned toward the understanding of their electronic structures and properties, and it is useful to collect the results and contemplate their implications. Developing a clear understanding of the electronic structure of these high-T_c materials is central not only to identifying the pairing mechanism, but also to describing the host of other essential, and often unusual properties displayed by these materials. Although a complete understanding of the important electronic properties would include the electronic response to perturbations of various kinds, this is an area in which little detailed work has been done.

1.2 Characteristics and properties of HTS

Some common characteristics of HTS are that they are ceramic, flaky oxides, which are poor metals at room temperature and are difficult materials with which to

work. They contain few charge carriers compared to normal metals and display highly anisotropic electrical and magnetic properties which are remarkably sensitive to oxygen content. While superconducting samples of the 1-2-3 material, $YBa_2Cu_3O_{7-x}$, can be easily made in a microwave oven, single crystals of the high purity required to determine the intrinsic physical properties of these systems are exceedingly difficult to make.

Various techniques have been adapted or developed successfully for the synthesis and fabrication of high quality HTS in various forms. They are from polycrystal to single crystal, from bulk to thin film, and from disk to wire, for scientific pursuit and device development. Some highlights are:

(1) More than 120 non-metallic HTS have been found with T_c's above 23K, the record for the conventional intermetallic superconductors. They fall into three diffe - rent compound groups, namely, the cuprate, the bismuthade, and the fullerite. All superconductors with T_c's above the liquid nitrogen boiling point of 77K are cuprates which have a distinct layered structure.

(2) These HTS are usually characterized by a low carrier concentration of $\sim 10^{21}/cm^3$, short coherence lengths of 10×10^{-8} cm and $\sim 3 \times 10^{-8}$ cm, along and perpendicular to the CuO_2-layer, respectively, and a large penetration depth of $\sim 3000 \times 10^{-8}$ cm.

(3) The T_c has risen rapidly t o the current record of 134 K $\left[in(HgBa_2Ca_2 - Cu_3O_{8+\delta}(Hg\text{-}1223) \right]$ at ambient pressure and 164K at 30GPa in the last ten years.

(4) The upper critical field H_{c2} has exceeded 150T $\left[inYBa_2Cu_3O_7\left(YBCO \right) \right]$.

(5) The critical current densities (J_c's) at77K in zero external field achieved are:

$\sim 5 \times 10^6 \text{ A}/\text{cm}^2$, in YBCO thin films; $\sim 10^6 \text{ A}/\text{cm}^2$ in YBCO/Ni flexible tapes; $\sim 8 \times 10^4 \text{A}/\text{cm}^2$ in YBCO melt-texture bulk; and $\sim 6 \times 10^4 \text{A}/\text{cm}^2$ in $Bi_2Sr_2Ca_{n-1}Cu_nO_{2n+\delta}$ (BSCCO) tapes. J_c decreases with externally applied field. However BSCCO (at 4.2K) and YBCO (at 77K) out perform the best conventional Nb_3Sn (at 4.2K) at high field.

With the continuing improvement in sample preparation and the successful development of new characterization techniques in recent years, experimental results from different groups converge and exhibit high quality enough for empirical rules to be drawn and theoretical models proposed to be tested. Some of the highlights are as following:

(1) All curates HTS have a layered structure and can be represented by a generic formula $A_mE_2R_{n-1}Cu_nO_{2n+m+2}\left[A - m2(n-1)n - E\right]$ with a stacking sequence of m (AO)-layers inserted between 2(EO)-layers on top of n CuO_2–layers interleaved by (n-1) (R)-layers, where A, E, and R are various cations. Layers of these compounds can be grouped into two blocks: the charge-reservoir block (CRB) of [(EO) (AO)$_m$ (EO)] and the active block (AB) of {(CuO$_2$) [(R) (CuO$_2$)]$_{n-1}$}. The CRB provides the sources of charge carriers for the AB which is considered to be the main component for superconductivity in the compound. As a result, a great majority of the theoretical models are built on a 2D-electron system in the CuO_2-layers.

(2) All cuprate HTS can be derived from their corresponding anti-ferromagnetic insulating parents via the so-called modulation doping over a very limited range. This is by introducing to or removing carriers from the AB without inducing in AB defects via anion or cation substitution, and / or addition or removal in the CRB. The overwhelming majority of HTS and all those with T_c's above 30K are hole-doped,

although HTS can be electron-doped. The compounds usually undergo the transformation with hole-doping: antiferromagnetic insulator $\rightarrow$ superconducting metal $\rightarrow$ non-superconducting metal and thus form a very interesting schematic phase diagram. The detection of antiferromagnetism of short correlation length deep into the superconducting doping-region has been one main inspiration for the magnetic superconducting mechanism proposed.

(3) T_c for all cuprate HTS varies almost universally with the carrier concentration per unit Cu-ion, p, as $T_c = T_c^{max} \left[1 - 82.6 \left(p - p_0 \right)^2 \right]$, where T_c^{max} is the maximum T_c of a compound system when optimally doped at p = p_0 which is ~ 0.16. Superconductors with p < p_0 are called underdoped and those with p > p_0 called overdoped. This T_c-p correlation has been the most effective guide to optimizing T_c of a compound. Few theoretical models advanced to date, while recognize the great significance of p; have dealt with the approximated quadratic dependence of T_c on p.

(4) Hole-doped cuprate HTS, when p is equal or close to p_0, exhibit salient features in many of their normal-state properties that are not in complete agreement with predictions of the well-accepted Fermi-liquid theory for metals. For instance, the resistivity $\left(\rho \right)$ decreases linearly as temperature decreases. The Hall resistivity $\left(\rho_H \right)$ also shows a strong temperature dependence which diminishes as the sample is made non-superconducting by changing its doping. For underdoped samples, anomalies are detected in measurements of magnetic susceptibility, thermal power, and nuclear magnetic resonance, attributed to the possible formation of a spin-gap below the characteristic temperature T_s.

(5) HTS display basically the same general magnetic phase diagram [H (T)] as the conventional low temperature superconductors, which is defined by the lower

critical field [H_{c1}], the irreversibility field [$H_i(T)$] and the upper critical field [$H_{c2}(T)$]. The region underneath $H_{c1}(T)$ is the Meissner state that between $H_{c1}(T)$ and $H_i(T)$ the vortex lattice state and that between $H_i(T)$ and $H_{c2}(T)$ the vortex liquid state. J_c becomes zero above $H_i(T)$. Because of the high T_c and high H_{c2} of HTS, the phase-space between $H_i(T)$ and $H_{c2}(T)$ is greatly expanded and thus reveal readily some features, which may or may not be unique to HTS. These features have been ascribed to the large fluctuation effect associated with weakly pinned magnetic fluxoids due to the quasi-2D nature of HTS.

(6) The holes in HTS form pairs below T_c with a total spin S = 0, and the evidence from experiments shows that this superconducting pairing state has an angular momentum L= 2, i.e., d-pairing. Magnetic pairing mechanism has long been predicted to give rise to a d-pairing, although other causes of non-magnetic origin have also been proposed.

It is instructive to contrast the properties of HTS and low temperature superconductors (LTS), which have important bearing in developing a comprehensive microscopic theory. It is easier to compare the similarities and differences of HTS and LTS in tabular form as shown below:

Table 1.1 Comparisons between HTS and LTS (Chu, 2004).

	HTS	LTS
Similarities		
$\rho = 0$ (when $H < H_i$)	yes	yes
Meissner state $\left(\text{when } H \leq H_{c1}\right)$	yes	yes
Charge-carrier pairing	yes	yes
Ginzburg-Landau theory	applicable	applicable
Differences		
T_c	$\leq 164K$	$\leq 23K$
Coherence length	$\sim 10^{-7}\,\text{cm}$	$\sim 10^{-5}\,\text{cm}$
Carrier concentration	$\sim 10^{21}\,\text{cm}^{-3}$	$\sim 10^{23}\,\text{cm}^{-3}$
Penetration depth	long	short
Type	all	some
Structure	$\sim$ 2D	3D
Anisotropy	large	small
Fluctuations	large	small
Normal state properties	abnormal	normal
Magnetic properties	complex	less complex
Pairing symmetry	d	s

Because of the properties discussed above, HTS can transmit a large electric current without loss at low frequencies and with only a small loss at high frequencies, trap and shield a strong dc magnetic field, shield an electromagnetic signal at high frequency display a drastic ρ-change near T_c and exhibit novel behaviour when made into tunnelling junctions. Many application concepts have exploited one or more of these characteristics. Many prototype devices have been build and tested successfully.

1.3 Development of theoretical models

After the discovery of the high-temperature superconductivity in cuprates, many kinds of theoretical models of the mechanism of the high-temperature superconductivity were proposed, but even today there is no consensus among theoretical physicists.There are so many various kinds of interactions in such complicated systems; electron-phonon interactions, spin-spin interactions, charge density waves, spin density waves, and so on. It may be considered that we are just beginning to understand the physics of these complex systems. Explaining this phenomenon clearly will take a long time.

There is, also, no consensus among theorists as to how to develop a more detailed theoretical description of the cuprates. The approaches which have been tried can be classified as top-down or bottom-up. In a top-down approach, one chooses a model early on (the Hubbard model is a typical example), develops solutions for alternative choices of model parameters, and then sees whether the solutions lead to results consistent with experiment. In a bottom-up approach one begins with the experimental results, and attempts to devise a phenomenological description of a subset of the experimental results. One then explores alternative scenario, until one arrives at a scenario and associated microscopic calculations which are consistent with experiment.

Then, and only then, does one search for a model Hamiltonian whose solution might provide the ultimate microscopic theory.

The theory of high temperature superconductivity has proven to be elusive to date. This is probably as much caused by the fact that in these complex materials it is very hard to establish uniquely even the experimental phenomenology, as well as by the evolution of many competing models, which seem to address only particular aspects of the problem. The Indian story of the blind men trying to characterize the main properties of an elephant by touching various parts of its body seems to be particularly relevant. It is not even clear whether there is a single theory of superconductivity or whether various mechanisms are possible. Thus it is impossible to summarize, or even give a complete general overview of all theories of superconductivity. The general view point (determined by majority vote) seems to be that low temperature superconductors are phonon mediated whereas high T_c ones are somehow "unconventional" and anisotropic, although the origin of the anisotropy remains controversial. Because of this, numerical studies in well-defined theoretical models may prove to be particularly illuminating and may help uncover the essence of superconductivity.

In the next section a simple model will be reconsidered to describe the HTS where the plasmons are assumed to be the attractive bosons in the pairing effect. The plasmon exchange model has indeed been presented and discussed by several authors as soon as the HTS were discovered. It is to be stressed that the high T_c in the new materials is due not to the plasmon mechanism itself. It has been realized that the phonons could also play a major role in the pairing effect as they do in the normal superconductors. On the other hand, there is experimental evidence that the electron-phonon interaction is very important, but it is not sufficient to lead to the observed

high T_c. This coexistence concept has received experimental support.

1.4 Concept of plasmon exchange model

Concerning with exchange by phonons and plasmons, one should note that these are not hypothetical, but real excitations. At the same time, the high anisotropy of the new oxides, caused by the presence of layer and chain structures, makes the plasmon mechanism very favourable. The behaviour of plasmons in quasi-low-dimensional materials, their dispersion relations, etc., differ in a striking way from those in the usual 3D systems. The electron-phonon interaction (EPI) leads to the appearance of an effective attraction between electrons. The interaction of an electron with the rest of the Fermi sea is a more complicated phenomenon than EPI. Namely, this interaction is not only responsible for the usual screening, but, in addition, it contains a dynamic part. This dynamic part corresponds to the collective motion of electrons with respect to the lattice or to the relative motion of two groups of carriers in a system with two energy bands. Plasmons are the quasi-particles describing such collective motion, and in this case, they are similar to phonons which are the quasi- particles describing the collective excitations of the lattice.

As mentioned earlier this approach is based on the concept of coexistence of the phonon and plasmon mechanisms. This concept is receiving various experimental support. Experimental data on thermal conductivity, photo-induced IR absorption, isotope shift, sound attenuation, etc., show that the electron-phonon coupling plays an important role.

The increase of the thermal conductivity at temperatures $T < T_c$ means that the phonons make a major contribution to the total thermal flow, and the electron-phonon interaction is a main relaxation mechanism (Morelli *et al*., 1987). The analysis of the

photo-induced IR absorption gives direct evidence for strong electron-phonon coupling in the high-T_c oxides (Kim *et al.*, 1987). The isotope shift $T_c \sim M$ which has been observed experimentally is also an important manifestation of the electron-phonon coupling (Cohen *et al.*, 1987).

The presence of the isotope shift is definite evidence of the contribution of EPI, although the question of the strength of EPI cannot be answered from the value of α alone. There are other experimental indications of strong electron-phonon coupling, such as ferroelectricity of the materials and drastic change of the phonon dispersion relation caused by the superconducting transition.

It is believed that strong electron-phonon coupling is very important for high T_c, but, nevertheless, it is not sufficient and there is a need for an additional mechanism (Kresin, 1987; Ashkenazi *et al.*, 1987; Ruvalds, 1987). Such a conclusion can be drawn from the analysis of neutron spectroscopy and tunnelling data.

Since many of the recent discovered superconducting materials have a layered structure. The layers are composed of Cu-O planes (or sheets) separated from each other by planes of various other oxides and rare earths as shown in Fig.1.1. The electrons interact with each other within the same layer as well as from layer to layer via an effective interaction involving plasmon exchanges among all layers. The CuO_2 layer is assumed to form a two-dimensional electron gas (2DEG) and that two electrons in a given layer can interact attractively by plasmon exchanges either within that layer or via the various neighbouring layers. An isolated layer has only one plasmon mode with a dispersion relation $\omega_p \propto q^{1/2}$. Interlayer interaction leads to a noticeable modification of the pure two-dimensional (2D) dispersion relation, namely, to the formation of plasmon bands. Nevertheless, anisotropy results in a picture which

differs in a striking way from the isotropic three-dimensional (3D) case. In addition, the maxima of the plasmon density of states are shifted toward the boundaries of the plasmon branches, which enhances the electron-plasmon coupling considerably.

It is the layered nature of the superconducting cuprates which confines the collective motion of the electrons predominantly to the planes and leads to the unusual features of its plasmon spectra. In addition, in the $YBa_2Cu_3O_7$ materials the appearance of one-dimensional chain structures introduces quasi-one-dimensional collective modes with similar unusual properties.

Indeed, it is a well-known fact that the spectrum of a layered electron gas (LEG) contains low-energy electronic collective modes, often called acoustic plasmons with a dispersion relation $\omega_p \propto q$. That such modes could not be observed experimentally at finite q so far is related to the fact that the only technique known to date to determine the plasmon energy as a function of its wave-vector (i.e., electron energy loss spectroscopy), has a resolution of 0.2-0.5 eV at best (Nücker *et al*., 1989; Stöckli *et al*., 2000). It remains thus an experimental challenge to measure collective charge excitations down to very low energies and finite q. It is also worth noting that the largest contribution of acoustic plasmons to physical quantities such as the condensation energy is expected to come from finite but rather small values of q with respect to the Fermi wave-vector. To study the effect of acoustic plasmons on superconductivity requires thus to probe finite q's.

Low energy electronic collective modes matter for superconductivity because they can act as intermediate bosons providing an effective attractive interaction between quasi-particles (Bill *et al*., 2000). Therefore, their importance is not limited to HTS. Organic or chalcogenide materials are other examples of layered systems that

undergo a superconducting phase transition. It is thus of fundamental interest to get insight into the relationship between acoustic plasmons and superconductivity.

The conventional theory of superconductivity has mostly dealt with 3D isotropic systems. In this theory the Coulomb repulsion is described by a static pseudopotential μ^* and its value is reduced because of the well-known logarithmic factor $\ln(E/\omega)$ where E is an electronic energy and ω is a characteristic bosonic (e.g. phonon) energy. Such a static approach is justified by the large value of the plasmon frequency $\omega_p(q=0) = (4\pi ne^2/m)^{1/2}$ which ranges between 5eV and 30eV. Such high energies imply a perfect, instantaneous screening of the Coulomb interaction.

Layered conductors have a structure of the plasmon spectrum that differs fundamentally from 3D metals. In addition to the high energy "optical" collective mode mentioned above, the spectrum contains also an important low-frequency part or acoustic plasmons (Kresin and Morawitz, 1988). The screening of the Coulomb interaction is incomplete and the dynamic nature of the interaction becomes important. As a result, the interplay between the attractive interaction and the Coulomb term is more subtle than introduced in the conventional theory of superconductivity (Bill *et al.*, 2003). It is on this screened Coulomb term and its interplay with the electron phonon mechanism that will be used to describe the superconducting state of layered conductors. It is assumed that the phonons themselves provide the pairing so that at T= 0 K the compound is in the superconducting state. In other words, the presence of phonons is sufficient to overcome the static Coulomb repulsive interaction. Within this scenario the dynamic screening acts as an additional factor. Therefore, in the absence of the plasmon term we obtain the conventional Eliashberg equations.

To study the impact of dynamic screening on the superconducting state we need to calculate the dielectric function, which contains the polarizability $\Pi(q, \omega_n)$. In particular, to obtain T_c, we have to determine these functions at finite temperatures and all values of (q, ω_n). The full temperature, frequency and wave-vector dependence of dielectric function and the effect on T_c will be studied in this research.

CHAPTER II

ELECTRONIC EXCITATION SPECTRUM

2.1 Dielectric function and plasmons

A plasmon or a plasma excitation is a fundamental elementary excitation of an electron system or any charged-particle system. It is the collective normal mode of charge-density oscillation in the free-carrier system, which is present both in classical and quantum plasma. Studying the collective plasmon excitation in the electron gas has been among the very first theoretical quantum-mechanical many-body problems studied in solid-state physics dating back to the early 1950s.

The collective motion of electrons corresponding to the density fluctuation is a wave motion with frequency ω_p, called plasma oscillations. When the interaction between particles is short ranged, frequency of oscillations with long wavelength are always proportional to the inverse wavelength as in sound waves. In contrast, charge density fluctuation can exert the long-range Coulomb force on each other, however for apart they appear. As a consequence the frequency remains finite in the limit of long wavelength.

In one-component plasma model, the electrons are considered in a background of positive ions forming a cloud of neutralizing charges. Being neutral, the response of plasma to an external electric field is characterized by a dielectric function. In general this is a function of position in the system and time. Therefore, its Fourier trans-

form $\varepsilon(q,\omega)$ is a function of wavenumber $\vec{q}$ and frequency ω. This function relates

the dielectric displacement vector $\vec{D}(\vec{q},\omega)$ to the electric field $\vec{E}(\vec{q},\omega)$ by the equa -

tion

$$\vec{D}(\vec{q},\omega) = \varepsilon(q,\omega)\vec{E}(\vec{q},\omega) \tag{2.1}$$

The dielectric displacement is determined through Poisson's equation by a test charge

density while the electric vector depends not only on the test charge but also on the

charge fluctuations induced by the test charge. Therefore,

$$i\vec{q}.\vec{D}(\vec{q},\omega) = 4\pi\rho_t(\vec{q},\omega) \tag{2.2}$$

$$i\vec{q}.\vec{E}(\vec{q},\omega) = 4\pi\left[\rho_t(\vec{q},\omega) + \langle\rho(\vec{q},\omega)\rangle\right]$$

where $\rho_t(\vec{q},\omega)$ is a test charge density and $\rho(\vec{q},\omega)$ is the fluctuational (variational)

charge density.

The average density $\langle\rho\rangle$ may be represented by the free particle polarization

function given by

$$\prod(q,\omega) = \frac{2}{(2\pi)^3}\int\frac{f(\varepsilon_{k+q})-f(\varepsilon_k)}{\varepsilon_{k+q}-\varepsilon_k+\omega+i\theta}dk \tag{2.3}$$

where ε_k is the kinetic energy and $f(\varepsilon_k)$ is the Fermi distribution function. The factor

2 is due to spin, and the imaginary notation $i\theta$ in the denominator means that it is

brought to zero after integration. The dielectric function is then given by

$$\varepsilon(q,\omega) = \frac{1}{1+V(q)\prod(q,\omega)} \tag{2.4}$$

where $\qquad V(q) = \dfrac{4\pi e^2}{q^2} \tag{2.5}$

is the Fourier transform of the Coulomb potential. The dielectric function thus obtained represents a result based on the random-phase approximation (RPA).

In Eq. (2.4), V (q) is the bare Coulomb potential. In a self-consistent approach this potential is replaced by $V(q)/\varepsilon$. In this case the dielectric function is given by

$$\varepsilon(q,\omega) = 1 - V(q)\prod(q,\omega) \qquad (2.6)$$

The polarization function corresponds to three dimensions. The static polarization function $\prod(q,0)$ is called Lindhard's function. The Lindhard model is used for the free electron gas where the wavefunctions are plane waves and the energies are $\varepsilon_k = \hbar^2 k^2/2m$. The occupancy of the states is determined by the Fermi distribution function $f(\varepsilon_k)$ at the temperature T = 0. The 3D analytic expression for the polarization function is given by

$$\prod(q,0) = \frac{k_F}{2\pi^2}\left[1 - \frac{1}{4}\left(s - \frac{4}{s}\right)\ln\left|\frac{s^2 + 2s}{s^2 - 2s}\right|\right] \qquad (2.7)$$

where $s = q/k_F$ is a dimensionless parameter and k_F is the Fermi wave-vector. The polarization function depends on dimension.

The RPA dielectric function has been used frequently, but it does not provide a good approximation for large q. Therefore, the dielectric function given by Eq. (2.4) is modified such that

$$\varepsilon(q,\omega) = 1 - \frac{V(q)\prod(q,\omega)}{1 + V(q)G(q,\omega)\prod(q,\omega)} \qquad (2.8)$$

where $G(q,\omega)$ is a correction function. This function is unknown, but it is expected to approach 1 for $q \to 0$ because the RPA is generally good in this limit.

The dielectric function can vanish at a plasmon frequency that depends on q.

The equation

$$\varepsilon(q, \omega_p) = 0 \tag{2.9}$$

provides a plasmon dispersion relation. For three dimensions, the plasmon in the long-wavelength limit is well defined and is given by

$$\omega_p = \left(\frac{4\pi n e^2}{m}\right)^{1/2} \tag{2.10}$$

where n is the electron density and typical values of $\hbar\omega_p$ are in the range 10-20 eV. The long-wavelength response of a 3D electron liquid is dominated by a strong resonance at the plasma frequency ω_p. The system will oscillate with this frequency without a driving external field. The restoring force is given by the internal field set up by the disturbance in the charge distribution. At shorter wavelengths, the plasma oscillations show dispersion, i.e., their frequency depends on the wave number q. At not too short wavelengths, the dispersion relation can be expanded as follows:

$$\omega_p(q) = \omega_p + \alpha q^2 + ... \tag{2.11}$$

where the dispersion coefficient is given by $\alpha = 3k_F^2/10m^2\omega_p$ in the Lindhard approximation (RPA).

The dielectric function is imaginary because of the small imaginary number in the integrand. Note that

$$\frac{i}{x + i\theta} = P\frac{1}{x} - i\pi\delta(x) \tag{2.12}$$

where P stands for taking the principal value and the symbol $i\theta$ is a small imaginary part which is brought to zero after it has been used.

The real part of the dielectric function is related to screening. In general, the real

part is large for small ω, indicating that screening in the static case is effective. The imaginary part is related to the Coulomb energy and describes the creation of real excitations of the system. In the dielectric response $\text{Im}1/\varepsilon$ describes the density fluctuation spectrum of the system.

The real part of the Lindhard dielectric function had been shown to be

$$\varepsilon_1(q,\omega) = 1 + \frac{2me^2}{\pi\hbar^2}\frac{k_F}{q^2} + \frac{me^2}{\pi\hbar^2}\frac{1}{q^3}\left[k_F^2 - \left(\frac{q}{2} - \frac{m}{\hbar}\frac{\omega}{q}\right)^2\right]\ln\left|\frac{2qk_F + q^2 - (2m/\hbar)\omega}{-2qk_F + q^2 - (2m/\hbar)\omega}\right|$$
$$+ \frac{me^2}{\pi\hbar^2}\frac{1}{q^3}\left[k_F^2 - \left(\frac{q}{2} + \frac{m}{\hbar}\frac{\omega}{q}\right)^2\right]\ln\left|\frac{2qk_F + q^2 + (2m/\hbar)\omega}{-2qk_F + q^2 + (2m/\hbar)\omega}\right|$$

(2.13)

In particular, for the static case we have

$$\varepsilon_1(q,0) = 1 + \frac{2me^2}{\pi\hbar^2}\frac{k_F}{q^2} + \frac{2me^2}{\pi\hbar^2}\frac{1}{q^3}\left(k_F^2 - \frac{q^2}{4}\right)\ln\left|\frac{2k_F + q}{2k_F - q}\right| \qquad (2.14)$$

The imaginary part of the Lindhard dielectric function is

$$\varepsilon_2(q,\omega) = \begin{cases} \dfrac{2m^2e^2}{\hbar^3}\dfrac{\omega}{q^3} & \text{if } q < 2k_F \text{ and } 0 \leq (2m/\hbar)\omega \leq 2qk_F - q^2 \\[2ex] \dfrac{me^2}{\hbar^2}\dfrac{1}{q^3}\left[k_F^2 - \left(\dfrac{q}{2} - \dfrac{m}{\hbar}\dfrac{\omega}{q}\right)^2\right] & \text{if } 2qk_F - q^2 \leq (2m/\hbar)\omega \leq 2qk_F + q^2 \\[2ex] 0 & \text{in the other cases} \end{cases} \qquad (2.15)$$

The (q,ω) plane of the imaginary part of the Lindhard dielectric function is shown in Fig.2.1.
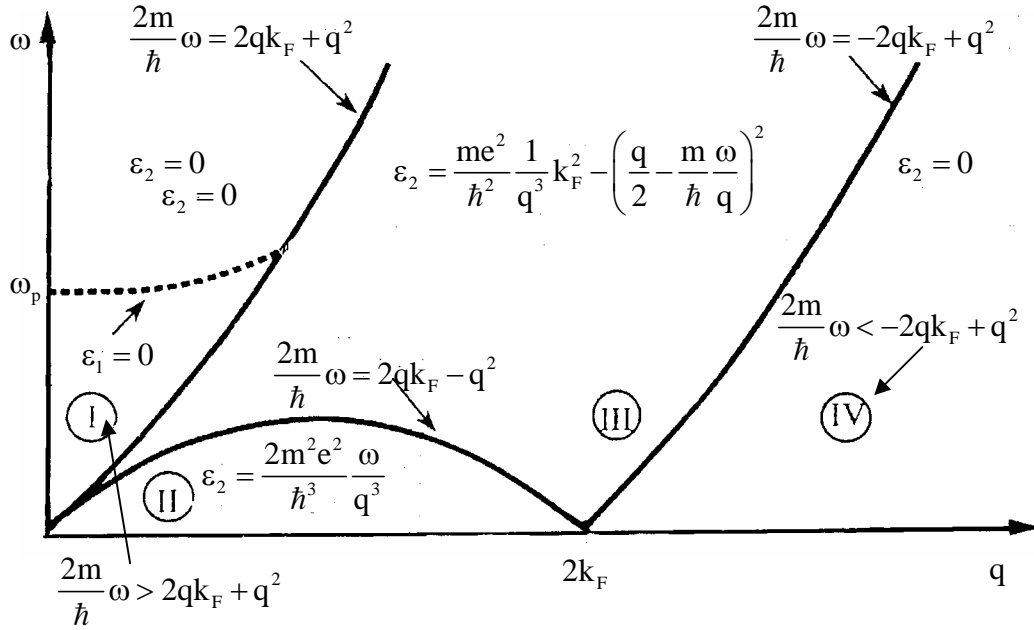
Figure 2.1 Imaginary parts of the Lindhard function. The dashed line, where

Simultaneously $\varepsilon_1(q,\omega)$ and $\varepsilon_2(q,\omega)$ vanish, gives the dispersion curve of

plasmon mode (Grosso and Parravicini, 2000).

It is seen from Fig. 2.1 that the (q,ω) plane is divided into 4 regions. The imagi-

nary part $\varepsilon_2(q,\omega)$ vanished in regions I and IV, while it is different from zero only in

regions II and III. It depends linearly on ω in the region II and quadratically in the

region III. Note that in the regions I and IV electron-hole single particle excitations of

wave-vector q are not possible (and thus ε_2 vanishes there).

Introducing the dimensionless quantity $x = q/2k_F$, the real part $\varepsilon_1(q,0) \equiv \varepsilon(q)$

for the static case given by Eq. (2.14) can be recast in the form

$$\varepsilon(q) = 1 + \frac{k_{TF}^2}{q^2} F(x) \tag{2.16}$$

where the function F(x) is given by

$$F(x) = \frac{1}{2} + \frac{1-x^2}{4x} \ln\left|\frac{1+x}{1-x}\right| \tag{2.17}$$

and $k_{TF}^2 = 4\pi e^2 D(E_F)$ is the Thomas-Fermi screening wavevector and D (E_F) is the density of states at the Fermi energy.

For small $q(q \ll 2k_F)$, we have $x \ll 1$ and $F(x) \approx 1$, therefore the Lindhard function gives the same result as the linearized Thomas-Fermi theory.

For large $q(q \gg 2k_F)$, we have $x \gg 1$ and $F(x) \approx 1/3x^2$, then the Lindhard function has the asymptotic behaviour

$$\varepsilon(q) \rightarrow 1 + \frac{4}{3}\frac{k_{TF}^2 k_F^2}{q^4}$$

A decrease of $\varepsilon(q) - 1$ as q^{-4} assure a well-behaved screening charge density at the origin.

For intermediate q $(q \approx 2k_F)$ the Lindhard dielectric function is continuous for $q \approx 2k_F$, but with a logarithmic singularity in the derivative i.e., $d\varepsilon(q)/dq \approx -\infty$. The singular in reciprocal space generates oscillation of the screening charge in real space known as Friedel oscillations.

2.2 Plasmons in two dimensions

The collective behavior in plasmons of lower dimensionality is quite different from that in 3D systems. The differences occur because the electric fields remain 3D while the induced charge densities have reduced dimensionality. The 2D plasmon is another different type of plasmon, the charge density distribution of which is restricted in 2D space and thus shows very different electrodynamic properties compared with those of 3D plasmons.

The static polarization function in 3D case given by Eq. (2.7) is different from that in 2D case. For 2D system at T = 0, it is given by

$$\Pi(q,0) = \frac{1}{2\pi}\begin{cases} 1, & s \le 2 \\ 1-\left(1-4s^{-2}\right)^{1/2} & s \ge 2 \end{cases} \tag{2.18a}$$

For 1D system, the static polarization is given by

$$\Pi(q,0) = \frac{1}{2\pi q}\ln\left|\frac{s^2+2s}{s^2-2s}\right| \tag{2.18b}$$

Figure 2.2 illustrate the Lindhard approximation for one-, two-, and three-dimensional cases of the static polarization function $\Pi(q,0)$ in units of $\Pi(0,0)$. The 1D curve with a divergence at $q = 2k_F$ shows relatively the strongest response to the test charge. In 2D case, the derivative of $\Pi(q,0)$ is singular at $q = 2k_F$, and the 3D curve has an inflection point. In these two cases, the response is strongest for q = 0. In all three cases, $\Pi(q,0)$ approaches 0 as $q \to \infty$.
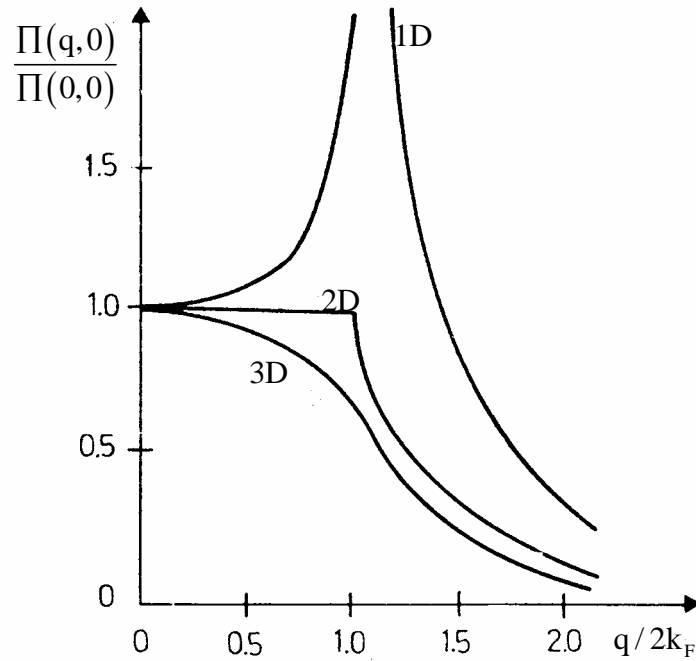
Figure 2.2 Lindhard approximation for static polarization in

one-, two-, and three-dimensional electron gas.

The Fourier transform of the Coulomb potential is also quite different from that

in 3D case which is given by Eq. (2.5). In 2D case, it has the form

$$V(q) = \frac{2\pi e^2}{q} \tag{2.19}$$

and the Fermi momentum is

$$k_F = (2\pi n)^{1/2} \tag{2.20}$$

For two dimensions, the plasmon dispersion relation at absolute zero is given in

the long-wavelength limit $(q \rightarrow 0)$ by

$$\omega_p = \left(\frac{2\pi n e^2}{m} q \right)^{1/2} \left(1 + \frac{3}{8} a_0 q \right) \tag{2.21}$$

Hence, a 2D plasmon is not defined in this limit. Here a_0 is the Bohr radius.

For electrons in the inversion layer, an effective Bohr radius must be used. It is given by

$$a_0^* = \frac{\hbar^2 \varepsilon^*}{m^* e^2} \frac{1}{g_v} \tag{2.22}$$

where ε^* is an effective dielectric constant m^* is an effective mass and g_v is the valley degeneracy.

In practice, a system like an inversion layer is not a truly 2D system. We shall therefore comment on the effect of a finite width of the layer and give the results for the quasi-2D electron liquid.

For a 2D classical electron gas between Si and SiO_2 in a MOSFET, the dispersion relation for small q is given by

$$\omega_p = \left(\frac{ne^2}{2\varepsilon^* m^*} q \right)^{1/2} \tag{2.23}$$

where

$$\varepsilon^* = \frac{1}{2}\left[\varepsilon_s + \varepsilon_{0x} \coth(qd) \right] \tag{2.24}$$

ε_s and ε_{0x} are the dielectric constants of Si and SiO_2 layers respectively, and d is the thickness of the oxide layer. The dispersion curve vanishes in the long-wavelength limit. This is a 2D characteristic that has been confirmed by experiment.

The special feature of the 2D system is that the plasmon dispersion at long-wavelengths is proportional to $q^{1/2}$ rather than being constant as in 3D case. Collective or plasmon modes of a 2D electron system have been known for many years to give an excitation spectrum that starts at zero energy, rather than at a finite energy as for bulk or surface plasmons. This was verified first for electron on liquid helium and later for electron in inversion layers. The plasmon dispersion of 2D system in classical

limit is given by (Fetter, 1974a)

$$\omega_p = \left(\frac{2\pi ne^2}{m}q\right)^{1/2}\left(1+3q/k_D\right)^{1/2} \tag{2.25}$$

where $k_D = 2\pi ne^2/k_B T$ is 2D Debye screening constant.

The specific theoretical issue is that the plasmon frequency ω_p is exactly known only at long wavelength $(q \to 0)$. At finite q, away from the long-wavelength limit, there are several corrections to the plasmon dispersion $\omega_p(q)$ arising from (finite wave vector) response, local-field corrections, finite temperature, and other mechanisms relevant to the specific electron system being studied.

2.3   Plasmons in layered systems

Electronic collective modes are notably different in layered systems as compared to 3D metals. A 3D electron gas has one degenerate "optical" plasmon branch with $\omega_p \neq 0$. In addition to this branch (corresponding to $q_z = 0$), layered systems display "acoustic" branches for all values of $q_z > 0$. Here, q_z is the wave vector normal to the conducting sheets. A layered conductor is characterized by a highly anisotropic plasmon band $\omega_p(q,q_z)$ without a gap at q = 0 except for the single branch for which $q_z = 0$ (q is a 2D wave vector in the plane of the sheets).

The detailed distribution of electric field intensities of the layer plasmons for a general value of q_z is very complicated due to interference from the contributions from different layers. It is physically instructive, however, to note that the upper and lower extrema of the plasmon branches correspond to physically transparent field patterns. The former ($q_z = 0$) has the carriers in adjacent sheets and hence the entire layered array moves in-phase against the uniform background- a type of motion which

for phonons is called acoustic- while it here leads to the highest frequency mode- the bulk plasmon. The latter ($q_z = \pi/L$ where L is the interlayer distance) has electrons on adjacent sheets moving out-of-phase against each other- a type of motion which for phonons leads to an optic mode. Note that these qualitative notions are interchanged here because for phonons one consideres the center-of-mass motion of the ions against one another, and the optic modes arise from having at least two atoms per unit cell. For the layer plasmons considered here the carriers are moving in the direction of the layers only against the uniform background density.

The band-width of the plasmon band, which is ω_p at q = 0, collapses to zero for q of order 1/L, and the singular upper and lower boundaries coalesce into the single-layer plasmon.

Two factors due to interlayer interactions affect the plasmon dispersion relation. First, the interlayer Coulomb interaction plays an important role. Second, one should consider interlayer transitions of the electrons, the importance of this factor increases with decreasing interlayer distance. It has been shown (Grecu, 1973) that introduction of a single hopping term for the electronic motion perpendicular to the layers introduces a finite gap at q = 0. Because of the small density of states in that region, we confine ourselves to pointing out that the major features of the layer plasmon bands, in particular, their singularities at their upper and lower boundaries, are not expected to be affected by inclusion of a small hopping term in the z-direction.

As a result, the polarization operator $\prod$ has the same form as in the 2D case, but the Coulomb potential V is different because of the Coulomb interlayer interaction.

Layered systems are characterized by a plasmon band $\Omega = f(q, q_z)$ where (q, q_z) are wave vectors in the planes and perpendicular to them. The z axis is chosen to be perpendicular to the layer. The collective excitation spectrum of the layered electron gas is shown in the Fig. 2.3.
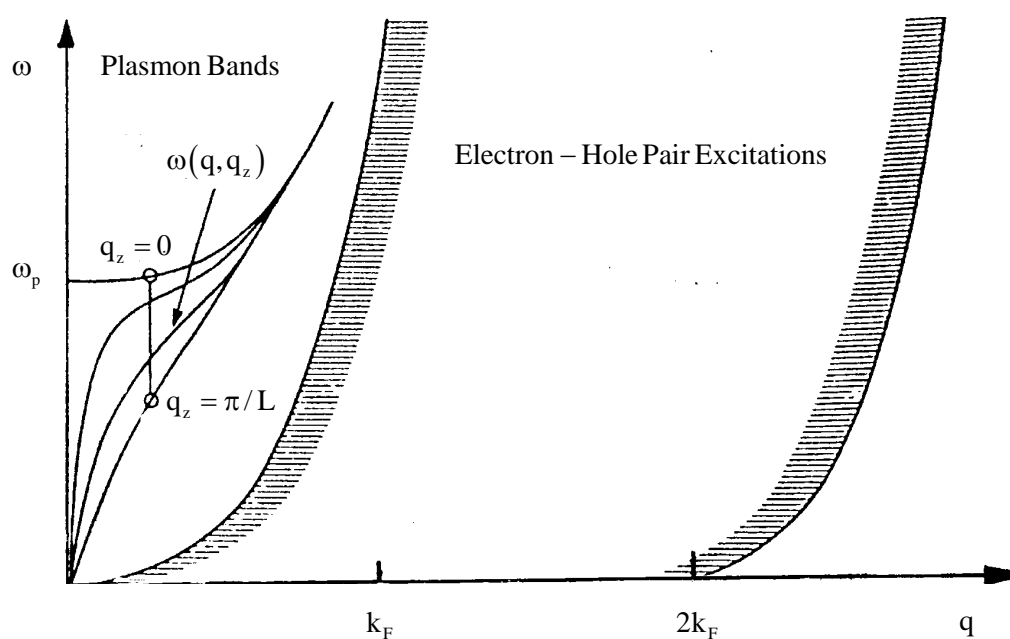
Figure 2.3 Plot of the various plasmon branches and electron-hole pair excitation as a function of q (absolute value of in-plane wave vector) and q_z for a layered electron gas (Kresin and Morawitz, 1988).

The values of Ω are restricted to lie between the upper and lower branches. These branches correspond to $q_z = 0$ and $q_z = \pi/L$ for the upper-most and the lowest branches, respectively. In addition, we note that these boundary modes correspond to in phase motion of electron on different planes ($q_z = 0$) and out-of-phase motion ($q_z = \pi/L$) on adjacent planes.

The upper branch correspond to 3D behavior, and the dependence of $\Omega(q,0)$ is similar to the behaviour of the usual 3D sample. On the other hand, the behaviour of the lowest branch $\Omega(q,\pi/L)$ is entirely different. It is important to note that in the limit $q_z \gg 1/L$ the interlayer interaction does not play an important role, and we are dealing with a two-dimensional dispersion relation $\omega \sim q$. There is a crossover from 3D to 2D behaviour in the region $q_z \sim 1/L$. This crossover corresponds to a maximum in the density of states (Landau and Lifshitz, 1976). This can be seen by considering the dependence of the plasmon frequency Ω on one less variable and, hence, the derivative with respect to this variable goes to zero. This leads to an effective increase in the density of states in this region.

Therefore, interlayer interaction leads to the formation of a highly anisotropic plasmon band $\Omega(q,q_z)$. A very important feature of this band is the nonuniform dis - tribution of the density of states. Indeed, the dispersion relation $\Omega(q,q_z)$ is described by the following equation (Morawitz et al., 1993):

$$\Omega_{\pm}(y,z) = v_F^2 y^2 + \frac{F^2(y,z)}{v_F^2 + 2F(y,z)/y} \tag{2.26}$$

where $\qquad F(y,z) = \dfrac{\sinh y}{\cosh y - \cos z} \tag{2.27}$

v_F is proportional to the Fermi velocity, $y \equiv qL$ and $z \equiv q_zL$.

It is easy to see that the derivative $\partial\Omega_+/\partial q_z$ vanishes at $q_z = 0, \pm\pi/L$. The sin- gularity $(\partial\Omega_+/\partial q_z)^{-1}$ implies a singularity in the plasmon density of states at both

boundaries. This singularity is transformed into a sharp peak if we take into account a small interlayer hopping term.

Hence, we see that the plasmon density of states has two peaked regions. The sharp increase of the density of states near the lower boundary is particularly important for the superconducting state in the layered superconductors.

The upper branch, Ω_+, and the lowest branch, Ω_-, of the layered electron gas in the plasmon region are shown to be (Molozovsky *et al.*, 1993)

$$\Omega_+ = \left(\frac{2\pi ne^2}{m}q\right)^{1/2} \left(\coth L/2\right)^{1/2} \tag{2.28}$$

which is the purely optical plasmon frequency, and

$$\Omega_- = \left(\frac{2\pi ne^2}{m}q\right)^{1/2} \left(\tanh qL/2\right)^{1/2} \tag{2.29}$$

which is the proper acoustic plasmon frequency.

The Ω_- plasmon involves charge fluctuations in the planes which, in the long-wavelength limit, are completely out of phase with each other. Consequently, in this limit, the Ω_- mode involves no net charge fluctuation and hence will not be excited by an electromagnetic wave. This feature is ultimately the reason why the Ω_- mode is acoustic, with its energy going to zero. Even more interesting is the role that the Ω_- mode might play as a new source of an attractive interaction between electrons in the CuO_2 sheets and hence high-temperature superconductivity.

CHAPTER III

TEMPERATURE AND FINITE-WAVE VECTOR

EFFECTS ON PLASMON DISPERSION RELATION

IN LAYERED CONDUCTORS

3.1 Interaction potential

Consider a layered system consisting of stacks of conducting sheets of CuO_2 which have a significant number of free charge carriers (electrons). These conducting sheets are along the z-axis and separated by dielectric spacer ε_M. A series of identical CuO_2 planes are separated by the interlayer distance L. The description of layered conductors can be made by neglecting the small interlayer hopping in a first approximation. The electrons in a CuO_2 plane interact via the Coulomb interaction with charge carriers both within and between the planes. The resulting potential has a particularly strong influence in the long-wavelength limit $(q \rightarrow 0)$.
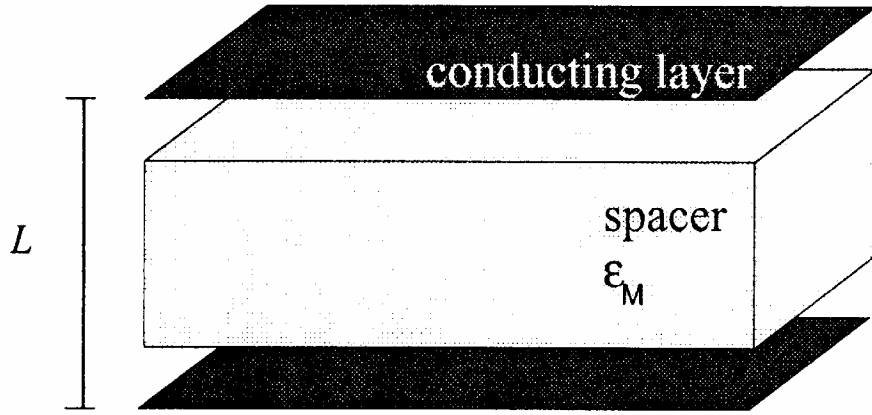
Figure 3.1 The layered electron gas model with two conducting sheets along z-axis and separated by dielectric spacer with dielectric constant ε_M.

The effective interaction between charge carriers is given by

$$V(q,\omega) = \frac{V_c(q)}{\varepsilon(q,\omega)} \tag{3.1}$$

where q is the wave vector along the plane and $V_c(q)$ is the bare Coulomb potential between the charge carriers. The function $\varepsilon(q,\omega)$ is the longitudinal dielectric function for a single band of charge carriers.

The Fourier transform of the Coulomb potential along the plane is

$$V_c(q,r,r') = \frac{2\pi e^2}{q\varepsilon_M}\exp(-q|r-r'|) \tag{3.2}$$

where r and r' are the coordinates of the planes and are discrete variables. The elec-

trons are assumed to be confined only in the conducting CuO_2 planes. In terms of the interlayer spacing L it is convenient to express.

$$r_j = jL \quad \text{and} \quad r_{j'} = j'L$$

where j and j′ denote the indices for the CuO_2 planes.

The bare Coulomb potential between the electrons in the $r - r'$ representation for fixed wave vector q becomes

$$V_c(q, r - r') = V_c(q, j, j')$$
$$= \frac{2\pi e^2}{q\varepsilon_M} \exp(-q|j - j'|L) \tag{3.3}$$

The effective interaction potential between electrons can be conveniently described by the perturbation approach and is

$$V(q, \omega, j, j') = V_c(q, j, j') - \sum_{j''} V_c(q, j, j'') \prod_{j'}(q, \omega) V(q, \omega, j, j'') \tag{3.4}$$

where $\prod(q, \omega)$ is the polarizability function for the jth layer. Since the system is translationally symmetric along the z-direction, we use following transformation

$$V(q_z) = \sum_{j,j'} V(j - j') \exp\left[i(j - j')L\right] q_z \tag{3.5}$$

and $\qquad V(j - j') = \frac{L}{2\pi} \int_{+\pi/L}^{-\pi/L} V(q_z) \exp\left[-i(j - j')q_z L\right] dq_z \tag{3.6}$

where q_z is the wave vector perpendicular to the plane. Performing the Fourier trans - formation of Eq. (3.4) and keeping in mind that the perioditicity of the layer is inde - pendent of j, the result is

$$V(q,q_z,\omega) = \frac{2\pi e^2}{q\varepsilon_M \varepsilon(q,q_z,\omega)} \sum_k \exp\left[-iq_k z_k - q|z_k|\right]$$

$$= \frac{2\pi e^2}{q\varepsilon_M \varepsilon(q,q_z,\omega)} R(q,q_z) \tag{3.7}$$

The function $R(q,q_z)$ is defined as the layer form factor, introduced by Fetter (Fetter, 1974a) in the hydrodynamic treatment of the layer plasmon dispersion and is

$$R(q,q_z) = \frac{\sinh(qL)}{\cosh(qL) - \cos(q_z L)} \tag{3.8}$$

The dielectric function for the layered system is then written in its general form as

$$\varepsilon(q,q_z,\omega) = 1 - V_c(q,q_z)\Pi(q,\omega) \tag{3.9}$$

where $\qquad V_c(q,q_z) = \dfrac{2\pi e^2}{q\varepsilon_M} R(q,q_z) \tag{3.10}$

The plasmon spectrum of a layered conductor is determined by the poles that correspond to the zeros of the real- frequency dielectric function

$$1 - V_c(q,q_z)\,\mathrm{Re}\,\Pi(q,\omega) = 0 \tag{3.11}$$

The temperature effect on the plasmon dispersion relation comes from the $\mathrm{Re}\,\Pi$ (q,ω) in Eq. (3.11).

Note that the layer form factor $R(q,q_z)$ given by Eq. (3.8) is applied only to the conducting CuO_2 layers which are stacked along the z-axis and separated by dielectric spacer with dielectric constant ε_M. This layered electron gas model can be applied to the high-temperature oxides such as lanthanum cuprates, layered organic supercon-

ductors, intercalated metal halide nitrides, etc. Other different structures such as a superlattice with a basis of two different kinds of metallic sheets (Bi-O and Cu-O sheets) and a coupled sheet-chain system (Y-Ba-Cu-O superconductors) will have different forms of $R(q, q_z)$.

The characteristic curve of the layer form factor $R(q, q_z)$ as a function of qL for five values of $q_z L$ is shown in Fig. 3.2. It is found that for large separation between the planes $qL \gg 1$ the function $R(q, q_z) \equiv R(Q) \rightarrow 1$ and $V_c(q, q_z) \equiv V_c(Q)$ reduces to that of a 2D Coulomb potential. For long in-plane wavelengths $(qL \ll 1)$, $R(Q) \rightarrow 2q/|Q^2|L$ and $V_c(Q)$ diverges as $1/|Q|^2$ for $|Q| \rightarrow 0$ in agreement with the 3D Coulomb interaction.
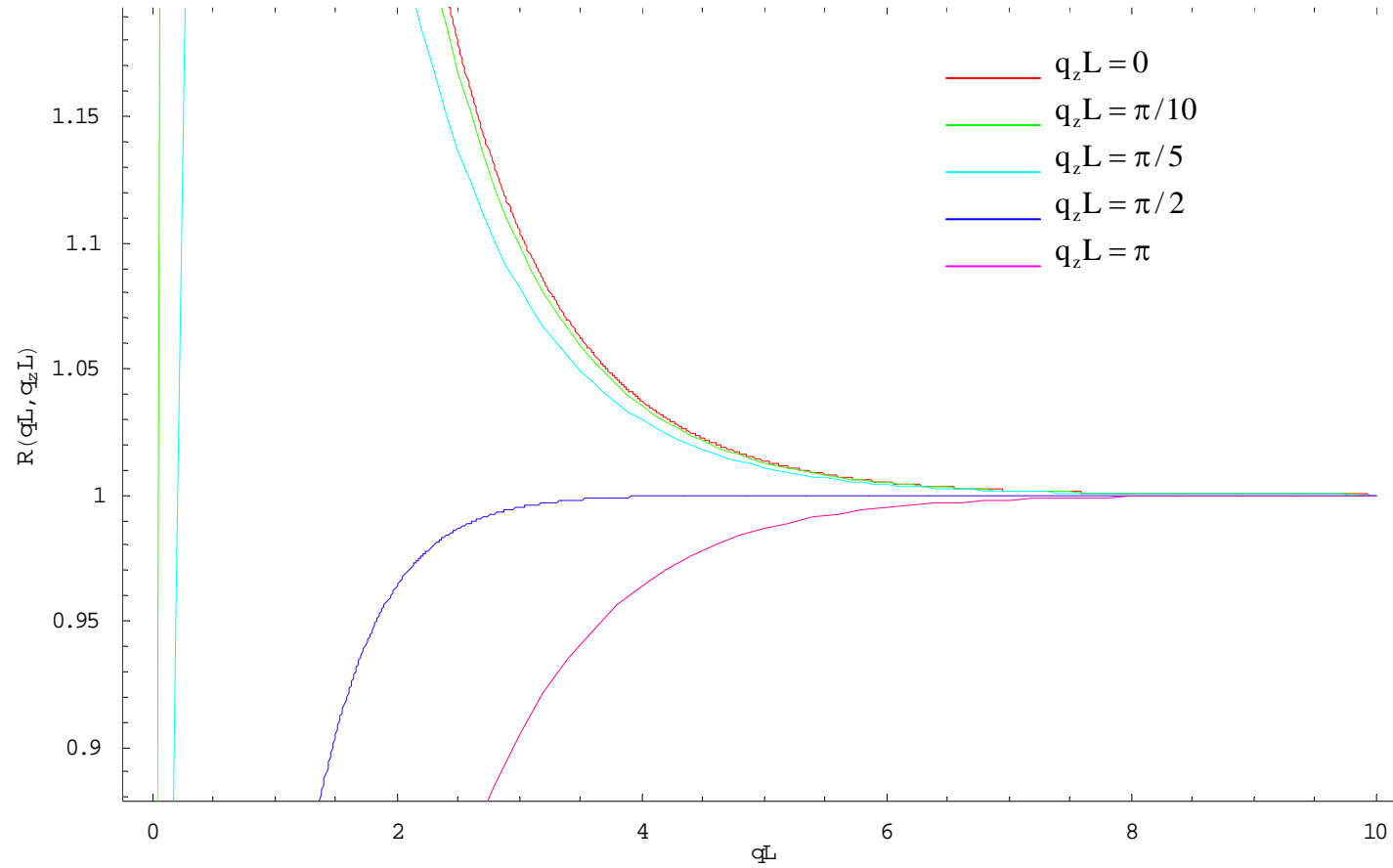
Figure 3. 2 Characteristic curves of the layer form factor $R\left(qL, q_zL\right)$.

3.2 Polarization as a function of temperature

The polarization propagator of a single layer takes the well-known form (Fetter and Walecka, 1971),

$$\Pi(q,\omega) = -\lim_{\eta \to 0} 2 \int \frac{d^2p}{(2\pi)^2} \left[\frac{f(\vec{p}+\vec{q}) - f(\vec{p})}{\hbar\omega + i\eta - \varepsilon_{\vec{p}+\vec{q}} + \varepsilon_{\vec{p}}} \right] \tag{3.12}$$

where f (p) is the Fermi-Dirac distribution function and $\varepsilon_p = \hbar^2 p^2 / 2m$. The factor 2 is due to spin degeneracy.

To find the real part and imaginary part of the polarization propagator, it is easier to rewrite Eq. (3.12) as

$$\Pi(q,\omega) = -2 \int \frac{d^2p}{(2\pi)^2} f(p) \left[\frac{1}{\hbar\omega + i\eta - \varepsilon_p + \varepsilon_{p-q}} - \frac{1}{\hbar\omega + i\eta - \varepsilon_{p+q} + \varepsilon_p} \right] \tag{3.13}$$

The real part of $\Pi(q,\omega)$ is then

$$\mathrm{Re}\,\Pi(q,\omega) = \frac{-2}{(2\pi)^2} P \int d^2p\, f(p) \left[\frac{1}{\hbar\omega - \varepsilon_p + \varepsilon_{p-q}} - \frac{1}{\hbar\omega + \varepsilon_p - \varepsilon_{p+q}} \right] \tag{3.14}$$

where P is the principal value.

Since
$$\varepsilon_{p-q} - \varepsilon_p = \frac{\hbar^2}{2m}\left(q^2 - 2pq\cos\theta\right)$$

$$\varepsilon_p - \varepsilon_{p+q} = -\frac{\hbar^2}{2m}\left(q^2 + 2pq\cos\theta\right)$$

Equation (3.14) then becomes

$$\operatorname{Re} \Pi(q,\omega) = \frac{2m}{\hbar^2 q (2\pi)^2} \int dp\, f(p) \int_0^{2\pi} d\theta \left[\frac{1}{\cos\theta - A} - \frac{1}{\cos\theta - B} \right] \qquad (3.15)$$

where
$$A = \left(\frac{m\omega}{\hbar q} + \frac{q}{2} \right) \frac{1}{p} \equiv \frac{a}{p} \qquad (3.16)$$

$$B = \left(\frac{m\omega}{\hbar q} - \frac{q}{2} \right) \frac{1}{p} \equiv \frac{b}{p} \qquad (3.17)$$

Consider the angular integral, $I_1(\theta) = \int_0^{2\pi} \frac{d\theta}{\cos\theta - A}$.

Let $z = e^{i\theta}$, $dz = iz\, d\theta$ and $\cos\theta = \frac{1}{2}\left(z + \frac{1}{z} \right)$, then

$$I_1(\theta) = \frac{2}{i} \oint_c \frac{dz}{z^2 - 2zA + 1}.$$

Poles of the angular integral are at $z_{1,2} = A \pm \sqrt{A^2 - 1}$. Now, suppose $A > 1$ then $|z_1| > 1$, $|z_2| < 1$ and since $z_1 . z_2 = 1$ it is seen that only z_2 lies inside the unit circle $|z| = 1$. The residue is $\frac{1}{z_2 - z_1}$, and hence

$$I_1(\theta) = \frac{-2\pi}{\sqrt{A^2 - 1}} = \frac{-2\pi p}{\sqrt{a^2 - p^2}}.$$

Similarly, suppose $B > 1$, then

$$I_2(\theta) = \int_0^{2\pi} \frac{d\theta}{\cos\theta - B} = \frac{-2\pi}{\sqrt{B^2 - 1}} = \frac{-2\pi p}{\sqrt{b^2 - p^2}}$$

For $|A, B| < 1$, it is easily seen that $I_1 = I_2 = 0$. Also for $B < -1$ i.e., for large q, I_2 has

the same value as given above except for a change of sign. We will not consider this case because it involves large q limit.

In general the Fermi function f (p) is a function of temperature defined by

$$f(p) = \frac{1}{e^{\beta(\varepsilon_p - \mu)} + 1} \tag{3.18}$$

where $\beta = 1/k_B T$, μ is the chemical potential and k_B is the Boltzmann constant. It is simpler to scale the parameters at finite temperature as follows:

$$x = p/k_F, \ t = T/T_F, \ z = x^2/t, \ \text{and} \ \alpha = \beta\mu \tag{3.19}$$

where k_F is the Fermi momentum T_F is the Fermi temperature, x, z and t are dimensionless variables. The Fermi function then becomes

$$f(x) = \frac{1}{e^{x^2/t - \alpha} + 1} \tag{3.20}$$

or $$f(z) = \frac{1}{e^{z - \alpha} + 1} \tag{3.21}$$

The degeneracy parameter, α, is determined from the condition that the total number N is fixed.

The value of the Fermi momentum k_F in terms of the electron density can be expressed at absolute zero as

$$N = 2\sum_p 1 = \frac{2A}{(2\pi)^2} \int_0^{k_F} d^2p = \frac{A}{2\pi} k_F^2$$

or $$n = \frac{N}{A} = \frac{k_F^2}{2\pi}$$

Thus,
$$k_F = (2\pi n)^{1/2}$$
(3.22)

However, the areal density, n, at finite temperature can be evaluated by

$$n = \frac{N}{A} = 2\int \frac{d^2 p}{(2\pi)^2} f(p) = \frac{k_F^2}{\pi} \int_0^\infty x f(x) dx$$
$$= nt \int_0^\infty f(z) dz$$

Hence,
$$\frac{1}{t} = \int_0^\infty \frac{dz}{e^{z-\alpha} + 1}$$

or
$$\alpha = \ln\left[e^{1/t} - 1 \right]$$
(3.23)

It is seen that for any given density and temperature, the ratio $t = T/T_F$ fixes the degeneracy parameter α and thus $f(z)$. Unlike 3D case, α can be expressed in closed form in 2D system.

Using the above angular integral $I_1(\theta)$ and the notations for parameters at finite temperature, the first term of Eq. (3.15) can be written in the form

$$\frac{-m}{\hbar^2 q\pi} \frac{k_F \sqrt{t}}{2} \int \frac{dz}{\left(e^{z-\alpha} + 1\right) \left(a^2 / tk_F^2 - z\right)^{1/2}}$$

Similarly for the second term in Eq. (3.15), thus the real part of $\Pi(q,\omega)$ becomes

$$\mathrm{Re}\,\Pi(q,\omega) = \frac{-m}{\hbar^2 q\pi} \frac{k_F \sqrt{t}}{2} \int \frac{dz}{e^{z-\alpha} + 1} \left[\frac{1}{\left(a^2 / tk_F^2 - z\right)^{1/2}} - \frac{1}{\left(b^2 / tk_F^2 - z\right)^{1/2}} \right]$$
(3.24)

This place an upper limit on z integral to be ξ_+ and ξ_- for the first and the second term

of Eq. (3.24) respectively where

$$\xi_{+} = \frac{a^2}{tk_F^2} \quad \text{and} \quad \xi_{-} = \frac{b^2}{tk_F^2}$$

or
$$\xi_{\pm} = \frac{1}{t}\left(\frac{m\omega}{\hbar q k_F} \pm \frac{q}{2k_F}\right) \tag{3.25}$$

Since the Fermi function at low temperature limit is quite different from that at high temperature, these two limits will be considered separately in the next two sections.

3.3 Low temperature limit

In the low temperature limit, it is necessary to consider 3 cases:

1. $\xi_{-} > \alpha$, obviously $\xi_{+} > \alpha$ automatically

2. $\xi_{\pm} < \alpha$

3. $\xi_{-} < \alpha$ and $\xi_{+} > \alpha$

Case 1. $\xi_{\pm} > \alpha$

Consider the integration

$$\int_0^{\xi_{-}} \frac{dz}{e^{z-\alpha}+1}\frac{1}{\sqrt{\xi_{-}-z}} = \int_0^{\alpha} \frac{dz}{\sqrt{\xi_{-}-z}} + \int_{\alpha}^{\xi_{-}} \frac{dz}{e^{z-\alpha}+1}\frac{1}{\sqrt{\xi_{-}-z}} - \int_0^{\alpha} \frac{dz}{e^{\alpha-z}+1}\frac{1}{\sqrt{\xi_{-}-z}}$$

$$= I_1 + I_2 + I_3$$

$$I_1 = \int_0^{\alpha} \frac{dz}{\sqrt{\xi_{-}-z}} = 2\sqrt{\xi_{-}} - 2\sqrt{\xi_{-}-\alpha}$$

Let $z - \alpha = x$ for I_2 and $\alpha - z = x$ for I_3, then

$$I_2 + I_3 = -\left\{ \int_\alpha^0 \frac{-dx}{e^x + 1} \frac{1}{\sqrt{\xi_- + x - \alpha}} - \int_0^{\xi_- - \alpha} \frac{dx}{e^x + 1} \frac{1}{\sqrt{\xi_- - x - \alpha}} \right\}$$

$$= -\left\{ \int_0^{\xi_- - \alpha} \frac{dx}{e^x + 1} \left[\frac{1}{\sqrt{\xi_- - \alpha + x}} - \frac{1}{\sqrt{\xi_- - \alpha - x}} \right] + \int_{\xi_- - \alpha}^\alpha \frac{dx}{e^x + 1} \frac{1}{\sqrt{\xi_- - \alpha + x}} \right\}$$

Since the last term is exponentially negligible, then

$$\therefore \quad I_2 + I_3 \approx -\left\{ \int_0^{\xi_- - \alpha} \frac{dx}{e^x + 1} \left[\frac{1}{\sqrt{\xi_- - \alpha}} \left(\left(1 + \frac{x}{\xi_- - \alpha}\right)^{-1/2} - \left(1 - \frac{x}{\xi_- - \alpha}\right)^{-1/2} \right) \right] \right\}$$

Also, since $\xi_- - \alpha$ is very large, this approximation will be

$$I_2 + I_3 \approx \frac{-1}{\sqrt{\xi_- - \alpha}} \left\{ \int_0^\infty \frac{dx}{e^x + 1} \left[1 - \frac{1}{2}\left(\frac{x}{\xi_- - \alpha}\right) - 1 - \frac{1}{2}\left(\frac{x}{\xi_- - \alpha}\right) + \ldots \right] \right\}$$

$$\approx \frac{1}{(\xi_- - \alpha)^{3/2}} \int_0^\infty \frac{x\,dx}{e^x + 1} = \frac{\pi^2}{12} \frac{1}{(\xi_- - \alpha)^{3/2}}$$

A similarly for the integration of z from 0 to ξ_+. Equation (3.24) becomes

$$\mathrm{Re}\,\Pi(q, \omega) = \frac{-m}{\hbar^2 q\pi} \frac{k_F \sqrt{t}}{2} \left\{ \left(2\sqrt{\xi_+} - 2\sqrt{\xi_-} + 2\sqrt{\xi_- - \alpha} - 2\sqrt{\xi_+ - \alpha} \right) + \right.$$

$$\left. + \frac{\pi^2}{12}\left(\frac{1}{(\xi_+ - \alpha)^{3/2}} - \frac{1}{(\xi_- - \alpha)^{3/2}} \right) \right\} \qquad (3.26)$$

where
$$\xi_\pm = \frac{\left(\dfrac{m\omega}{\hbar q} \pm \dfrac{q}{2}\right)^2}{tk_F^2} = \frac{1}{t}\left[\frac{m\omega}{\hbar qk_F} \pm \frac{q}{2k_F}\right]^2 \equiv \frac{A_\pm^2}{t} \qquad (3.27)$$

and
$$A_\pm = \frac{m\omega}{\hbar qk_F} \pm \frac{q}{2k_F}$$

Since, $\sqrt{\xi_+} - \sqrt{\xi_-} = \dfrac{1}{\sqrt{t}}\left(A_+ - A_-\right)$

$$= \frac{1}{\sqrt{t}}\left[\left(\frac{m\omega}{\hbar qk_F} + \frac{q}{2k_F}\right) - \left|\frac{m\omega}{\hbar qk_F} - \frac{q}{2k_F}\right|\right]$$

$$= \frac{1}{\sqrt{t}}\left(\frac{q}{k_F}\right) \qquad \text{(if } \frac{m\omega}{\hbar qk_F} > \frac{q}{2k_F} \text{ i.e., small q limit)}$$

and the approximation

$$\xi_\pm - \alpha \approx \frac{1}{t}\left[A_\pm^2 - 1\right]$$

will be used, then Eq. (3.26) becomes

$$\mathrm{Re}\,\Pi(q,\omega) = \frac{-m}{\hbar^2 q}\frac{k_F}{\pi}\left\{\frac{q}{k_F} + \left[\left(A_-^2 - 1\right)^{1/2} - \left(A_+^2 - 1\right)^{1/2}\right] + \right.$$

$$\left. + \frac{\pi^2 t^2}{24}\left[\left(A_+^2 - 1\right)^{-3/2} - \left(A_-^2 - 1\right)^{-3/2}\right]\right\}, \qquad \text{for}\quad \frac{m\omega}{\hbar q} \gg \frac{q}{2}$$

The term in the bracket can be approximated as follows:

$$\left(A_-^2 - 1\right)^{1/2} - \left(A_+^2 - 1\right)^{1/2} \approx A_- - A_+ + \frac{1}{2}\left(\frac{1}{A_+} - \frac{1}{A_-}\right) + \frac{1}{8}\left(\frac{1}{A_+^3} - \frac{1}{A_-^3}\right)$$

$$\approx -\frac{q}{k_F} - \frac{q}{2k_F}\left(\frac{\hbar q k_F}{m\omega}\right)^2 - \frac{3}{8}\frac{q^5}{k_F}\left(\frac{\hbar k_F}{m\omega}\right)^4$$

and
$$\left(A_+^2 - 1\right)^{-3/2} - \left(A_-^2 - 1\right)^{-3/2} \approx \frac{A_-^3 - A_+^3}{A_-^3 A_+^3} \approx -\frac{3q}{k_F}\left(\frac{\hbar q k_F}{m\omega}\right)^4$$

Collecting these terms we, therefore, obtain the real part of the polarization propagator in the case $\xi_\pm > \alpha$ as

$$\operatorname{Re}\Pi(q,\omega) = \frac{mk_F}{\hbar^2 q\pi}\left[\frac{q^3}{2k_F}\left(\frac{\hbar k_F}{m\omega}\right)^2 + \left(\frac{3}{8} + \frac{\pi^2 t^2}{8}\right)\frac{q^5}{k_F}\left(\frac{\hbar k_F}{m\omega}\right)^4\right] \qquad (3.28)$$

Case 2. $\xi_\pm < \alpha$

This condition of $\xi_\pm < \alpha$ is equivalent to $\left|\frac{m\omega}{\hbar q k_F} \pm \frac{q}{2k_F}\right| < 1$. Equation (3.24) be - comes

$$\operatorname{Re}\Pi(q,\omega) = \frac{-m}{\hbar^2 q\pi}\frac{k_F\sqrt{t}}{2}\left[\int_0^{\xi_+}\frac{dz}{e^{z-\alpha}+1}\frac{1}{\sqrt{\xi_+ - z}} - \int_0^{\xi_-}\frac{dz}{e^{z-\alpha}+1}\frac{1}{\sqrt{\xi_- - z}}\right]$$

The first integral can be approximated as follows:

$$\int_0^{\xi_+}\frac{dz}{e^{z-\alpha}+1}\frac{1}{\sqrt{\xi_+ - z}} = \int_0^{\xi_+}\frac{dz}{\sqrt{\xi_+ - z}} - \int_0^{\xi_+}\frac{dz}{e^{\alpha-z}+1}\frac{1}{\sqrt{\xi_+ - z}}, \qquad \text{let } \alpha - z = x$$

$$\approx 2\sqrt{\xi_+} + \int_{\alpha-\xi_+}^{\alpha}\frac{e^{-x}dx}{\sqrt{\xi_+ - \alpha + x}}$$

Put $\xi_+ - \alpha + x = y$, the second term of the last equation becomes

$$\int_0^{\xi_+} \frac{e^{\xi_+ - \alpha - y} dy}{\sqrt{y}} = e^{\xi_+ - \alpha} \int_0^{\xi_+} \frac{e^{-y}}{\sqrt{y}} dy \approx \sqrt{\pi} \, e^{\xi_+ - \alpha} - \frac{1}{\sqrt{\xi_+}} e^{-\alpha}$$

Similarly for the z-integration from 0 to ξ_-. Hence

$$\mathrm{Re}\,\Pi(q,\omega) \approx \frac{-m}{\hbar^2 q \pi} \frac{k_F \sqrt{t}}{2} \left[2\sqrt{\xi_+} - 2\sqrt{\xi_-} + \sqrt{\pi} \, e^{\xi_+ - \alpha} - \sqrt{\pi} \, e^{\xi_- - \alpha} \right]$$

$$= \frac{-m}{\hbar^2 q \pi} k_F \sqrt{t} \left[\frac{A_+}{\sqrt{t}} - \frac{A_-}{\sqrt{t}} + \frac{\sqrt{\pi}}{2} e^{-\alpha} \left(e^{\xi_+} - e^{\xi_-} \right) \right]$$

$$= \frac{-m}{\hbar^2 q \pi} k_F \left\{ \frac{q}{k_F} \theta \left(\frac{m\omega}{\hbar q k_F} - \frac{q}{2k_F} \right) + \frac{2m\omega}{\hbar q k_F} \theta \left(\frac{q}{2k_F} - \frac{m\omega}{\hbar q k_F} \right) + \right.$$

$$\left. + \left[e^{A_+^2/t} - e^{A_-^2/t} \right] e^{-1/t} \frac{\sqrt{\pi t}}{2} \right\}$$

For the case $\dfrac{q}{2k_F} > \dfrac{m\omega}{\hbar q k_F}$, the lowest order of the real part of polarization propagator

has the approximated form as

$$\mathrm{Re}\,\Pi(q,\omega) \approx \frac{-m k_F}{\hbar^2 q \pi} \cdot \frac{2m\omega}{\hbar q k_F}$$

which is a negative quantity. Hence, there is no plasmon mode in this case.

Case 3. $\xi_- < \alpha$ and $\xi_+ > \alpha$

An analysis similar to the one given above shows that $\mathrm{Re}\,\Pi(q,\omega)$ is also negat-

ive in this case and hence there is no plasmon mode too.

Therefore, the real part of the polarization propagator which is to be used for the

calculation of plasmon dispersion relation is given by Eq. (3.28) only.

3.4 High temperature limit

In high temperature limit, we approximate the Fermi function by Boltzman fun-

ction. Thus, Eq. (3.24) becomes

$$\text{Re}\,\Pi(q,\omega) = \frac{-m}{\hbar^2 q\pi}\frac{k_F\sqrt{t}}{2}e^{\alpha}\int e^{-z}dz\left[\frac{1}{\sqrt{\xi_+ - z}} - \frac{1}{\sqrt{\xi_- - z}}\right]$$

where $\qquad e^{\alpha} \sim \dfrac{1}{t}$

The first integral can be evaluated as

$$\int_0^{\xi_+}\frac{e^{-z}dz}{\sqrt{\xi_+ - z}} = \int_0^{\xi_+}\frac{e^{-z}}{\sqrt{\xi_+}}\left(1 - \frac{z}{\xi_+}\right)^{-1/2}dz$$

$$= \frac{1}{\sqrt{\xi_+}}\int_0^{\xi_+}e^{-z}\left(1 + \frac{z}{2\xi_+} + \frac{3}{8}\frac{z^2}{\xi_+^2} + \ldots\right)dz \text{ , provided } \xi_{\pm} > 1$$

$$\approx \frac{1}{\sqrt{\xi_+}}\left(1 + \frac{1}{2\xi_+} + \frac{3}{4\xi_+^2}\right) \qquad \text{(to the order of } e^{-\xi_+} \text{ and } \frac{1}{\xi_{\pm}^3}\text{)}$$

Similarly for the z-integration from 0 to ξ_- , hence,

$$\text{Re}\,\Pi(q,\omega)\frac{-m}{\hbar^2 q\pi}\frac{k_F\sqrt{t}}{2}\left\{\frac{1}{\sqrt{\xi_+}} + \frac{1}{2\xi_+^{3/2}} + \frac{3}{4\xi_+^{5/2}} - \frac{1}{\sqrt{\xi_-}} - \frac{1}{2\xi_-^{3/2}} - \frac{3}{4\xi_-^{5/2}}\right\}$$

Consider the following terms:

$$\frac{1}{\sqrt{\xi_+}} - \frac{1}{\sqrt{\xi_-}} = \sqrt{t}\left(\frac{1}{A_+} - \frac{1}{A_-}\right)$$

$$= \sqrt{t} \cdot \frac{\hbar q k_F}{m\omega} \left[\left(1 + \frac{\hbar q^2}{2m\omega}\right)^{-1} - \left(1 - \frac{\hbar q^2}{2m\omega}\right)^{-1} \right]$$

$$\approx \sqrt{t} \cdot \frac{\hbar q k_F}{m\omega} \left[1 - \frac{\hbar q^2}{2m\omega} - 1 - \frac{\hbar q^2}{2m\omega} \right]$$

$$= -\sqrt{t} \frac{\hbar^2 q^3 k_F}{m^2 \omega^2}$$

and

$$\frac{1}{\xi_+^{3/2}} - \frac{1}{\xi_-^{3/2}} \approx t\sqrt{t} \left(\frac{\hbar q k_F}{m\omega}\right)^3 \left[1 - \frac{3\hbar q^2}{2m\omega} - 1 - \frac{3\hbar q^2}{2m\omega} \right]$$

$$= -t\sqrt{t} \frac{3\hbar^4 k_F^3 q^5}{m^4 \omega^4}$$

Substituting these values into the above equation, the high temperature limit of the real part of polarization propagator will be

$$\mathrm{Re}\,\Pi(q,\omega) = \frac{q^2 k_F^2}{2\pi m\omega^2} \left(1 + \frac{3}{2} t \frac{\hbar^2 q^2 k_F^2}{m^2 \omega^2} \right) \tag{3.29}$$

3.5 Plasmon dispersion relation in layered superconductors

The plasmon dispersion relation in layered system is determined by the poles that correspond to the zeros of real-frequency dielectric function and given by Eq. (3.11), i.e.,

$$1 - V_c(q, q_z)\,\mathrm{Re}\,\Pi(q,\omega) = 0$$

where the bare Coulomb potential $V_c(q, q_z)$ is given by Eq. (3.10). The real part of the polarization propagator at low temperature limit is given by Eq. (3.28) and by Eq. (3.29) for the high temperature limit.

At low temperature limit, the plasmon dispersion relation becomes

$$\omega_p^2 = \left(\frac{4e^2\varepsilon_F}{\varepsilon_M L}\right)\left(\frac{L}{2\hbar^2}\right) q\, R(Q)\left[1 + \left(\frac{3}{4} + \frac{\pi^2 t^2}{4}\right)\frac{\hbar^2 q}{me^2}\right] \tag{3.30}$$

where $\varepsilon_F = \hbar^2 k_F^2/2m$ is the Fermi energy. The dispersion relation consists of two parts. The first part, that appears as prefactor of Eq. (3.30), comes from the modified Cou-lomb interaction given by Eq. (3.10) with the layer form factor $R(q,q_z)$ given by Eq. (3.8). This part reflects the finite-thickness effect of a layered system. Since $V_c(Q) \equiv V_c(q,q_z)$ diverges as $1/|Q|^2$ for $|Q| \to 0$ in agreement with the 3D case, therefore the prefactor of Eq. (3.30) at $q_z = 0$ and $qL \ll 1$ reduces to the value $4\pi ne^2/\varepsilon_M Lm$ of 3D optical plasmon. On the other hand, for $q_z L = \pi$ and $qL \ll 1$, the prefactor of Eq. (3.30) becomes a function of q^2 and the plasmon dispersion reduces to the acoustic plasmon $(\omega_p \propto q)$. The plasmon band is, therefore, confined between the upper branch with $q_z L = 0$ and the lower branch with $q_z L = \pi$. Since for large separation between the planes $(qL \gg 1)$, $V_c(Q)$ reduces to the 2D coulomb interaction, then the prefactor of Eq. (3.30) becomes the value $2\pi ne^2 q/\varepsilon_M m$ of 2D case. Figure 3.3 shows the charac-teristic curves of the layer plasmon dispersion in unit of the usual optical mode $\omega_{op}^2 = \omega_p^2(q=0, q_z=0) = 4e^2\varepsilon_F/\varepsilon_M L$.

The second part of the layer plasmon dispersion at low temperature limit is the terms in bracket of Eq. (3.30). This part comes from the 2D nature of the polarization propagator $\Pi(q,\omega)$ given by Eq. (3.28). It contains the finite-wave-vector (higher

order in q) effect and the temperature effect. At $T = 0K$, the effect of the leading higher order in q, which is $(3/4)\hbar^2 q / me^2$, in agreement with the term $(3/4)(q/q_{TF})$ reported by Hwang and Sarma (Hwang and Sarma, 2001) and the previous work (Rajagopal, 1977). The electronic excitation spectrum for the layered system at $T = 0$ is shown in the Figure 3.2(b) and shows similar curves that reported by the others (Bill *et al.*, 2003).The finite-temperature effect, which is $(\pi^2 t^2 / 4)\hbar^2 q / me^2$, is quite small and negligible for $t \equiv T / T_F \ll 1$ as seen in Figure 3.2 (c)-(f) and confirmed by Hwang and Sarma (Hwang and Sarma, 2001).

From Eqs. (3.8), (3.10) and (3.29) we obtain the plasmon dispersion at high temperature limit:

$$\omega_p^2 = \left(\frac{4e^2\varepsilon_F}{\varepsilon_M L}\right)\left(\frac{L}{2\hbar^2}\right) q\, R\,(Q)\left[1 + \frac{3}{2}t\frac{\hbar^2 q}{me^2}\right] \tag{3.31}$$

Since the finite-temperature effect comes from the 2D nature of $\prod(q,\omega)$ which is the term $(3/2)t\hbar^2 q / me^2$ in the bracket of Eq. (3.31). For $t \gg 1$, this term is in agreement with the term $3q / k_D$ calculated by Fetter (Fetter, 1974b) for the classical electron surface layer ($k_D = 2\pi n e^2 / k_B T$ is the 2D analog of the Debye $-$ Hückel screening cons - tant). This term is also in agreement with the term $(3/2\sqrt{2})(T/T_F)(q/r_s)$ reported by Hwang and Sarma (Hwang and Sarma, 2001) for a very-low-density electron system on the surface of liquid helium. It must be noted that this result is valid only in a very narrow range of q due to the condition $\xi_\pm > 1$ or $(me^2 / \hbar qt) < 1$. Since $t \gg 1$, this expre-

ssion limits the range of q values very near zero. If $\xi_\pm > 1$ is not satisfied we do not get any plasmon mode as may be easily seen by the explicit calculation.

It is easily seen from Figure 3.3 that the inclusion of the second term in the dispersion relation makes the slope of the acoustic plasmon increase significantly. The finite-wave-vector effect is therefore, important at low temperature limit. The temperature dependence shows a smaller effect compare to the effect by higher order in q. The dispersion relation at high temperature limit given by Eq. (3.31) is proved to be valid compared with the classical limit of the 2D system such as the system of electrons on the surface of liquid helium, but valid only in a very narrow range of q near zero.
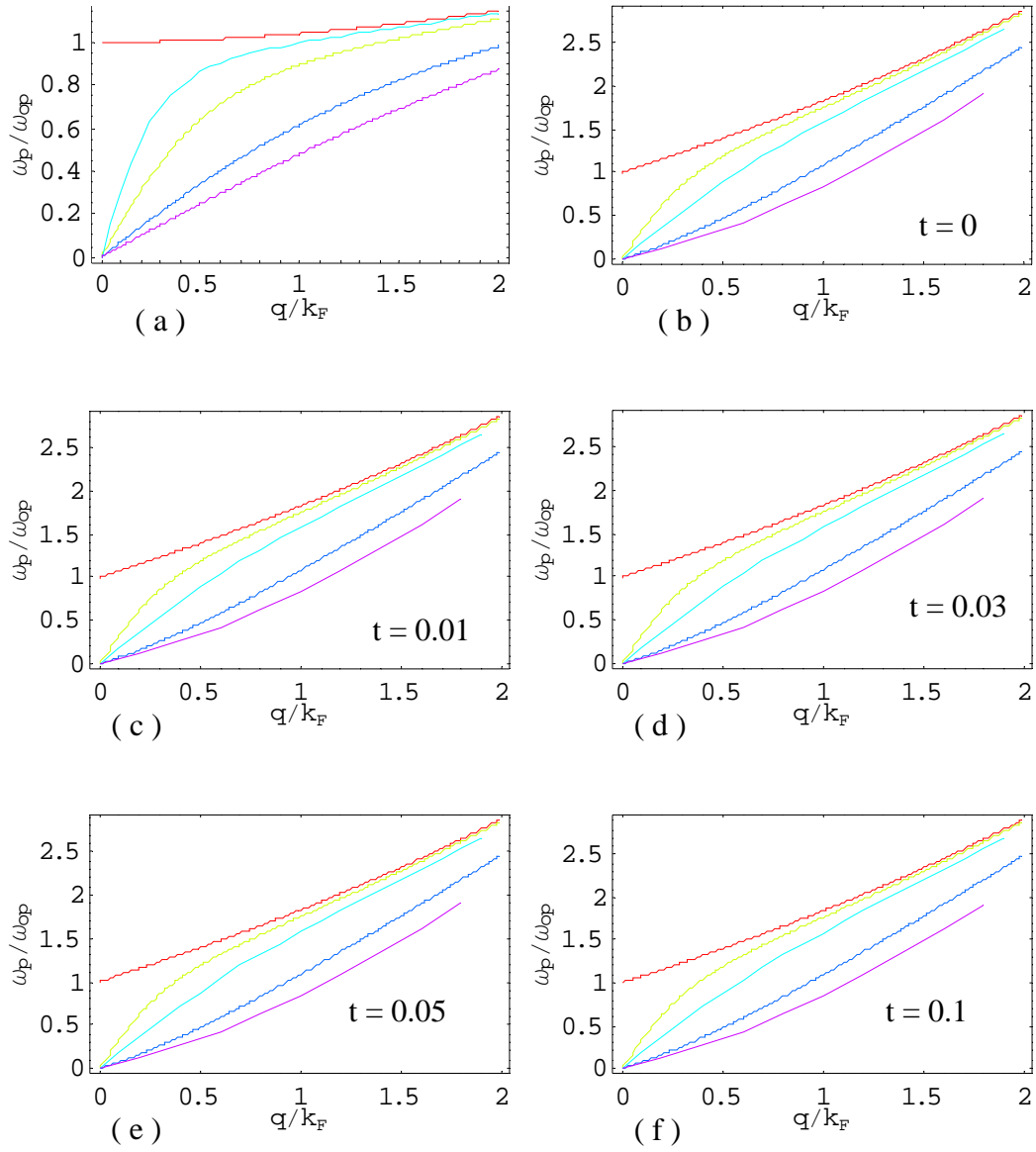
Figure 3. 3 Layer plasmon dispersion as given by Eq. (3. 30) for which:

(a) containing only the first term

(b) with the second term at t = 0

(c)-(f) with the second term at various small t
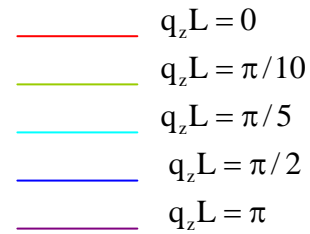
CHAPTER IV

FULL TEMPERATURE, FREQUENCY AND WAVE VECTOR DEPENDENCE OF DIELECTRIC FUNCTION IN LAYERED SUPERCONDUCTORS

4.1 Screening of the Coulomb interaction

It is known that the bare Coulomb interaction, $V(q) = 4\pi e^2 / q^2$, is not the actual interaction between any two electrons. In fact, the interaction between any two electrons will be far weaker because all of the other electrons will act to screen the Coulomb interaction. The correct strategy for dealing with electrons with Coulomb interaction is to do perturbation theory in the screened Coulomb interaction. In a metal, the screening is complete; the bare Coulomb potential is modified into a screened Coulomb potential with the following peculiar properties: (i) The screened Coulomb field is cut off at a characteristic distance of the order of k_F^{-1}. (ii) Weakly decaying long-range oscillations of electron density occur (Friedel oscillations). (iii) The change of electron density must be finite at the origin.

To understand qualitatively the highly effective shielding in metals, the Thomas-Fermi model has been used. This simple model illustrates the basic physics in the low q, ω limit and explains quite well the exponential screening at intermediate distance. It fails in predicting finite induced charge at the origin and long-range oscillations. To

understand the physics at $q \to 2k_F$, we have to use more sophisticate approximations such as the RPA.

In the Thomas-Fermi model, the bare Coulomb interaction has been replaced by a screened Coulomb interaction:

$$\frac{4\pi e^2}{q^2} \quad \to \quad \frac{4\pi e^2}{q^2 + k_{TF}^2} \tag{4.1}$$

or
$$\frac{1}{r} \quad \to \quad \frac{e^{-k_{TF} r}}{r} \tag{4.2}$$

Thus, the bare long-range Coulomb interaction e^2 / r is transformed into an exponenti-ally damped interaction with screening length $1/k_{TF}$, where k_{TF} is the inverse of the Thomas-Fermi screening length. For a free-electron gas, one has

$$k_{TF}^2 \quad = \quad \frac{4}{\pi} \frac{k_F}{a_B} \tag{4.3}$$

where $a_B = \hbar^2 / m e^2$ is the Bohr radius. The static dielectric function $\varepsilon(q, \omega = 0) \equiv \varepsilon(q)$, which is known as the Thomas-Fermi dielectric function has the form

$$\varepsilon(q) \quad = \quad 1 + \frac{k_{TF}^2}{q^2} \tag{4.4}$$

However, the Thomas-Fermi dielectric screening needs improvements to provide the correct behaviour of the induced electron charge density at small and large distances. A more refined result may be obtained by replacing the bare Coulomb interaction by the sum of the bubble diagrams, known as the RPA approximation. The effective interaction, $V_{eff}^{RPA}(q, \omega)$ is

$$V_{eff}^{RPA}(q,\omega) = V(q) + V(q)\Pi(q,\omega)V(q) + V(q)\Pi(q,\omega)V(q)\Pi(q,\omega)V(q) + \ldots$$

$$= \frac{V(q)}{1 - \Pi(q,\omega)V(q)} \tag{4.5}$$

where $\Pi(q,\omega)$ is the particle-hole bubble. For small q and $\omega = 0$,

$$V_{eff}^{RPA}(q,\omega = 0) = \frac{4\pi e^2}{q^2 + q_{TF}^2} \tag{4.6}$$

which is the same as the Thomas-Fermi result and the dielectric function is given by Eq. (4.4). However, for $\omega \neq 0$, the RPA result contains additional information about the dynamics of the electrons. Also, for $q \to 2k$, the RPA result contains information about the Fermi surface. For $\omega \neq 0$ and $q \to 2k_F$, the RPA approximation can be called into question.

The dynamic $(\omega \neq 0)$ dielectric function for $q = 0$ is given by

$$\varepsilon(0,\omega) = 1 + \frac{\omega_p^2}{\omega^2} \tag{4.7}$$

where $\omega_p^2 = 4\pi n e^2 / m$ is the plasma frequency and the dynamic dielectric function is exact in the limit $q = 0$ and $\omega > 0$ (Nozie`re and Pines, 1989). Eq. (4.7) can be recognized as the Drude model for the dielectric function of a free-electron gas.

Screening of the Coulomb interaction takes very different forms in layered conductors and 3D isotropic metals. The description of layered conductors can be made by neglecting the small interlayer hopping in a first approximation. On the other hand, it is essential to take into account the screened interlayer Coulomb interaction which has an important dynamic part. It is known that for usual 3D materials this

interaction can be consider in the static limit since electronic collective modes are very high in energy of the optical plasmon energies of the order 5-30 eV in metals. Such high energies imply a perfect, instantaneous screening of the Coulomb interaction. Therefore, the Coulomb repulsion enters the conventional theory of superconductivity as a single static pseudopotential μ^*.

The situation is very different in layered conductors. Layered conductors have a structure of the plasmon spectrum that differ fundamentally from 3D metals. In addition to the high energy optical plasmon mode, the spectrum contains also on important low-frequency part or the acoustic plasmons. The screening of the Coulomb interaction is incomplete which is a result from the layered structure. The dynamic nature of the Coulomb interaction becomes important since the response to a charge fluctuation is time dependent and hence the frequency dependence of the screened Coulomb interaction. As a result, the interplay between the attractive interaction and the Coulomb part is more subtle than introduced in the conventional theory of superconductivity. The dynamic screening in layered systems can lead to a Coulomb-induced enhancement of the superconducting pairing and might be an essential addition to the usual electron-phonon contribution.

The electronic screening of the Coulomb interaction in the layered conductors is described by the dielectric function $\varepsilon(q, q_z, \omega_n, T)$ written in its most general form as

$$\varepsilon(q, q_z, \omega_n, T) = 1 - V_c(q, q_z) \Pi(q, \omega_n, T) \qquad (4.8)$$

where
$$V_c(q, q_z) = \frac{2\pi e^2}{q \varepsilon_M} R(q, q_z) \qquad (4.9)$$

$$R(q, q_z) = \frac{\sinh(qL)}{\cosh(qL) - \cos(q_zL)} \tag{4.10}$$

and
$$\Pi(q, \omega_n, T) = -2\int \frac{d^2p}{(2\pi)^2} \frac{f(\vec{p}+\vec{q}) - f(\vec{p})}{i\hbar\omega_n - (\varepsilon_{\vec{p}+\vec{q}} - \varepsilon_{\vec{p}})} \tag{4.11}$$

q is the in-plane wave vector, q_z is the wave vector perpendicular to the plane and two conducting planes are separated by spacer with dielectric constant ε_M and L is the interlayer distance. This model of the layered conductor has been shown in Figure 3.1. The layer form factor $R(q, q_z)$ has a characteristic curve as shown in Figure 3.2. To study the impact of dynamic screening on superconducting state we need to calcu-late the dielectric function, Eq. (4.8) which contains the polarization $\Pi(q, q_z, \omega_n)$. To obtain T_c we have to determine these functions at finite temperatures. In general, the proper account of dynamic screening requires to consider all three parameters of the polarization.

In this chapter we will consider the static polarization separately from the dynamic one. Numerical results will be reported and the analytical limits will be discussed.

4.2 Static polarization

The static polarization corresponds to the term n = 0 in Eq. (4.11), i.e.,

$$\Pi(q, \omega_n = 0, T) \equiv \Pi(q, T) = -2\int \frac{d^2p}{(2\pi)^2} \frac{f(\vec{p}+\vec{q}) - f(\vec{p})}{\varepsilon_{\vec{p}} - \varepsilon_{\vec{p}+\vec{q}}} \tag{4.12}$$

By transformation $\vec{p} + \vec{q} \to \vec{k}$ for $f(\vec{p}+\vec{q})$ and $\varepsilon_{\vec{p}+\vec{q}}$ and the transformation $\vec{p} \to -\vec{p}$ for $f(\vec{p})$ and $\varepsilon_{\vec{p}}$, using the fact that $\varepsilon_{-\vec{p}} = \varepsilon_{\vec{p}}$ and $f(-\vec{p}) = f(\vec{p})$, then

$$\Pi(q,T) = \frac{4}{(2\pi)^2} \int d^2 p \frac{f(\vec{p})}{\varepsilon_{\vec{p}} - \varepsilon_{\vec{p}-\vec{q}}}$$

$$= \frac{2m}{\hbar^2 \pi^2 q} \int_0^\infty p f(p) dp \int_0^{2\pi} \frac{d\theta}{2p\cos\theta - q} \qquad (4.13)$$

Consider the angular integral

$$I(\theta) = \int_o^{2\pi} \frac{d\theta}{2p\cos\theta - q} = \frac{1}{q} \int_0^{2\pi} \frac{d\theta}{a\cos\theta - 1}$$

where $a = 2p/q$. Now, let $z = e^{i\theta}$ and $\cos\theta = \frac{1}{2}\left(z + \frac{1}{z}\right)$, it follows that

$$I(\theta) = \frac{1}{iq} \oint \frac{dz}{\frac{a}{2}z^2 - z + \frac{a}{2}}$$

$$= -\frac{2i}{aq} \oint_{|z|=1} \frac{dz}{\left(z - \frac{1}{a}\right)^2 + \left(1 - \frac{1}{a^2}\right)}$$

It is easily seen that the poles of the integral are at the point

$$z = \frac{1}{a} \pm i\left(1 - \frac{1}{a^2}\right)^{1/2} \qquad \text{for} \quad a^2 > 1$$

$$= \frac{1}{a} \pm \left(\frac{1}{a^2} - 1\right)^{1/2} \qquad \text{for} \quad a^2 < 1$$

For $a^2 > 1$, the residue $\mathrm{Res}_+(1)$ for $z = 1/a + i\left(1 - 1/a^2\right)^{1/2}$ is $1/2i\left(1 - 1/a\right)^{1/2}$ whereas

the residue $\mathrm{Res}_-(1)$ for $z = 1/a - i\left(1 - 1/a^2\right)^{1/2} = -\mathrm{Res}_+(1)$. Since the sum of the re-

sidue is zero then there is no contribution to the integration from $a^2 > 1$.

Now, for $a^2 < 1$, the poles are at $z_{1,2} = 1/a \mp \left(1/a^2 - 1\right)^{1/2}$. Since $z_1 . z_2 = 1$, only the

pole z_1 lies inside the unit circle $|z| = 1$ and the maximum value of a is unity. It follows

that the upper limit of the p-integration of Eq. (4.13) is q/2. Also, since the residue for

z_1 is equal to $-1/2\left(1/a^2 - 1\right)^{1/2}$, then the value of $I(\theta)$ is equal to $-2\pi / (q^2 - 4p^2)^{1/2}$

and Eq. (4.13) becomes

$$\Pi(q,T) = \frac{-4m}{\hbar^2 \pi q} \int_0^{q/2} \frac{p f(p) dp}{\left(q^2 - 4p^2\right)^{1/2}} \tag{4.14}$$

As before, it is simpler to scale the parameter at finite temperatures as follows:

$$x = p/k_F, \quad y = q/k_F, \quad t = T/T_F \quad \text{and} \quad \alpha = \beta\mu = \ln\left[e^{1/t} - 1\right]$$

The static polarization, then, becomes

$$\Pi(y,t) = \frac{-4m}{\hbar^2 \pi q} \int_0^{y/2} \frac{x f(x) dx}{\left(y^2 - 4x^2\right)^{1/2}} \tag{4.15}$$

where

$$f(x) = 1/\left(e^{x^2/t - \alpha} + 1\right) \tag{4.16}$$

The variation of $\Pi(y,t)$ for various y and t is shown in Figure 4.1 where the unit that

$\hbar^2 = 2m = 1$ and $e^2 = 2$ have been used.
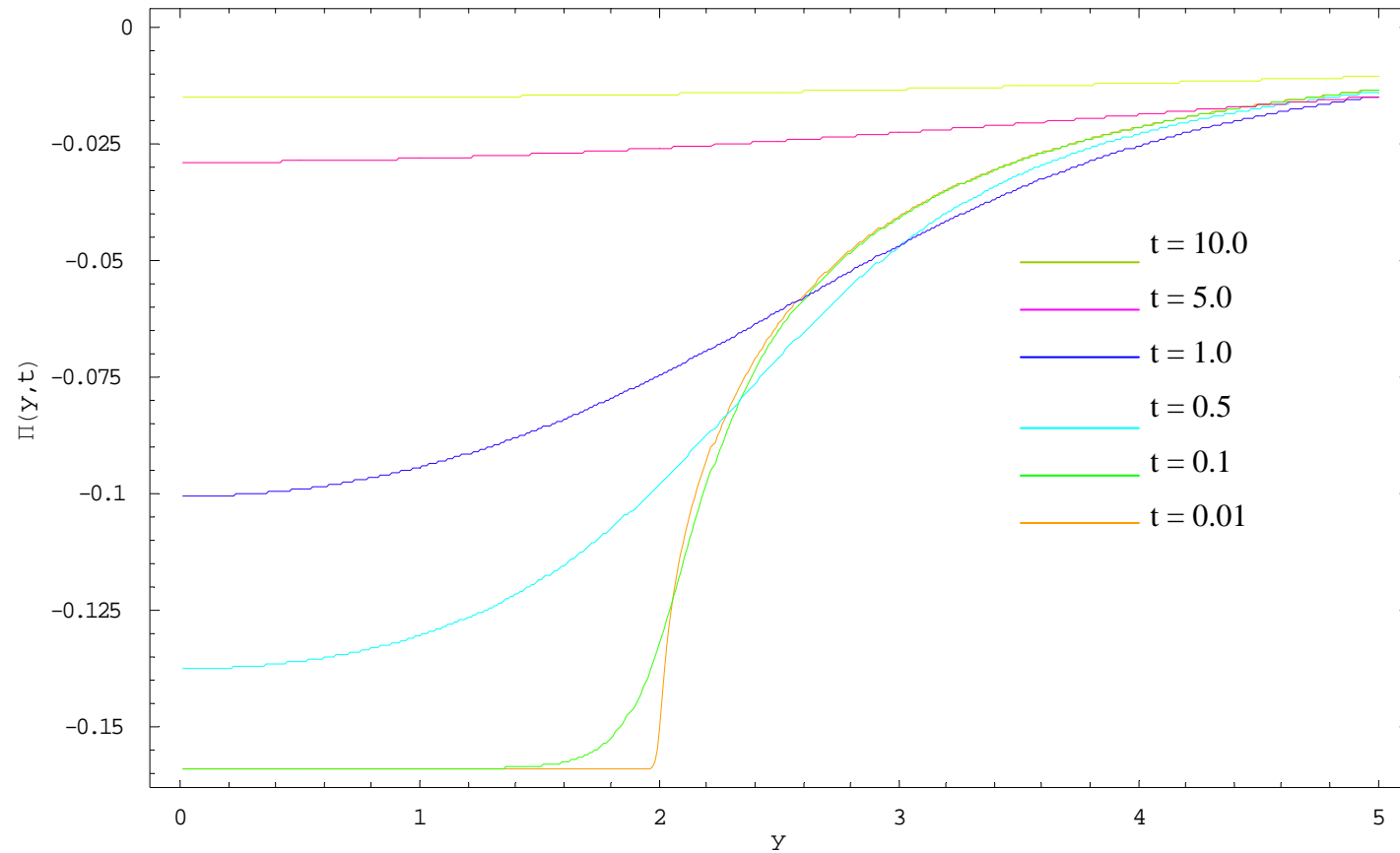
Figure 4. 1 Variation of static polarizability with $y = q/k_F$ for various $t = T/T_F$. At $t = 0$, it is constant of the value -0.159 up to $y = 2$ and drastically change to zero for large y. At higher temperatures they tend to be a function of t alone for small y and a function of y alone for large y.

Since the static polarization is a function of scaled wave vector y and the scaled temperature t, we will consider 4 limits of this function

a. Low temperature, small y limit

b. Low temperature, large y limit

c. High temperature, small y limit, and

d. High temperature, large y limit

4.2.1. Low temperature, small y limit

Let $x^2 / t = z$ and the Fermi function can be split to

$$\frac{1}{e^{z-\alpha} + 1} = 1 - \frac{1}{e^{\alpha-z} + 1}$$

and with the unit $\hbar^2 = 2m = 1$ and $e^2 = 2$ then Eq. (4.15) becomes

$$\Pi(y,t) = \frac{-t}{\pi y} \left[\int_0^{y^2/4t} dz - \int_0^{y^2/4t} \frac{dz}{e^{\alpha-z} + 1} \right] \left(\frac{1}{y^2 - 4tz} \right)^{1/2}$$

At low temperature the second integral can be approximated to $y/2t \; e^{\alpha}$ and $\alpha \sim 1/t$, thus it can be approximate to zero, while the first integral gives the value $y/2t$. Hence the polarization in this limit will be

$$\prod_{\substack{t \to 0 \\ y \to 0}}(y,t) \sim \frac{-1}{2\pi} \equiv -0.159 \tag{4.17}$$

4.2.2. Low temperature, large y limit

For small t and large y, the upper limit of the integration, $y^2/4t$, can be appro - ximated to ∞. Thus

$$\Pi(y,t) \sim \frac{-t}{\pi y} \int_0^\infty \frac{dz}{\left(e^{z-\alpha}+1\right)\left(y^2-4tz\right)^{1/2}}$$

The integral can be carried out by using the Sommerfeld method (Sommerfeld and Bethe, 1933) and has the value:

$$\Pi(y,t) = \frac{-t}{\pi y}\left[\int_0^\alpha g(z)dz + \frac{\pi^2}{6}\frac{dg(z)}{dz}\bigg|_{z=\alpha} + \text{higher term}\right]$$

$$\sim \frac{-t}{\pi y}\left[-\frac{1}{2t}\left(\sqrt{y^2-4}-y\right)+\frac{\pi^2}{3}\frac{t}{\left(y^2-4\right)^{3/2}}\right]$$

where $g(z) = 1/\left(y^2-4tz\right)^{1/2}$. The second term in the bracket goes to zero for small t and large y. Thus,

$$\prod_{\substack{t\to 0\\ y\to\infty}}(y,t) \sim -\frac{1}{2\pi}\left(1-\sqrt{1-4/y^2}\right) \approx -\frac{1}{\pi y^2} \tag{4.18}$$

which is a function of y only.

4.2.3. High temperature, small y limit

In the high temperature limit the Fermi function can be approximated by the Boltzmann distribution function, i. e.,

$$f(x) = 1/\left(e^{x^2/t-\alpha}+1\right) \sim \frac{1}{t}e^{-x^2/t} \qquad \text{where} \qquad e^\alpha \sim 1/t$$

The polarization in this limit becomes

$$\Pi(y,t) \sim \frac{-2}{\pi y^2 t}\int_0^{y/2}\frac{x\, e^{-x^2/t}\, dx}{\left(1-4x^2/y^2\right)^{1/2}}$$

Let $2x/y \equiv u$ and expanding the exponential value as

$$e^{-y^2 u^2/4t} = 1 - \frac{y^2 u^2}{4t} + \frac{y^2 u^4}{32t^2} - \cdots$$

$$\sim 1 - \frac{y^2 u^2}{4t}$$

The polarization in this limit then becomes

$$\Pi(y,t) \sim \frac{-1}{2\pi t}\left[\int_0^1 \frac{u\,du}{\sqrt{1-u^2}} - \frac{y^2}{4t}\int_0^1 \frac{u^3\,du}{\sqrt{1-u^2}}\right]$$

$$= \frac{-1}{2\pi t}\left[1 - \frac{y^2}{6t}\right]$$

$$\therefore \qquad \prod_{\substack{t\to\infty\\ y\to 0}}(y,t) \sim \frac{-1}{2\pi t} \qquad\qquad (4.19)$$

which is approximately a function of temperature alone.

4.2.4. High temperature and large y limit

Similarly to the case (4.2.3), we have

$$\Pi(y,t) = \frac{-1}{2\pi t}\int_0^1 \frac{u\,e^{-y^2 u^2/4t}\,du}{\left(1-u^2\right)^{1/2}}$$

Since $\qquad 1/\left(1-u^2\right)^{1/2} \sim 1 + \frac{1}{2}u^2 \qquad$, then

$$\Pi(y,t) \sim \frac{-1}{2\pi t}\left[\int_0^1 u\,e^{-y^2 u^2/4t}du + \frac{1}{2}\int_0^1 u^3\,e^{-y^2 u^2/4t}\,du\right]$$

$$= \frac{-1}{2\pi t}\left[\frac{-2t}{y^2}\left(e^{-y^2/4t}-1\right) - \frac{t}{y^2}\,e^{-y^2/4t} - \frac{4t^2}{y^4}\left(e^{-y^2/4t}-1\right)\right]$$

$$\approx \frac{-1}{\pi y^2}\left(1-\frac{3}{2}e^{-y^2/4t}\right)$$

$$\therefore \qquad \prod_{\substack{t\to\infty \\ y\to\infty}}(y,t) \sim -1/\pi y^2 \qquad\qquad (4.20)$$

It is to be noted from Eqs. (4.18) and (4.20) that as $y\to\infty$, the value of the polarization can be approximated to be a function of y only and goes to zero slowly for large y. Thus, the values in the two limits are almost flat which can be seen from Figure 4.1.

We then conclude that in the low temperature limit $(t\to 0)$, the polarization is approximately constant with the value of -0. 159. This constant agrees quite well with that calculated by the previous work (Maldague, 1978) or the recent work (Bill *et al.*, 2003). The values are drastically change for $y\gg 2$ and go to zero as $y\to\infty$. If one evaluate the dielectric function, $\varepsilon(q,\omega=0)$, by using Lindhard's formula, then it is found that the behaviours of 2D case is quite different from 3D case. In 2D case, the polarization is exactly constant at T = 0 up to $q=2k_F$ whereas it has a logarithmic slope at $q=k_F$ in 3D case (Ziman, 1964). In the low temperature limit, the polarization decrease as $1/q^2$ in 2D case but it is proportion to $1/q^2$ for $q\gg k_F$ in 3D case. At higher temperature the curves converge slowly in 2D case and the sharpness near $q=2k_F$ is disappears.

4.3 Dynamic polarization

The dynamic polarization corresponds to the term $n\neq 0$ in Eq. (4.11). It must be noted that the name is correct only for T = 0. At finite temperature the frequencies ω_n

are related with β, however, we still use the same name. From Eq. (4.11), we have

$$\Pi(q,\omega_n,T) = -2\int\frac{d^2p}{(2\pi)^2}\frac{f(\vec{p}+\vec{q})-f(\vec{p})}{i\hbar\omega_n-\left(\varepsilon_{\vec{p}+\vec{q}}-\varepsilon_{\vec{p}}\right)}$$

$$= \frac{-2}{(2\pi)^2}\int d^2p\,f(p)\left[\frac{1}{i\hbar\omega_n+\left(\varepsilon_{\vec{p}+\vec{q}}-\varepsilon_{\vec{p}}\right)}-\frac{1}{i\hbar\omega_n+\left(\varepsilon_{\vec{p}}-\varepsilon_{\vec{p}+\vec{q}}\right)}\right]$$

$$= -\frac{1}{\pi^2}\frac{2m}{\hbar^2q}\int_0^\infty p\,f(p)\,dp\int_0^{2\pi}d\theta\,\frac{q+2p\cos\theta}{(q+2p\cos\theta)^2+(2m\omega_n/\hbar q)^2}$$

$$= \frac{-m}{\hbar^2\pi^2q}\int_0^\infty dp\,p\,f(p)\int_0^{2\pi}d\theta\left[\frac{1}{(q+2p\cos\theta)+i(2m\omega_n/\hbar q)}+cc.\right] \quad (4.21)$$

where cc denotes its complex conjugate.

Consider the angular integral,

$$I_1(\theta) = \int_0^{2\pi}\left[q+2p\cos\theta+i(2m\omega_n/\hbar q)\right]^{-1}d\theta$$

$$= \frac{1}{2p}\int_0^{2\pi}(A+\cos\theta)^{-1}d\theta$$

where $\qquad A = q/2p+im\omega_n/\hbar pq$

Let $\quad z=e^{i\theta}\quad$ and $\quad\cos\theta=\frac{1}{2}(z+1/z)$, then

$$I_1(\theta) = \frac{1}{ip}\oint_{|z=1|}\left(z^2+2Az+1\right)^{-1}dz$$

There are two poles at $z_{1,2}=-A\pm\left(A^2-1\right)^{1/2}$. Since $z_1.z_2=1$, one root $\quad z_1=-A+\left(A^2-1\right)^{1/2}$ must be inside the unit circle $|z|=1$, while the other root z_2 be outside the

unit circle. Hence

$$I_1(\theta) = \frac{1}{ip} \oint \left[(z - z_1)(z - z_2) \right]^{-1} dz = \frac{1}{ip} \frac{2\pi i}{z - z_2} = \frac{\pi}{p} \left(A^2 - 1 \right)^{-1/2}$$

Similarly for its complex conjugate denoted by $I_2(\theta)$,

$$I_2(\theta) = \frac{\pi}{p} \left(A^{*2} - 1 \right)^{-1/2}$$

where $\qquad\qquad A^* = q/2p - im\omega_n / \hbar pq$

The total angular integration then becomes

$$I(\theta) = I_1(\theta) + I_2(\theta)$$

$$= \frac{\pi}{p} \left\{ \frac{\left(A^2 - 1 \right)^{1/2} + \left(A^{*2} - 1 \right)^{1/2}}{\left[\left(A^2 - 1 \right)\left(A^{*2} - 1 \right) \right]^{1/2}} \right\}$$

Now, let

$$A^2 - 1 = R^2 e^{i2\phi} = (q/2p)^2 - (m\omega_n / \hbar pq)^2 - 1 + im\omega_n / \hbar p^2$$

$$A^{*2} - 1 = R^2 e^{-i2\phi} = (q/2p)^2 - (m\omega_n / \hbar pq)^2 - 1 - im\omega_n / \hbar p^2$$

where $\quad R^2 = \left[\left\{ (q/2p)^2 - (m\omega_n / \hbar pq)^2 - 1 \right\}^2 + (m\omega_n / \hbar p^2)^2 \right]^{1/2}$

$\therefore \qquad \left(A^2 - 1 \right)^{1/2} + \left(A^{*2} - 1 \right)^{1/2} = R \left(e^{i\phi} + e^{-i\phi} \right) = 2R \cos\phi$

$$\left[\left(A^2 - 1 \right)\left(A^{*2} - 1 \right) \right]^{1/2} = R^2$$

where $\quad \tan 2\phi = \left(m\omega_n / \hbar p^2 \right) / \left[(q/2p)^2 - (m\omega_n / \hbar pq)^2 - 1 \right]$

Finally, the angular integral becomes

$$I(\theta) = 4\pi\cos\phi \Big/ \left[\left(q^2 - 4p^2 - 4m^2\omega_n^2/\hbar^2 q^2\right)^2 + \left(16m^2\omega_n^2/\hbar^2\right)\right]^{1/4}$$

and the dynamic polarization reduces to

$$\Pi(q,\omega_n,T) = \frac{-4m}{\hbar^2\pi q}\int\limits_0^\infty \frac{pf(p)\cos\phi\,dp}{\left[\left(q^2 - 4p^2 + 4m^2\omega_n^2/\hbar^2 q^2\right)^2 + \left(16m^2\omega_n^2/\hbar^2\right)\right]^{1/4}} \tag{4.22}$$

Again, with the same notation as before;

$$x = p/k_F \ , \ \ y = q/k_F \ , \ \ t = T/T_F \ , \ \ \alpha = \beta\mu = \ln\left[e^{1/t}-1\right] \ \text{ and } \ \omega_n = 2\pi n/\beta\hbar \,,$$

Also together with unit $\hbar^2 = 2m = 1$ has been used, then the dynamic polarization in convenient form for numerical evaluation is

$$\Pi(y,n,t) = -\frac{2}{\pi}\int\limits_0^\infty \frac{xf(x)\cos\phi\,dx}{\left[\left(y^4 - 4x^2y^2 - 4n^2\pi^2 t^2\right)^2 + \left(4n\pi ty^2\right)^2\right]^{1/4}} \tag{4.23}$$

where $\quad \tan 2\phi = \dfrac{4n\pi ty^2}{y^4 - 4x^2y^2 - 4n^2\pi^2 t^2} \tag{4.24}$

$$f(x) = \frac{1}{e^{x^2/t-\alpha}+1} \tag{4.25}$$

Note that the upper limit of the p-integration is ∞ in contrast to the value y/2 for the case of static polarization. Both of the polarizations are the function of y and t but independent of the density of electron gas.

Graphs of $\Pi(y,n,t)$ versus y for different values of n and some fixed t values are shown in Figure 4.2 (a)-(j). It is equal to zero at y = 0 for all temperatures and n's which can be proved as follow. By geometry and Eq. (4.24) we have

$$\cos 2\phi = \frac{y^4 - 4x^2y^2 - 4n^2\pi^2t^2}{\left[\left(y^4 - 4x^2y^2 - 4n^2\pi^2t^2\right)^2 + \left(4n\pi ty^2\right)^2\right]^{1/2}} \tag{4.26}$$

At $y = 0$, $\cos 2\phi = -1$ or $\cos \phi = 0$, then the polarization given by Eq. (4.23) is equal to zero.

At very low temperature $\left(t \sim 0.01\right)$ it abruptly increases (negative side) with y to different values for different n up to $y \sim 2$, and then decreases rapidly to zero for $y \gg 2$. The behaviour of the polarization for $y \gg 2$ at fixed t for different values of n is identical. At high temperatures, the sharpness of the curves around $y \sim 2$ are broaden and the peaks are shifted to higher values of y.
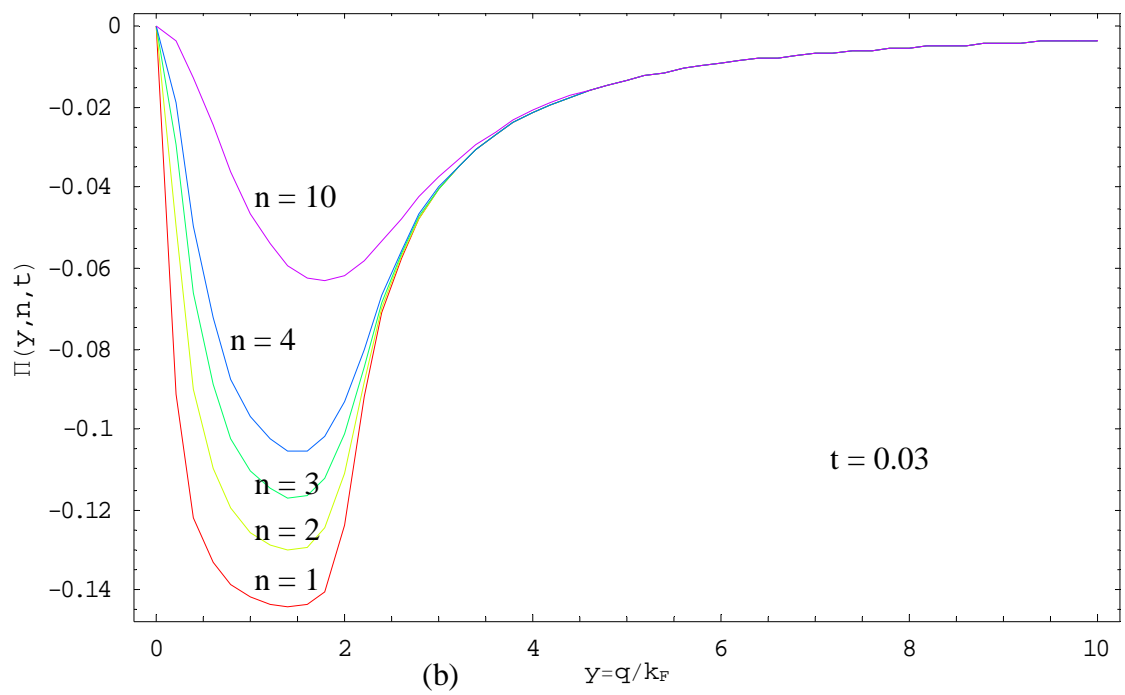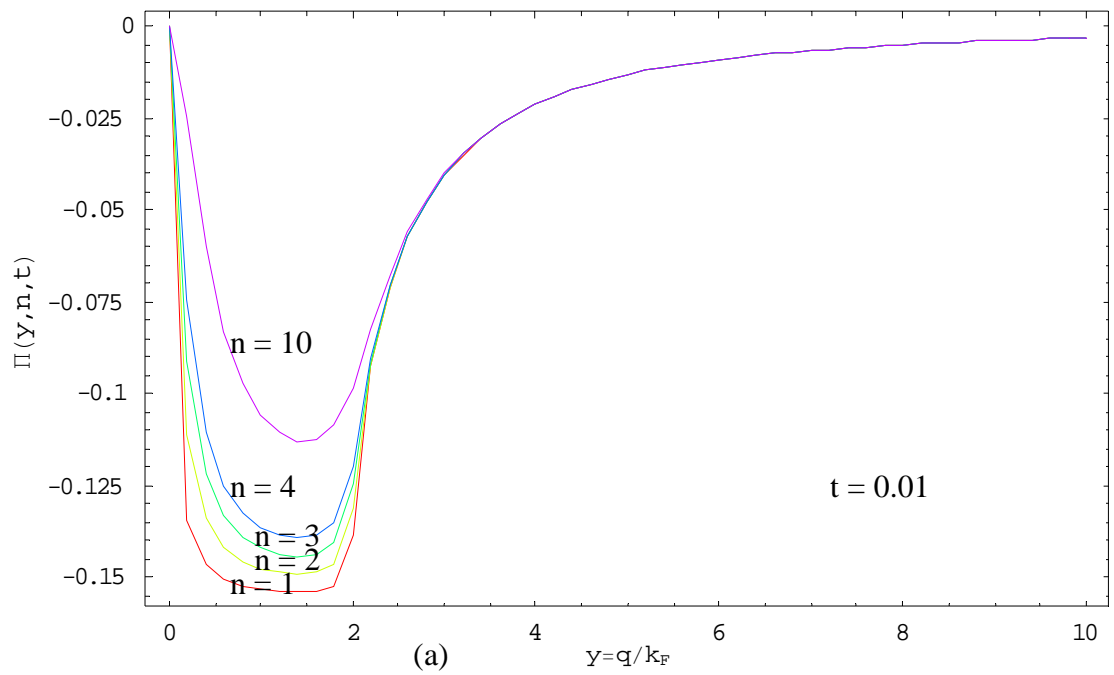
Figure 4.2 Dynamic polarizability in RPA as a function of $y = q/k_F$

for various values of n and $t = T/T_F$.

(c)

(d)
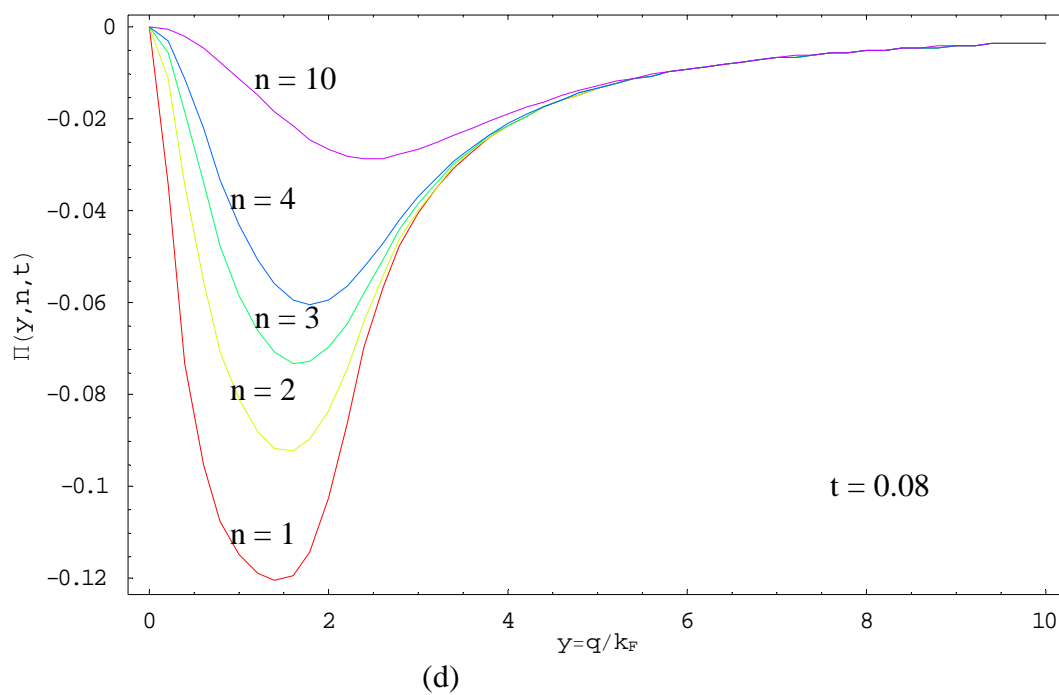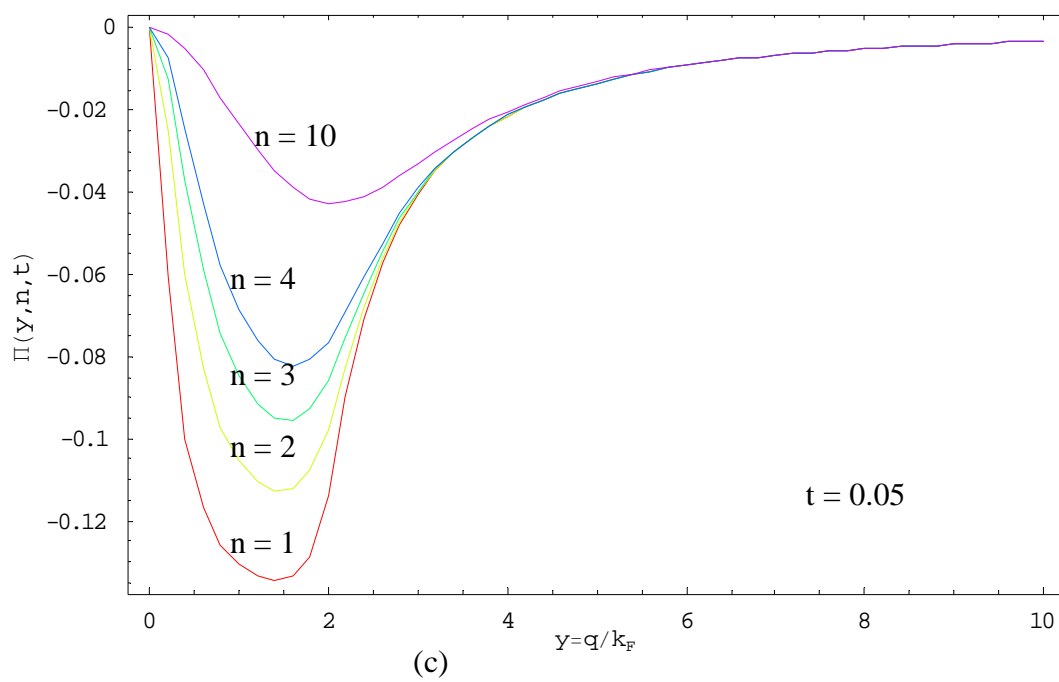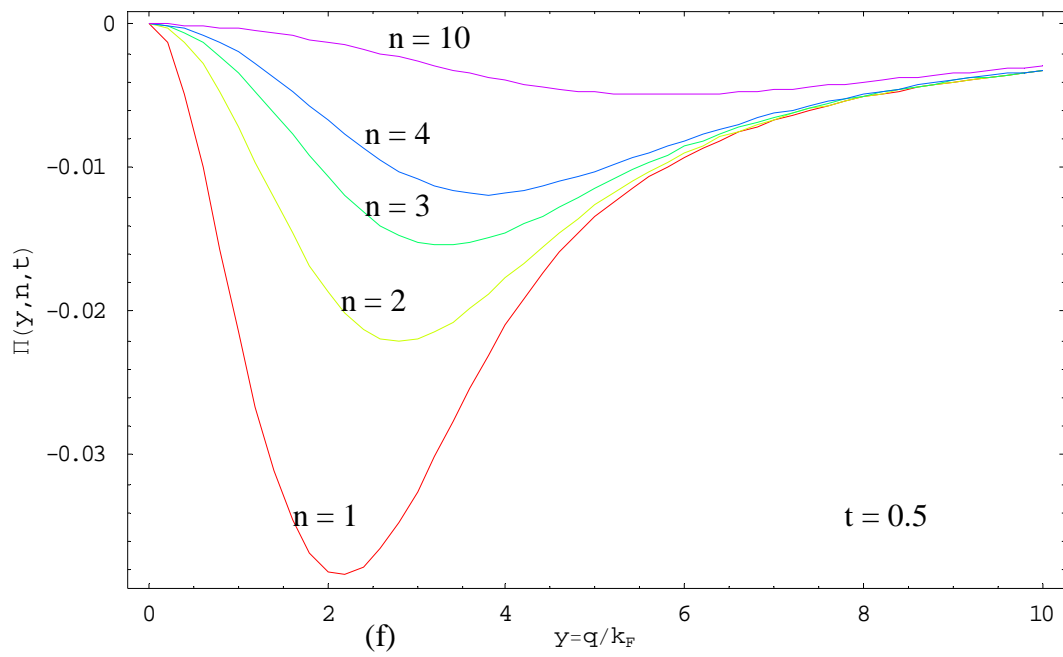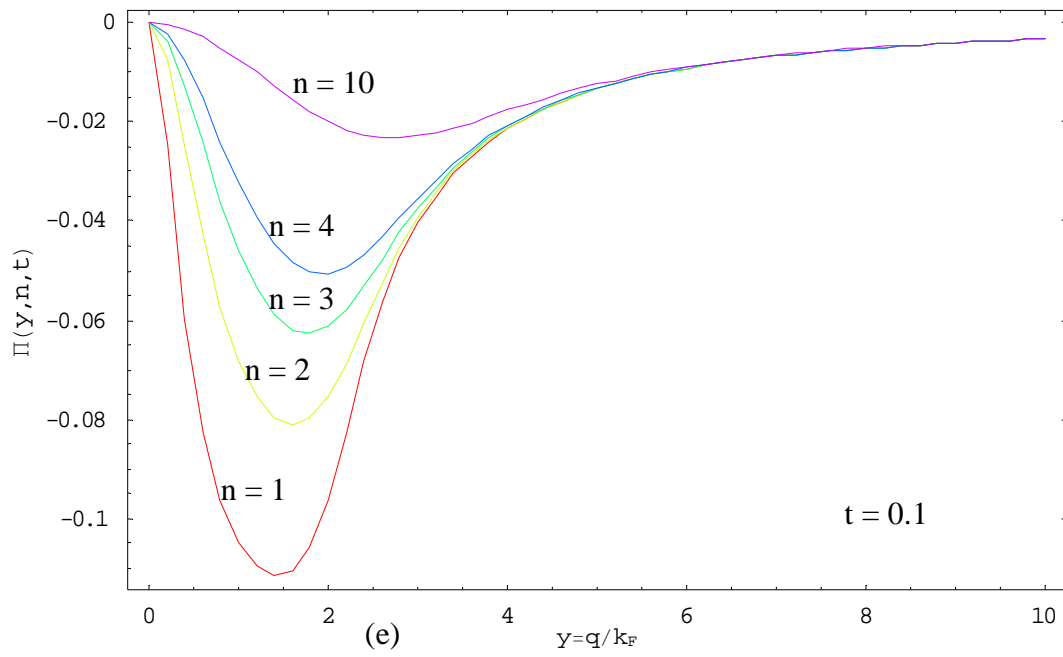
Figure 4.2 (Continued)

Figure 4.2 (Continued)

(g)

(h)

Figure 4.2 (Continued)

(i)

(j)
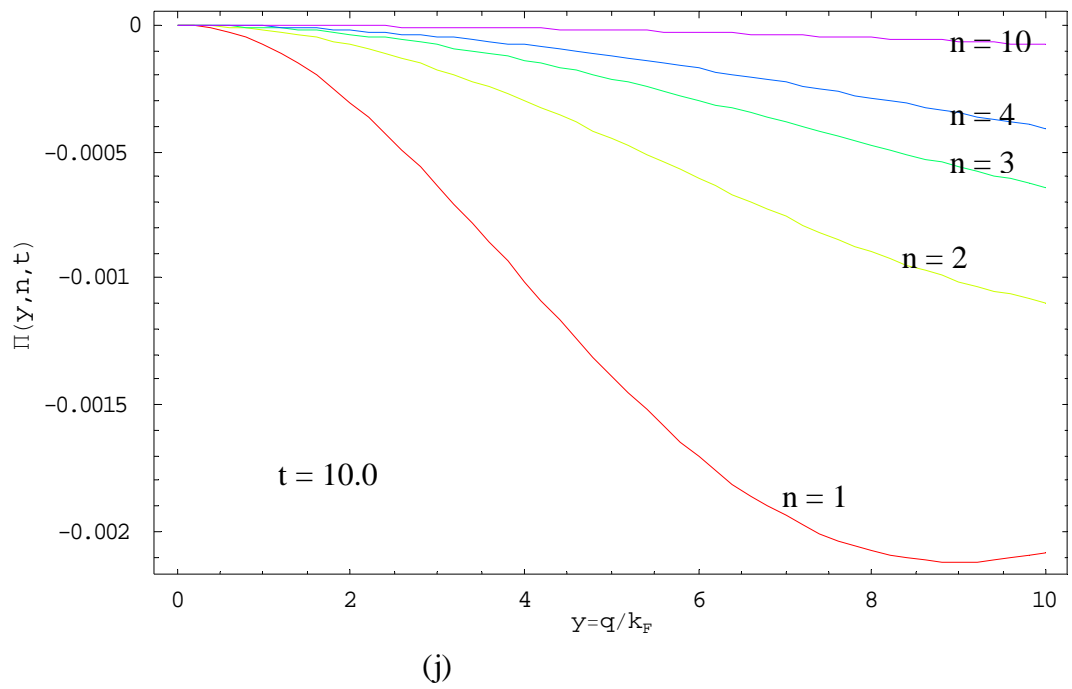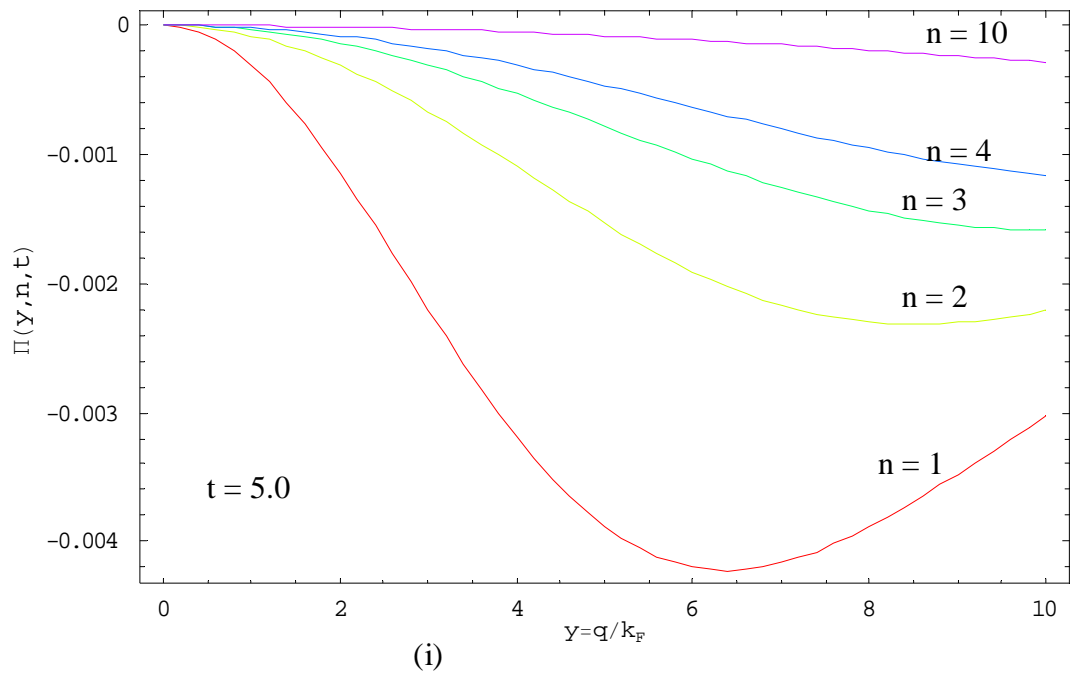
Figure 4.2 (Continued)

As before, we will consider four limits of the dynamic polarization.

4.3.1 Low temperature, small y limit

At low temperature and small y, $\cos 2\phi$ given by Eq. (4.26) can be approximated

to

$$\cos 2\phi \approx \frac{-\left(4x^2y^2 + 4n^2\pi^2t^2\right)}{\left[\left(4x^2y^2 + 4n^2\pi^2t^2\right)^2 + \left(4n\pi ty^2\right)^2\right]^{1/2}}$$

$$\approx -1 + \frac{1}{2}\frac{n^2\pi^2t^2y^4}{\left(x^2y^2 + n^2\pi^2t^2\right)^2}$$

and since $\cos 2\phi = 2\cos^2\phi - 1$, then

$$\cos\phi = \frac{1}{2}\frac{y^2}{n\pi t}\left[1/\left(1 + x^2y^2/n^2\pi^2t^2\right)\right]$$

The dynamic polarization, therefore, reduces to

$$\Pi(y,n,t) \approx -\frac{2}{\pi}\int_0^\infty \frac{x f(x)\cos\phi\,dx}{\left[4x^2y^2 + 4n^2\pi^2t^2\right]^{1/2}}$$

$$= -\frac{1}{2\pi}\left(\frac{y}{n\pi t}\right)^2\int_0^\infty \frac{x f(x)\,dx}{\left[1 + \left(xy/n\pi t\right)^2\right]^{3/2}}$$

Let $x^2/t = z$, $a = y^2/n^2\pi^2t$ then

$$\Pi(y,n,t) = -\frac{a}{4\pi}\int_0^\infty \frac{g(z)\,dz}{e^{z-\alpha} + 1}$$

where $g(z) = \left(1 + az\right)^{-3/2}$. Using Sommerfeld approximation

$$\therefore \qquad \Pi(y,n,t) \sim \frac{-a}{4\pi}\left[\int\limits_{0}^{\alpha} g(z)\,dz + \frac{\pi^2}{6}\frac{dg(z)}{dz}\bigg|_{z=\alpha}\right]$$

$$= \frac{-1}{2\pi}\left[1-(1+a\alpha)^{-1/2}+\frac{a^2\pi^2}{8}(1+a\alpha)^{-5/2}\right]$$

$$= \frac{-1}{2\pi}\left[1-\left\{1+(y/n\pi t)^2\right\}^{-1/2}\right]$$

$$\therefore \qquad \prod_{\substack{y\to 0 \\ t\to 0}}(y,n,t) \approx \frac{-1}{2\pi}\left[1-\left\{1+(y/n\pi t)^2\right\}^{-1/2}\right] \qquad (4.27)$$

Note that the polarization is also dependent on n, and if n = 0 it reduces to the value $-1/2\pi$ of the static case.

4.3.2 Low temperature, large y limit

In this limit $\cos 2\phi$ can be approximated as

$$\cos 2\phi \approx \left(y^4-4x^2y^2\right)/y^2\left[\left(y^2-4x^2-4n^2\pi^2t^2/y^2\right)^2+(4n\pi t)^2\right]^{1/2}$$

$$\approx 1$$

or $\cos\phi \sim 1$, then the polarization becomes

$$\Pi(y,n,t) \approx -\frac{2}{\pi}\int\limits_{0}^{\infty}\frac{x\,f(x)\,dx}{(y^4-4x^2y^2)^{1/2}}$$

Let $x^2/t = z$ and using Sommerfeld expansion, we have

$$\Pi(y,n,t) = \frac{-t}{\pi y^2}\left[\int\limits_{0}^{\alpha} g(z)\,dz + \frac{\pi^2}{6}\frac{dg(z)}{dz}\bigg|_{z=\alpha}\right]$$

where
$$g(z) = \left(1 - 4tz/y^2\right)^{-1/2}$$

Finally, we get

$$\prod_{\substack{t\to 0 \\ y\to\infty}}(y,n,t) \sim \frac{-1}{2\pi}\left[1 - \left(1 - 4/y^2\right)^{1/2}\right] \sim -1/\pi y^2 \tag{4.28}$$

which is independent of integer n as we expect and has the same form with Eq. (4.18) of the static case.

4.3.3 High temperature, small y limit

The value of $\cos 2\phi$ in this limit can be approximated as

$$\cos 2\phi \approx -\left(4n^2\pi^2t^2 + 4x^2y^2\right) / \left[\left(4n^2\pi^2t^2 + 4x^2y^2\right)^2 + \left(4n\pi ty^2\right)^2\right]^{1/2}$$

$$= -1 + n^2\pi^2t^2y^4 / 2\left(x^2y^2 + n^2\pi^2t^2\right)^2$$

or
$$\cos\phi = \left(y^2/2n\pi t\right)\left[1 + \left(xy/n\pi t\right)^2\right]^{-1}$$

The polarization becomes

$$\prod(y,n,t) \approx -\frac{2}{\pi}\int_0^\infty \frac{x f(x)\cos\phi\, dx}{\left[4x^2y^2 + 4n^2\pi^2t^2\right]^{1/2}}$$

At high temperature, the Fermi function $f(x) \sim \frac{1}{t}e^{-x^2/t}$

$$\therefore \qquad \prod(y,n,t) \approx \frac{-y^2}{2n^2\pi^3t^3}\int_0^\infty \frac{x\,e^{-x^2/t}\, dx}{\left[1 + \left(xy/n\pi t\right)^2\right]^{3/2}}$$

$$\approx \frac{-y^2}{2n^2\pi^3t^3}\left(\frac{t}{2} - \frac{3y^2}{4n^2\pi^2}\right)$$

or
$$\prod_{\substack{t\to\infty \\ y\to 0}}(y,n,t) \sim -y^2/4n^2\pi^3 t^2 \tag{4.29}$$

4.3.4 High temperature, large y limit

Since $\cos 2\phi \sim 0$ or $\cos\phi \sim 1/\sqrt{2}$ and $f(x) \sim \dfrac{1}{t}e^{-x^2/t}$, then

$$\Pi(y,n,t) \sim -\frac{2}{\pi}\int_0^\infty \frac{x f(x)\cos\phi\, dx}{2y(n\pi t)^{1/2}}$$

or
$$\prod_{\substack{t\to\infty \\ y\to\infty}}(y,n,t) \sim -1/2\pi y(2n\pi t)^{1/2} \tag{4.30}$$

which is a very small quantity

4.4 Evaluation of the dielectric function in its full form

To study the impact of static and dynamic screening in the layered system we need to calculate the dielectric function given by Eq. (4.8). In particular, to obtain T_c of HTS we have to determine these functions at finite temperatures. Since the inverse $\varepsilon^{-1}(q,q_z,n,t)$ of the dielectric function is the quantity that enters the vertex $\Gamma_c = V_c(q,q_z)/\varepsilon(q,q_z,n,t)$ the result of this quantity is shown separately between the static and dynamic cases.

4.4.1 Static case

The static polarization, which enters in the static case of the dielectric function is given by Eq. (4.15). The result is shown in Figure 4.3 for the same values of para-meters as in Figure 4.2

Figure 4.3 Inverse dielectric function of layered electron gas for static case.

(c)
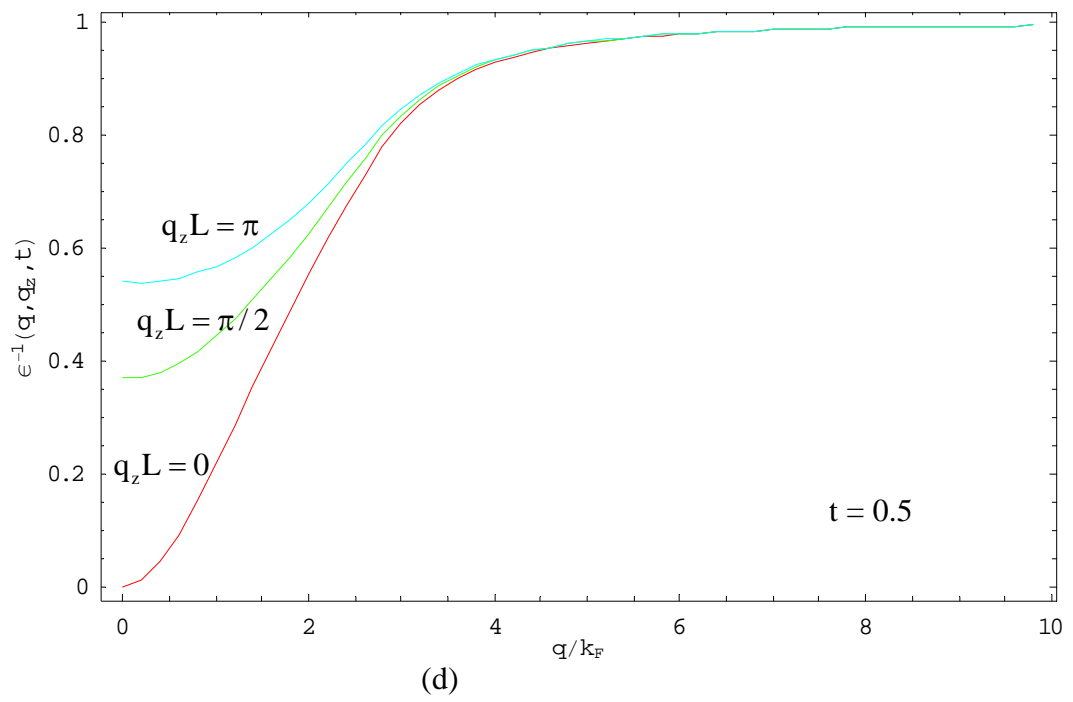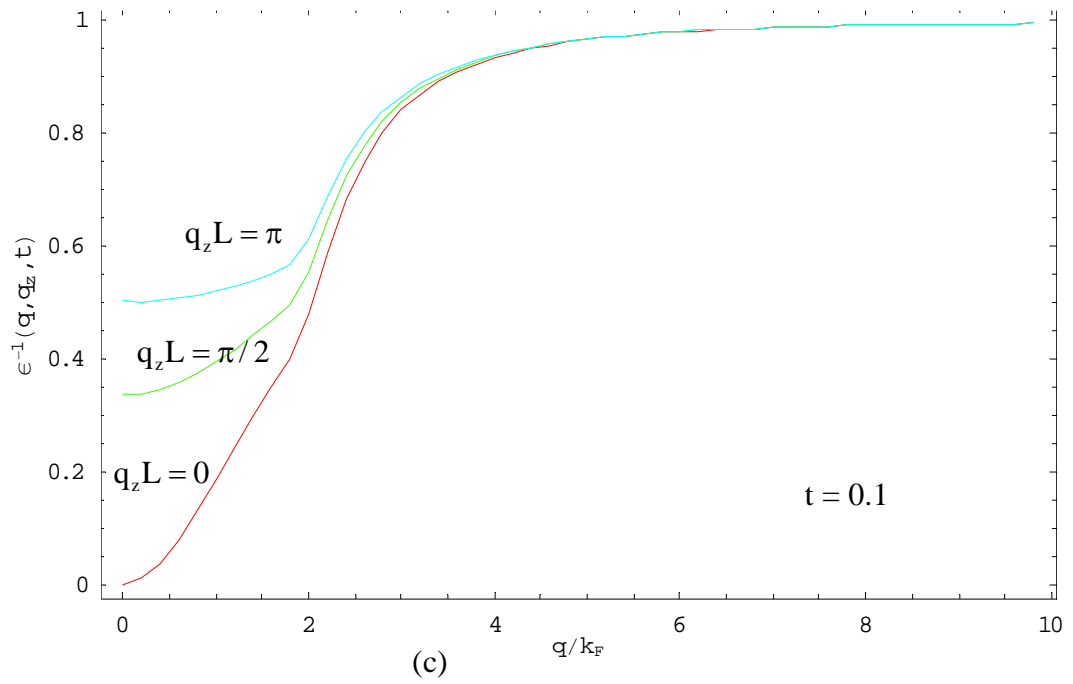
(d)

Figure 4.3 (Continued)

(e)

(f)
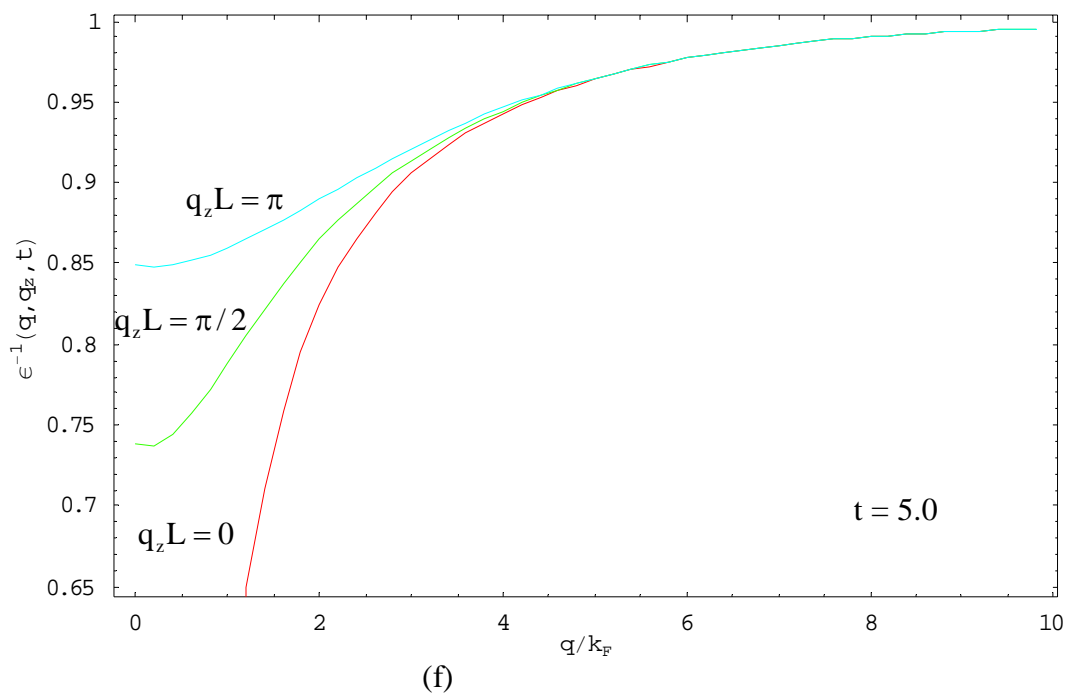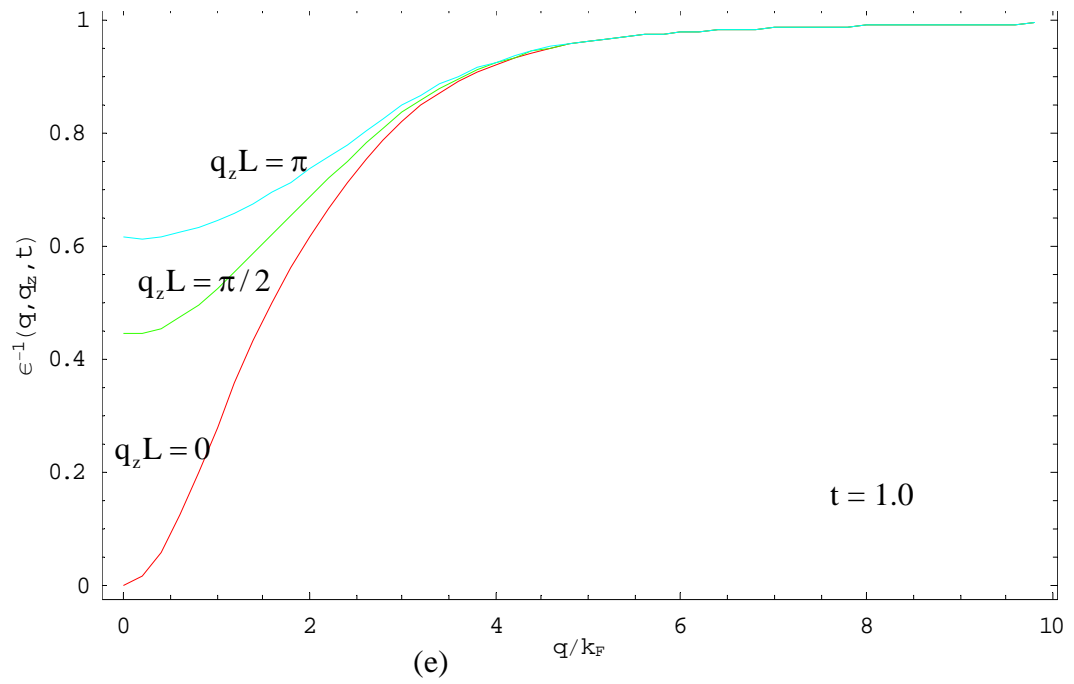
Figure 4.3 (Continued)

4.4.2 Dynamic screening

The dynamic polarization given by Eq. (4.23) is used for the evaluation of the dielectric function necessary to study the dynamic screening. The inverse

$\varepsilon^{-1}\left(q,q_z,\omega_n,T\right)$ of the dielectric function as a function of $y = q/k_F$ at various t and n

is shown in Figure 4.4. Note the strong q and ω_n dependence of the function at finite temperatures. This shows the necessity to consider the dielectric function in its full form to study the dynamical screening of the Coulomb interaction. Also note that the inverse dielectric function is zero (perfect screening) only in the static limit
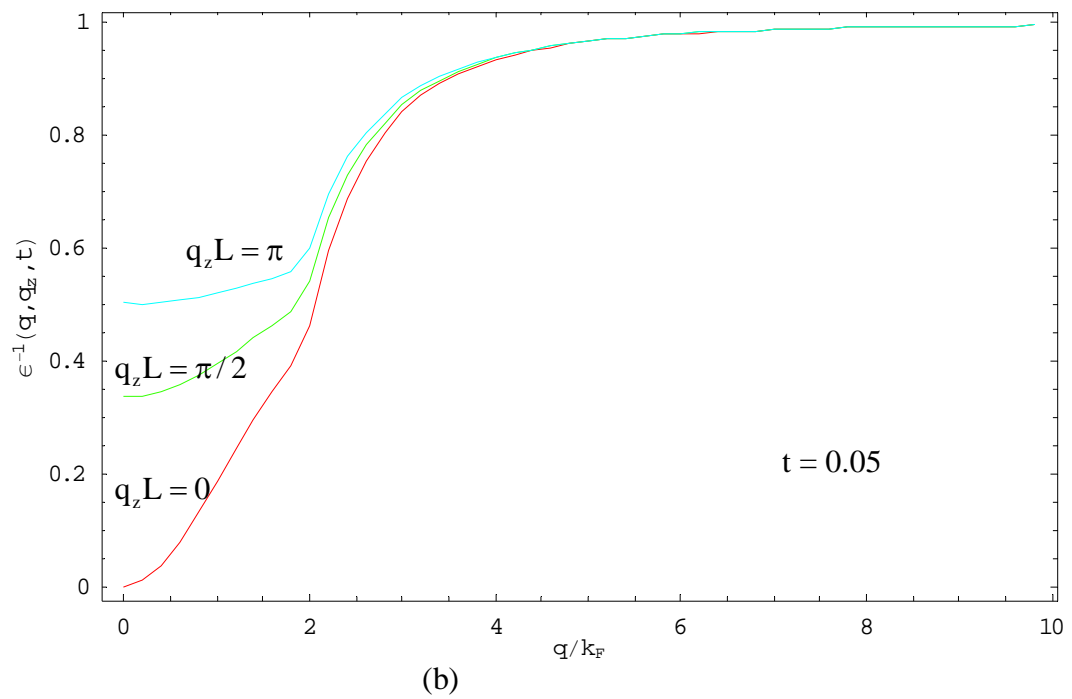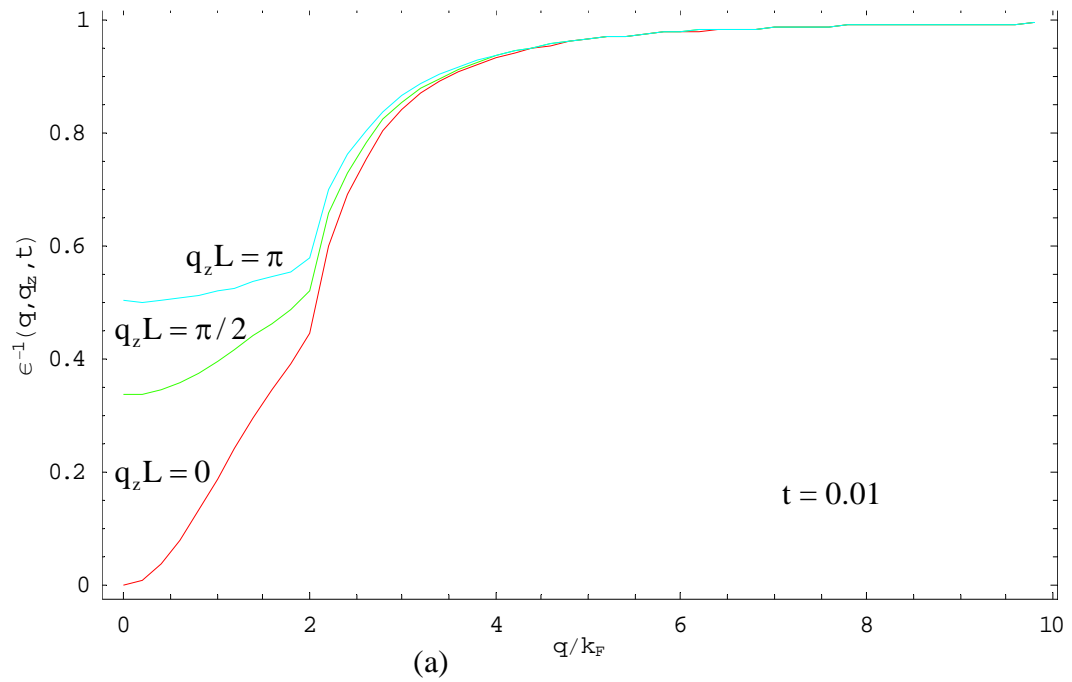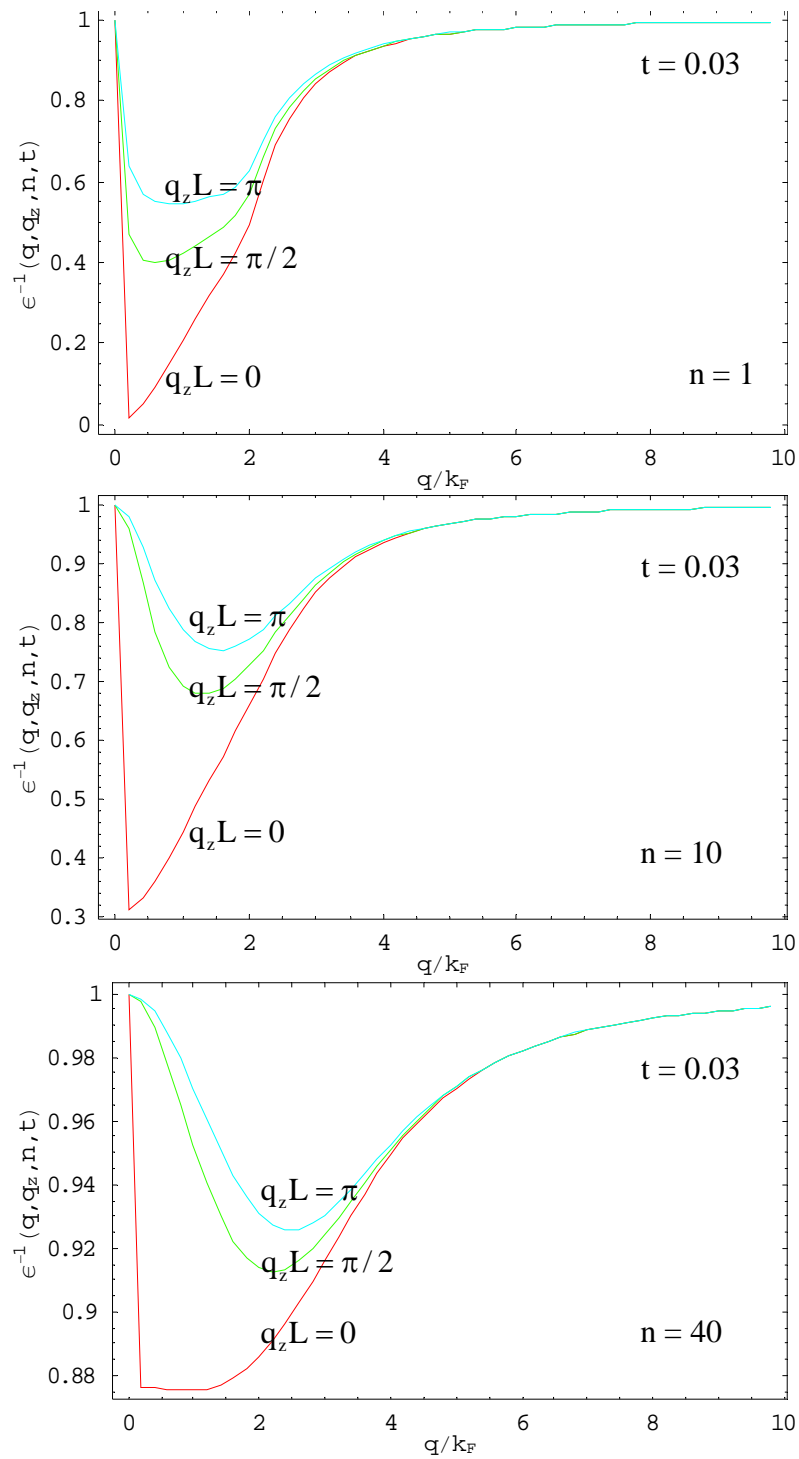
Figure 4.4 Inverse dielectric function of layered electron

gas for dynamic case.
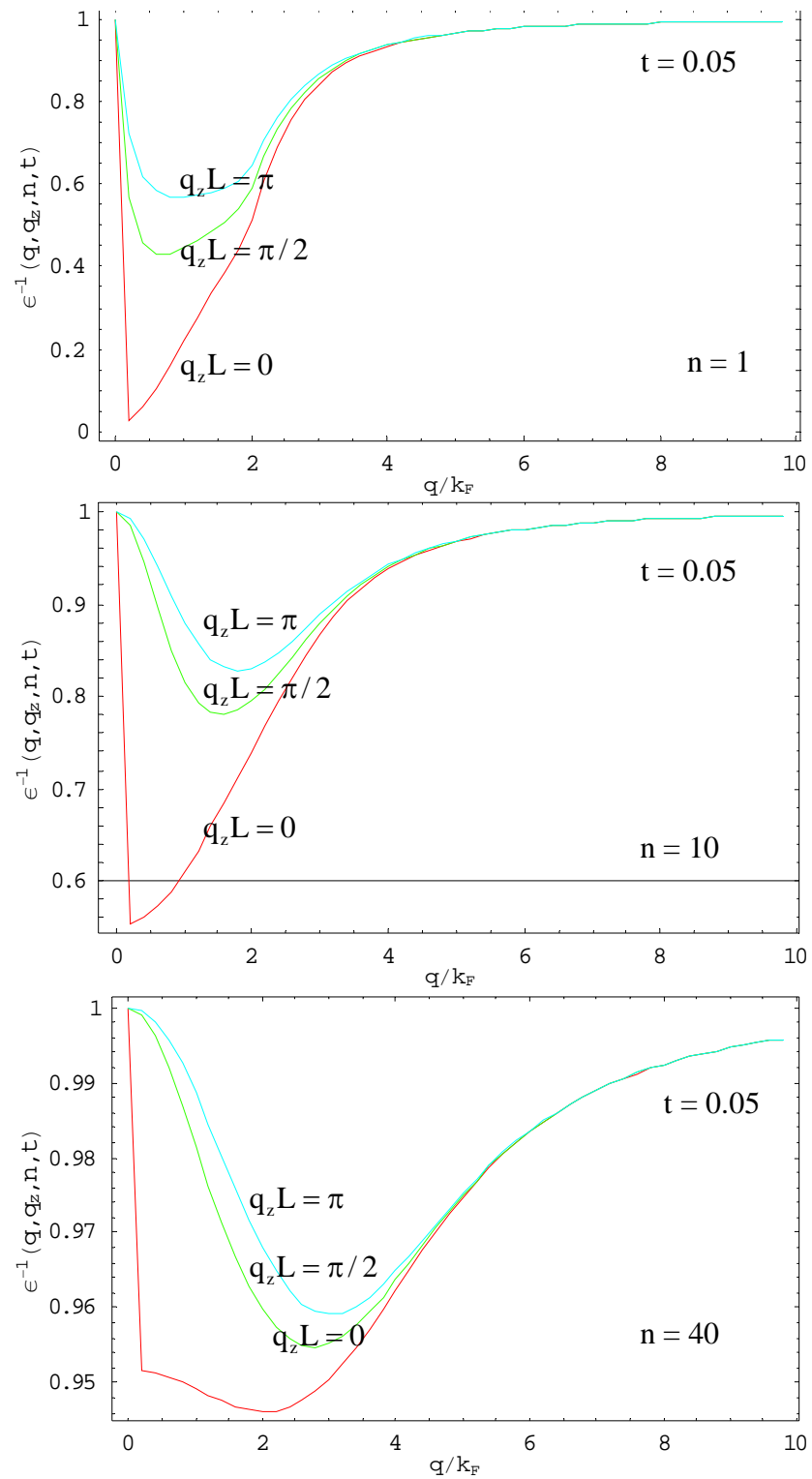
Figure 4.4 (Continued)
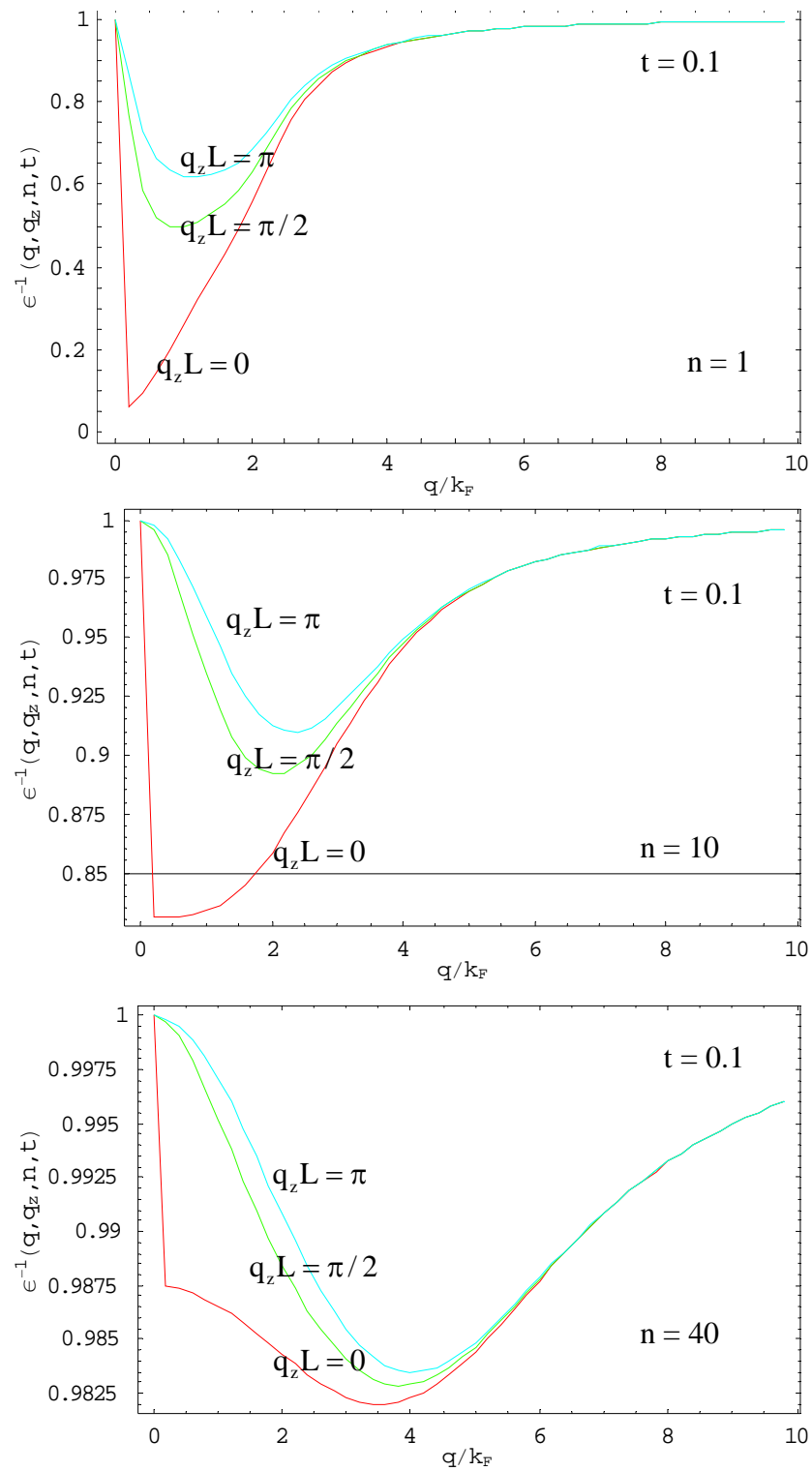
Figure 4.4 (Continued)
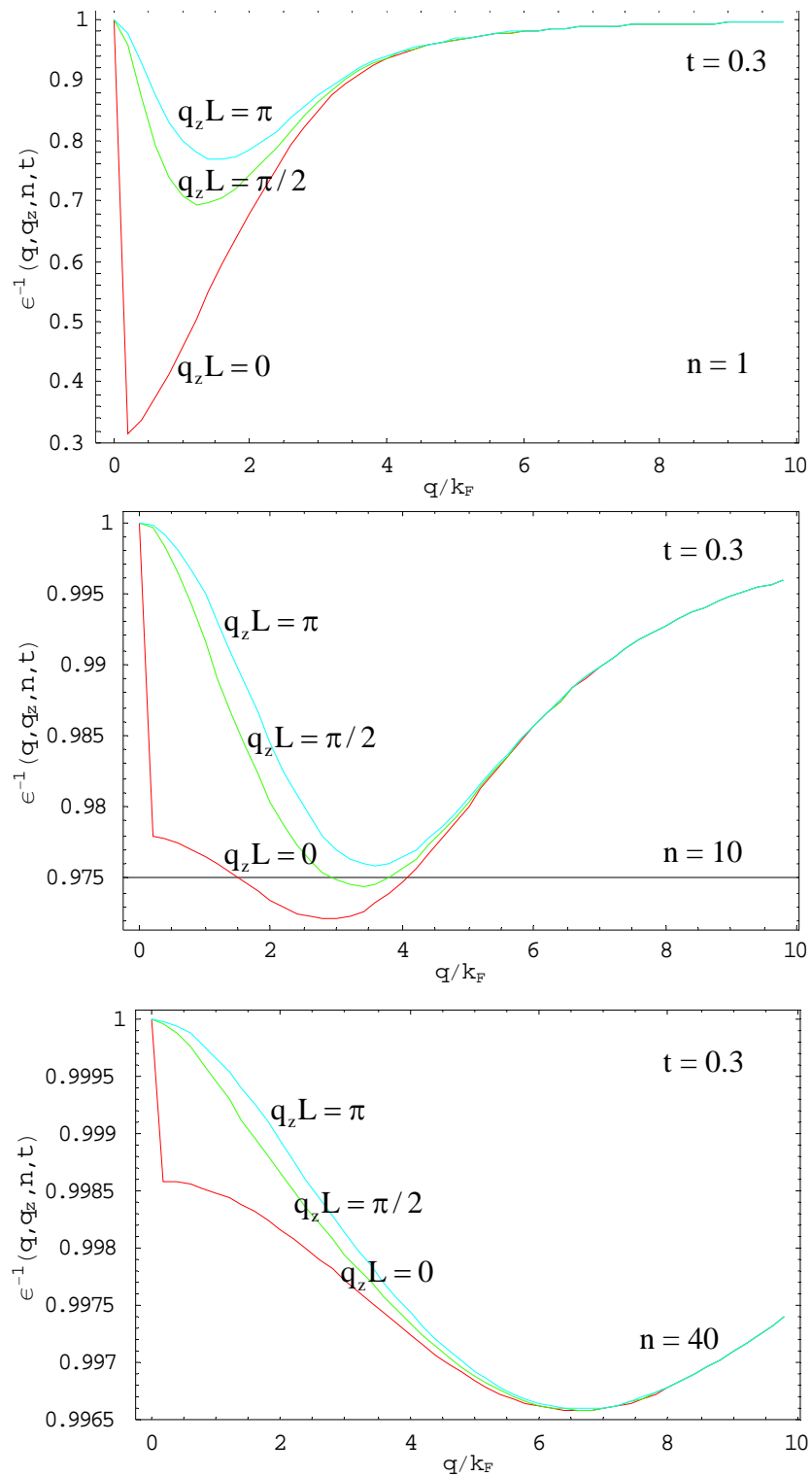
Figure 4.4 (Continued)

A few important properties of the inverse dielectric function will be pointed out. The function is bounded for all q and ω_n. For high frequencies and / or large wave vectors, the inverse dielectric function goes to 1. This means that the Coulomb interaction is unscreened and thus long-range in these limits. However, the unscreened limits are shifted to larger wave vectors with the increasing of frequencies and temperatures. At sufficiently high frequencies, the inverse dielectric function takes the form

$$\lim_{\omega_n \to \infty} \varepsilon^{-1}(q, q_z, \omega_n, T) \approx 1 - \frac{\omega_p^2}{\omega_n^2} \tag{4.31}$$

which is the so-called Drude limit (Nozie`res and Pines, 1989) where $\omega_p^2 = \omega^2(q = 0, q_z = 0)$ is the usual 3D optical plasmon. It is only at zero frequency or in the static case (n = 0) that the Coulomb interaction is perfectly screened and the inverse dielectric function takes the form of the Thomas-Fermi type.

$$\varepsilon^{-1}(q, q_z, \omega_n = 0, T) = \left[1 + k_{TF}^2 / |q, q_z|^2 \right]^{-1} \tag{4.32}$$

Where k_{TF} is the Thomas-Fermi screening wave vector which is given by $k_{TF}^2 = m\omega_n^2 / 2\hbar^2$ for the layered system.

The full temperature, frequency and wave-vector dependence of the dielectric function describing the screening in layered superconductors will be useful to study the effect on T_c. The additional impact of dynamic screening on pairing in layered superconductors had been discussed (Bill *et al.,* 2003). Three classes of layered superconductors had been studied: metal-intercalated halide nitrides, layered organic materials and high-T_c oxides. They showed that the plasmon contribution is dominant in

the first class of layered materials. They obtained $T_c \approx 24.5K$ which is very close to the observed value $T_c = 25.5K$. In the absence of the plasmon contribution they obtained $T_c^{ph} \ll 1K$. For the layered organic superconductors, they obtained $T_c = 10.4K$ while in the absence of acoustic plasmons they obtain $T_c^{ph} = 6.3K$. Therefore, 40% of the value of T_c is due to the pairing of electrons via the exchange of acoustic plasmon. In the case of high-T_c oxides they obtained $T_c = 36.5K$ which is close to the experimental value $T_c = 38K$. In the absence of the screened Coulomb interaction they obtained $T_c^{ph} = 30K$, thus about 20% of the observed value of T_c is due to acoustic plasmons. Thus the dynamically screened interlayer Coulomb interaction has been shown to be important for superconductivity in the cuprates.

In the next chapter the evaluation of the T_c of these materials will be considered.

CHAPTER V

CALCULATION OF CRITICAL TEMPERATURE OF

LAYERED SUPERCONDUCTORS

5.1 Strong-coupled superconductors

The BCS theory provides a complete though approximate theory of both thermal as well as dynamic properties of superconductors in the weak coupling limit. According to the BCS theory, the transition temperature T_c depends upon the product

$$\lambda \;=\; N(0)V \tag{5.1}$$

of the single spin density of states at the Fermi surface N (0) with the pairing potential V, and a cutoff frequency of order the Debye frequency θ_D. When λ is small, in practice less than 0.25, the BCS theory predicts that

$$T_c \;=\; 1.14\theta_D \exp(-1/\lambda) \tag{5.2}$$

In this same weak-coupling limit, the gap at zero temperature is given by

$$2\Delta(0)/k_B T_c \;=\; 3.53 \tag{5.3}$$

which is frequently used as a test for the applicability of the BCS model.

Generalizations of the BCS treatment concentrate on two main problems:

(1) inclusion of the repulsive Coulomb interaction between the electrons, and

(2) extension of the BCS theory to the situation with arbitrarily large electron-phonon coupling by generalizing the treatment of normal metals, with electron-lattice interac-

tions incorporated in a systematic fashion. Both of these factors have been included in the Eliashberg approach to superconductivity (Eliashberg, 1966).

The Coulomb repulsive interaction reduces the effective attractive interaction between the electrons, so that instead of Eq. (5.2) one obtains in the BCS approximation

$$T_c = 1.14\theta_D \exp\left(-\frac{1}{\lambda - \mu^*}\right) \tag{5.4}$$

where μ^* is the so-called pseudo-Coulomb potential (Morel and Anderson, 1962). The Eliashberg correction to the BCS theory must be evaluated numerically. Extending this idea so that comparison to experiments could be made, Mc Millan (1968) calculated the self-energies of normal and paired electrons and used a dimensionless electron-phonon coupling parameter,

$$\lambda \equiv 2 \int_0^{\omega_{max}} \alpha^2(\omega)\, F(\omega)\, \frac{d\omega}{\omega} \tag{5.5}$$

where $\alpha^2(\omega)$ is the average electron-phonon interaction at frequency ω, $F(\omega)$ is the phonon density of states, and ω_{max} is the maximum phonon frequency. (Note: this α^2 has nothing to do with the α associated with the isotope effect). Equation (5.5) should be general and apply for any boson–mediated pairing, not just phonon-mediated pairing. The ω^{-1} in λ increases the importance of the low-frequency bosons with respect to those at higher frequency. He numerically solved the finite temperature, nonlinear Eliashberg equations finding T_c for various classes of strong-coupled superconductors. From these solutions, he constructed an approximate equation that relates T_c to a small number of parameters by the form

$$T_c = \frac{\theta_D}{1.45} \exp\left[-\frac{1.04(1+\lambda)}{\lambda - \mu^*(1+0.62\lambda)} \right] \tag{5.6}$$

The most interesting feature of McMillan's expression is the fact that the phonon contribution is effectively reduced by $0.62\mu^*\lambda$. This arises because the time correlation between paired electrons are distorted by the repulsive Coulomb interaction so that in the presence of the Coulomb interaction a member of a pair cannot take full advantage of the attractive lattice polarization produced by its partner.

Due to the screening by the other electrons, the effective Coulomb repulsion μ^* differs from the instantaneous Coulomb repulsion μ by the relation

$$\frac{1}{\mu^*} = \frac{1}{\mu} + \ln\left(\frac{\omega_{el}}{\omega_{ph}} \right) \tag{5.7}$$

where ω_{el} can be taken as the plasma frequency ω_p, or the Fermi energy ε_F, whereas ω_{ph} corresponds to the high-frequency cutoff of the phonons or Debye frequency. Usually μ^* is in range $0 - 0.2$ and $\mu^* \approx 0.1$ being the typical value for most superconductors.

One should mention a very important feature of the phonon-mediated electron pairing. Namely; the transition temperature is proportional to the Debye temperature θ_D. Hence, T_c given by Eq. (5.4) depends on the mass M of the atoms composing the lattice. In the simplest situation we expect that $T_c \approx M^{-1/2}$. If the Coulomb repulsion between electrons is taken into account, then the relation is $T_c \approx M^{-\alpha}$ where α is obtained by using Eq. (5.6) and was shown by Mc Millan to be

$$\alpha = \frac{1}{2}\left\{1 - \frac{(1+\lambda)(1+0.62\lambda)}{\left[\lambda - \mu^*(1+0.62\lambda)\right]^2}\right\} \tag{5.8}$$

In the strong coupling limit $(\lambda \geq 1)$ the exponent α is largely reduced from its initial value of ½. Therefore, if the value of α is small, one may interpret this fact as either the evidence for strong electron-phonon coupling or that a new nonphonon mecha - nism is needed to explain superconductivity.

5.2 Coexistence of the phonon and plasmon mechanisms

A simple analytical expression describing T_c for any strength of the electron-phonon coupling λ_{ph} is derived directly from the Eliashberg equation (Kresin, 1987a). It is given by

$$T_c = \frac{0.25\,\overline{\omega}}{\left[e^{2/\lambda_{eff}} - 1\right]^{1/2}} \tag{5.9}$$

where $\overline{\omega} = \left\langle \omega^2 \right\rangle^{1/2}$, $\left\langle \omega^2 \right\rangle = \int d\omega\, \alpha^2(\omega)F(\omega)\omega$, $F(\omega)$ is the phonon density of states; $\alpha^2(\omega)$ describes the electron-phonon interaction. The effective interaction strength is

$$\lambda_{eff} = \frac{\lambda - \mu^*}{1 + 2\mu^* + \lambda\mu^* t(\lambda)} \tag{5.10}$$

The function $t(\lambda)$ is defined graphically for all λ, but analytically for $\lambda \leq 1$ and for $\lambda \gg 1$ only.

Let us apply Eq. (5.9) to the La-Sr-Cu-O system in order to estimate the value of λ_{ph}. According to data obtained by neutron inelastic spectroscopy, the phonon densi-ty of states $F(\omega)$ in the $La_{1.8}Sr_{0.2}CuO_4$ system exhibits two sharp peaks at $\omega_1 \simeq 100K$ and $\omega_2 \approx 200K$. Therefore, it is reasonable to put $\omega = 150K$. Let $\mu^* = 0.1$ and $\alpha^2(\omega)$

can be determined by the tunneling spectroscopy technique, then from Eq. (5.9) we obtain $\lambda_{ph} \approx 5$. This means that we require very strong electron-phonon coupling to account for the experimentally observed $T_c \approx 40K$. However, from measurements of the energy gap and the ratio $\beta = 2\Delta(0)/T_c$ that depends on the value of λ_{ph} shows that $\beta \leq 5$. This implies that λ_{ph} for the system does not exceed the value $\lambda_{ph} = 2$, which is not sufficient to provide the experimentally observed $T_c \approx 40K$ and the corresponding value $\lambda_{ph} = 5$. Hence, we come to the conclusion that the electron-phonon interaction plays an important role in the La-Sr-Cu-O system but, nevertheless, there is need for an additional mechanism of attraction between the carriers.

As mentioned earlier that the electron-plasmon interaction is believed to be an additional mechanism which, jointly with the strong electron-phonon coupling, is responsible for high-T_c superconductivity. The concept of coexistence means that the electron-phonon plays an important role. The Coulomb repulsion is overcome mainly by the electron-phonon interaction. As for the plasmon contribution, the electron-plasmon interaction provides an additional mechanism of electron-electron attraction, and in the presence of electron-phonon interaction it leads to an additional increase in T_c. For a rough estimate the expression for T_c can be written in the form (Kresin, 1987b):

$$T_c = T_c^{ph} \left(\frac{\overline{\omega}_{pl}}{T_c^{ph}} \right)^{\alpha} \tag{5.11}$$

where

$$\alpha = \frac{\lambda_{pl}}{\lambda_{pl} + \lambda_{ph}} \tag{5.12}$$

and T_c^{ph} is the critical temperature in the absence of the plasmon mechanism. One can see that the large value of plasmon energy $\overline{\omega}_{pl}$ make the plasmon contribution noticeable, even for small λ_{pl}. For example, if $\lambda_{ph} \approx 2$ (this value corresponds to $2\Delta(0)/k_B T_c \approx 5$) and $\lambda_{pl} \approx 0.3$, $\overline{\omega}_{pl} \approx 60$ meV, we obtain $T_c^{ph} \approx 22K$ and $T_c \approx 38K$. If we use an experimental value of 1eV for the bulk plasmon frequency (Sulewski *et al.,* 1987), which is a lower limit for the 3D to 2D crossover, we estimate a $\lambda_{pl} \approx 0.2$ for $T_c \approx$ 38K. It is clear that an increase of $\overline{\omega}_{pl}$ results in a decrease of λ_{pl}. Plasmon –induced pairing can, therefore, make a noticeable change in T_c relative to T_c^{ph} even for small values of λ_{pl} and it arises from the large value of the plasmon frequency.

Using the plasmon exchange model, the T_c observed in the thallium-based and bismuth-based compounds was shown (Bose and Long, 1990) to increase with the number of CuO layers per unit cell, which is in agreement with observed result. The thallium-based compound with only one CuO layer per cell has a T_c of 80K; with two CuO layers its T_c is 105K, whereas with three CuO layers it is raised to 125K. Similar conclusions have also been drawn for the bismuth-based compounds.

The Eliashberg model, on the basis that the attractive interaction is provided by the plasmon mediated effective interaction between charge carriers, has been developed (Longe and Bose, 1992a) to calculate the critical temperature in high-T_c supercon-ductors. The effective interaction between the electrons are described within the RPA. This interaction can be written in the standard form

$$V(q,\omega) = V_0(q)\left[1 + \int\limits_{-\pi/L}^{\pi/L} dq_z \frac{2\omega_p(q,q_z)|M(q,q_z)|^2}{\omega^2 - \omega_p^2(q,q_z)}\right] \qquad (5.13)$$

where $V_0(q) = 2\pi e^2 / \varepsilon_M q$ is the bare 2D Coulomb interaction, $\omega_p(q, q_z)$ is the plasmon frequency and $|M(q, q_z)|^2$ is the square of the electron-plasmon matrix element. Indeed, it has been shown (Allen and Dynes, 1975) that if the effective interaction between electrons in a superconductor can be written as given by Eq. (5.13), then the parameters λ and $\langle \omega^2 \rangle$ can be obtained from

$$\lambda = N(0) \left\langle \frac{2|M(q, q_z)|^2}{\omega_p(q, q_z)} \right\rangle_{FS} \tag{5.14}$$

and $\qquad \lambda \langle \omega^2 \rangle = N(0) \left\langle 2|M(q, q_z)|^2 \, \omega_p(q, q_z) \right\rangle_{FS} \tag{5.15}$

where $N(0)$ is the density of states of the electrons at the Fermi surface and $\langle ... \rangle_{FS}$ indicated that an average of the expression is taken over the Fermi surface. Hence, the frequency $\bar{\omega}$ is given by the square root of the ratio of (5.15) and (5.14). Equations (5.14) and (5.15) had been shown (Longe and Bose, 1992b) to be

$$\lambda = \frac{2N(0)}{\pi} \int_{q_m}^{2k_F} dq \, \frac{V_0(q)}{\left(4k_F^2 - q^2\right)^{1/2}} \tag{5.16}$$

and $\qquad \lambda \langle \omega^2 \rangle = \frac{2N(0)}{\pi} \frac{2\pi n e^2}{\varepsilon_M m^*} \int_{q_m}^{2k_F} dq \, \frac{q \, V_0(q) \coth(Lq)}{\left(4k_F^2 - q^2\right)^{1/2}} \tag{5.17}$

First it is interesting to note that λ, as given by Eq. (5.16), does not depend on the interlayer distance L. This is due to the analytic properties of the RPA potentials given by Eq. (5.13). Another important point has to be noted. The integrals (5.16) and (5.17) diverge for small momentum transfers q. The technique to address this difficulty is to introduce a finite q_m (replacing 0) as the lower limit of integration in the two equations to obtain finite results. Physically one would expect that the effective range

of q_m should be of the order of inverse coherence length ξ, since charge carriers at distances larger than ξ do not contribute significantly to Cooper pairing. Therefore, one can write $q_m = 1/\xi$ and thus T_c must obviously depend on the value of ξ.

It is also interesting to note that even though integrals (5.16) and (5.17) diverge for small q_m, but their ratio $\left(\text{i.e.}\left\langle \omega^2 \right\rangle\right)$ however does not. On the other hand, for q_m large i.e. $q_m \rightarrow 2k_F$, $\left\langle \omega^2 \right\rangle$ tends rather slowly to the upper limit $2k_F \sigma \coth\left(2k_F L\right) \sim 2k_F \sigma$ where $\sigma = 2\pi n e^2 / \varepsilon_M m^*$. Hence the range of variation of $\left\langle \omega^2 \right\rangle$ as a function of q_m is not very extended. This is not the case for λ which diverges linearly for small q_m.

As before, it is simpler to scale the parameter, $y = q/k_F$. Then Eqs. (5.16) and (5.17) become

$$\lambda = N\left(0\right) \frac{2\pi e^2}{\varepsilon_M} \frac{1}{\pi k_F} \int\limits_{1/k_F\xi}^{2} \frac{dy}{y\left(1 - y^2/4\right)^{1/2}} \tag{5.18}$$

$$\lambda\left\langle \omega^2 \right\rangle = N\left(0\right) \frac{2\pi e^2}{\varepsilon_M} \frac{\sigma}{\pi} \int\limits_{1/k_F\xi}^{2} dy \frac{\coth\left(k_F Ly\right)}{\left(1 - y^2/4\right)^{1/2}} \tag{5.19}$$

where $\quad N\left(0\right) = \dfrac{m^*}{2\pi}$ (5.20)

$$\sigma = \frac{2\pi e^2 n}{\varepsilon_M m^*} \tag{5.21}$$

and $\quad k_F^2 = 2\pi n$ (5.22)

It is seen from Eqs. (5.18) and (5.19) that the two parameters obviously depend on the dielectric constant ε_M, the effective mass m^*, the surface number density n of the electron gas (or equivalently the Fermi wave vector k_F and hence the Fermi ener-

gy ε_F) and the coherence length ξ. The Coulomb repulsion parameter μ^* depends on other boson frequencies and like many other investigators its numerical value is cho - sen to be 0.1. However, its value is still a matter of discussion and will be a second parameter to be varied around 0.1. Substituting these values of $\bar{\omega}$, λ and μ^* in the Mc Millan's equation and the Kresin's equation for T_c, the critical temperature of the cuprate superconductors will be obtained and discussed.

5.3 Critical temperature of $La_{1.85}Sr_{0.15}CuO_4$

In this section we will focus on the $La_{1.85}Sr_{0.15}CuO_4$ for which most parameters have been determined and it deserves special attention because of the simplicity of its structure. This system plays a role similar to the hydrogen atom in atomic physics. It is the best test system for understanding the basic principles of high-temperature superconductivity.

Followings are the normal state parameters (Bill *et al.,* 2003):

the interlayer distance $\qquad$ $L = 6.5 \,\dot{A}$

the Fermi wave-vector $\qquad$ $k_F = 3.5 \times 10^7 \ cm^{-1}$

the dielectric constant $\qquad$ $\varepsilon_M \simeq 5-10$

the effective mass $\qquad$ $m^* = 1.7 \, m_e$

the coherence length $\qquad$ $\xi = 35 \,\dot{A}$

and the Coulomb pseudopotential is taken to be $\mu^* = 0.1$ (here, m_e being the mass of the bare electron)

Two equations, Mc Millan's equation and Kresin's equation, will be used for the calculation of T_c of this material. The Mc Millan's equation for the plasmon exchange model is similar to Eq. (5.6) and has the form

$$T_c = \frac{\bar{\omega}}{1.45} \exp\left[-\frac{1.04(1+\lambda)}{\lambda - \mu^*(1+0.62\lambda)}\right] \qquad (5.23)$$

where the Debye frequency θ_D is replaced by the average frequency of plasmon, the exchange of which is responsible for superconductivity.

The Kresin's equation for the plasmon exchange model to calculate the value of T_c is given by Eq. (5.9), i.e.,

$$T_c = \frac{0.25\,\bar{\omega}}{\left[e^{2/\lambda_{\text{eff}}} - 1\right]^{1/2}}$$

where the effective interaction strength λ_{eff} is given by Eq. (5.10), i.e.

$$\lambda_{\text{eff}} = \frac{\lambda - \mu^*}{1 + 2\mu^* + \lambda\mu^* t(\lambda)}$$

and the analytical expression for the function $t(\lambda)$ is given (Long and Bose, 1992b) by

$$t(\lambda) = 0.75 + 0.8/(1+\lambda) - 0.12(\lambda - 0.5) \qquad (5.24)$$

The results of T_c obtained by these two equations will be compared with the recent work by Bill *et al.* (2003). We will start with the calculation of λ and $\bar{\omega}$ given by Eqs. (5.18) and (5.19) respectively. As can be seen from the given parameters that the value of dielectric constant ε_M is in range 5-10, and λ and $\bar{\omega}$ obviously sensitive to this choice of ε_M. We, therefore, calculate the values of λ, $\bar{\omega}$ and then T_c^{pl} by using different values of ε_M. The result is shown in Table 5.1. The finite-wave vector (higher order in q) effect of plasmon dispersion relation given by Eq. (3.30), which is

the term $(3/4)\hbar^2 q/me^2$, on T_c^{pl} is also shown in the table. It is seen that the values of T_c^{pl} obtained by using Kresin's equation are higher than that by using McMillan's equation and the finite-wave vector effect enhances the values of T_c^{pl} significantly.

Table 5.1 The calculated values for T_c^{pl} as obtained from Kresin's equation (T_{c1} and T_{c2}) and from McMillan's equation (T_{c3} and T_{c4}).

T_{c1} and T_{c3} are the values without the finite-wave vector effect whereas T_{c2} and T_{c4} are the values including that effect.

ε_M	By Kresin's equation				By McMillan's equation			
	T_{c1}		T_{c2}		T_{c3}		T_{c4}	
	(eV)	(K)	(eV)	(K)	(eV)	(K)	(eV)	(K)
5	0.0117898	136.821	0.0126273	146.54	0.0112205	130.213	0.0120175	139.463
6	0.004993	57.943	0.00534767	62.059	0.00460658	53.459	0.0049338	57.256
7	0.00198005	22.978	0.0021207	24.610	0.0017475	20.279	0.00187163	21.720
8	0.00072192	8.377	0.00077320	8.973	0.00059975	6.960	0.00064236	7.454
9	0.00023725	2.753	0.00025411	2.948	0.00018176	2.109	0.00019467	2.259
10	0.00006867	0.797	0.00007355	0.854	0.00004722	0.548	0.00005057	0.587

As reported by Bill *et al.* (2003), the experimental value of T_c of $La_{1.85}Sr_{0.15}$ - CuO_4 is $T_c^{exp} \approx 38K$. Their numerical result is $T_c = 36.5K$ whereas in the absence of acoustic plasmon it is $T_c^{ph} = 30K$. Therefore, the value of T_c due to acoustic plasmons is $T_c^{pl} = 6.5K$. The expected result (due to acoustic plasmons) to fit the experimental value is $T_c^{pl} \approx 8K$. It is seen from table 5.1 that the expected results correspond to the dielectric constant $\varepsilon_M = 8$ (8.38K and 8.97K by Kresin's equation, 6.96K and 7.45K by Mc Millan's equation). These results are quite different from the values that correspond to $\varepsilon_M = 7$ and $\varepsilon_M = 9$. It is, therefore, necessary to obtain T_c^{pl} that correspond to the dielectric constant around $\varepsilon_M = 8$. The result is shown in Table 5.2. It is seen from Table 5.2 that the appropriated value of the dielectric constant is $\varepsilon_M \simeq 8.0$ for $\mu^* = 0.1$.

Table 5.2 The calculated values for T_c^{pl} as obtained from the same process of Table 5.2 with dielectric constant around $\varepsilon_M = 8$

ε_M	By Kresin's equation				By McMillan's equation			
	T_{c1}		T_{c2}		T_{c3}		T_{c4}	
	(eV)	(K)	(eV)	(K)	(eV)	(K)	(eV)	(K)
7.5	0.00120965	14.0379	0.00129557	15.0351	0.00103812	12.0473	0.00111186	12.9031
7.75	0.00093736	10.8781	0.00100395	11.6508	0.000791967	9.19075	0.000848223	9.8436
8	0.00072192	8.3779	0.00077320	8.9730	0.000599759	6.96018	0.000642362	7.4545
8.25	0.00055241	6.4107	0.00059165	6.8661	0.000450694	5.23028	0.000482708	5.6018
8.5	0.00041983	4.8721	0.00044965	5.2182	0.000335921	3.89835	0.000359782	4.1752

.

Finally, to find the proper value of effective repulsive strength μ^* (rather than 0.1) that fit the expected result of $T_c^{pl} \approx 8K$, we use it here as a second parameter varying from 0.07 to 0.13 in steps of 0.01. The critical temperature T_c^{pl} as a function of the dielectric constant ε_M for 7 values of μ^* is shown in Table 5.3 and Figure 5.1. It is seen from the figure that the proper value of ε_M and μ^* that fit the expected result of $T_c^{pl} \approx 8K$ are $\varepsilon_M = 8.0$ and $\mu^* = 0.1$.

Table 5.3 The calculated values for T_c^{pl} (in Kelvin, K) as a function of ε_M by using Kresin's equation for various values of effective repulsive strength around $\mu^* = 0.1$. The Kresin's equation without finite-wave vector effect has been used.

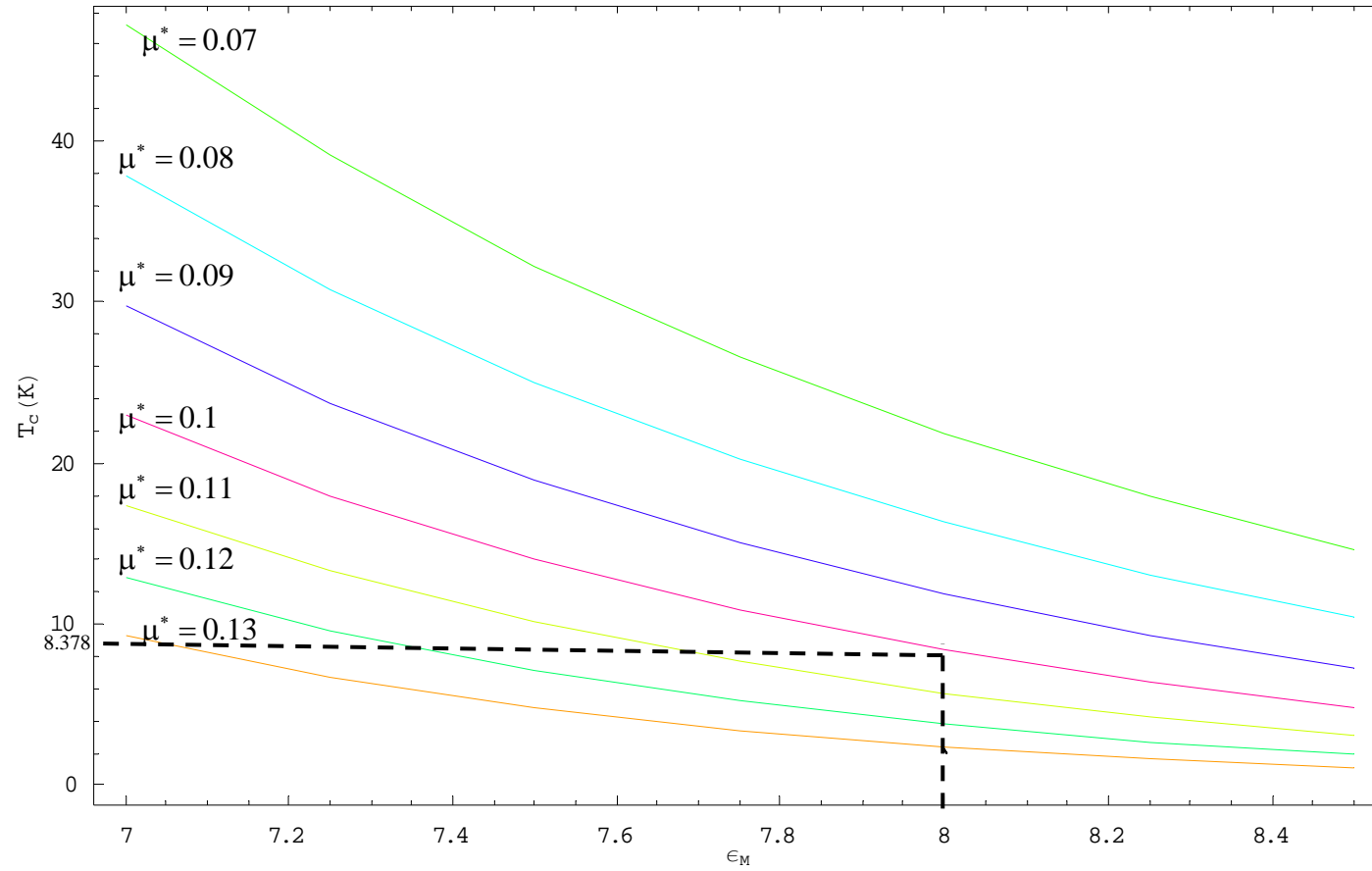| μ^*	ε_M				
	7.5	7.75	8.0	8.25	8.5
0.07	32.286	26.591	21.845	17.899	14.625
0.08	24.980	20.211	16.296	13.091	10.477
0.09	18.940	15.018	11.853	9.310	7.274
0.10	14.038	10.878	8.378	6.411	4.872
0.11	10.141	7.654	5.731	4.255	3.131
0.12	7.116	5.210	3.776	2.706	1.917
0.13	4.830	3.414	2.381	1.637	1.109

Figure 5.1 The critical temperature as a function of dielectric constant ε_M for seven values of

electron-electron repulsive strength μ^*, varying from 0.07 to 0.13 in steps of 0.01.

CHAPTER VI

DISCUSSION AND CONCLUSION

The purpose of this research is to study the impact of plasmon exchange mechanism on high temperature superconductivity in layered superconductors. Particular emphasis is set on the temperature effect and finite-wave vector (higher order in q) effect on plasmon dispersion relation in layered system. The particular emphasis is also set on the dynamically screened Coulomb interaction and the calculation of critical temperature of layered superconductor, i.e., $La_{1.85}Sr_{0.15}CuO_4$.

The plasmon exchange model has been proposed and discussed by several authors as soon as the high temperature superconductivity were discovered. This is because many of the discovered superconducting materials have a layered structure. It is believed that the layered nature of the superconducting cuprates which confines the collective motion of the electrons predominantly to the planes and leads to the unusual features of its plasmon spectra. The spectrum of a layered electron gas contains low-energy electronic collective modes called acoustic plasmons with a dispersion relation $\omega_p \propto q$ that differs fundamentally from 3D metals. The screening of the Coulomb interaction in this system is incomplete and the dynamic nature of the interaction becomes important. As a result, the interplay between the attractive interaction and the Coulomb term is more subtle than the BCS theory. The electronic screening of the Coulomb interaction is described by the dielectric function which contains the polarization propagator. To obtain the critical temperature we have to determine these

functions at finite temperatures. In this research, the static polarization is evaluated and analyzed separately from the dynamic one. The inverse of the dielectric function is evaluated numerically and the results can be compared with the previous work.

The plasmon dispersion relation in the layered superconductor is determined by the poles that correspond to the zeros of the real part of dielectric function. The layer form factor given by Eq. (3.8) which reflects the layered nature of the system is applied only to this layered electron gas model. Other different structures will have different form factor. The temperature effect and the finite–wave vector effect comes from the 2D nature of the polarization propagator given by Eq. (3.28). Numerical result shows that the finite-wave vector effect makes the slope of the dispersion relation inc- rease significantly. This effect is, therefore, important at low temperature limit. The temperature effect is quite small and can be negligible in this limit. The dispersion relation at high temperature is proved to be valid and comparable with the classical limit such as the system of electrons on the surface of liquid helium.

The dynamical screening of the Coulomb interaction is an essential feature of layered structure that provides for an additional contribution to the pairing. The polarization that enters in the calculation of the dielectric function has a static characteristics differ from the dynamic one. The static polarization in the low temperature limit is approximately constant with the value of -0.159 and drastically changes to zero for $q \geq 2k_F$. At higher temperature the curve converge slowly and the sharpness near $q = 2k_F$ is disappear. The dynamic polarization is equal to zero at $y = q / k_F = 0$ for all temperatures and n's. At very low temperature it abruptly increase with y up to $y = 2$ and then decreases rapidly to zero for $y \gg 2$. At higher temperatu-res, the curves are broaden and the peaks are shifted to higher values of y. The different

characteristics between static and dynamic polarizations causes the different curves of the inverse of dielectric function. The inverse dielectric function is shown to be zero only in the sta - tic case which means perfect or complete screening. The dynamic polarization leads to strong q and ω_n dependence of the inverse dielectric function at finite temperatu- res. This is the reason why it is necessary to consider the dielectric function in its full form to study the dynamical screening of the Coulomb interaction.

Using the plasmon exchange model in the framework of the Eliashberg theory for strong coupling superconductors, the plasmon contribution to the critical tempera- ture T_c^{pl} could be obtained. In this model the plasmons are assumed to be the attractive bosons in the pairing effect. The effective interactions between the electrons are des- cribed within the RPA. The electrons interact with each other within the same layer as well as from layer to layer via an effective interaction involving plasmon exchanges among all layers. Eliashberg's equation for the calculation of T_c has been modified into the McMillan's equation and Kresin's equation. These two equations contain two basic parameters to be evaluated, λ and $\bar{\omega}$. The quantity λ represents the attractive strength between electrons, which in this model is essentially mediated by plasmons. The quantity $\bar{\omega}$ is the average value of the frequency of the plasmons, the exchange of which is responsible for superconductivity. Both λ and $\bar{\omega}$ obviously depend on the dielectric constant ε_M, the effective mass m^*, the Fermi wave-vector k_F, the interlayer distance L, and the coherence length ξ (to specify the lower limit of integration for λ and $\bar{\omega}$). The third parameter enters in the two equations for T_c^{pl} is the Coulomb repul - sion strength μ^*. This parameter is generally not well known, but one knows that it is

limited by the condition $0 < \mu^* < 0.5$. Many other investigators take its numerical value to be 0.1. In this work, μ^* is kept as an undefined parameter around 0.1.

A specific cuprate superconductor, $La_{1.85}Sr_{0.15}CuO_4$, for which most parameters have been determined, is selected for the calculation of T_c^{pl}. Since the experimental value of T_c of this material is $T_c^{exp} \approx 38K$ and the phonon contribution to the T_c is shown to be $T_c^{ph} = 30K$, hence the plasmon contribution should be $T_c^{pl} \approx 8K$. Indeed the critical temperature is sensitively dependent on parameters mentioned above. However, only ε_M is not known precisely and the value of μ^* should be tested around the value of 0.1. Variation of ε_M and μ^* shows that the proper values of them for $T_c^{pl} \approx 8K$ are $\varepsilon_M \approx 8$ and $\mu^* \approx 0.1$.

The plasmon exchange model is very simple since the microstructure of the superconductors is completely neglected. The model is characterized by four parameters only. For reasonable values of these parameters the calculated value of T_c^{pl} is found to be in reasonable agreement with the experimental values of the materials. In the case of high-temperature oxides, the contribution of low-energy plasmons to the criti- cal temperature is significant but not dominant. The phonon contribution is still largest in this model. In some classes of layered superconductors, the acoustic plasmon contribution are shown to be dominant or of the same order by phonon contribution.

REFERENCES

Allen, P. B. and Dynes, R. C. (1975). Transition temperature of strong-coupled super-conductors reanalyzed. **Physical Review B** 12(3):905.

Anderson, P. W. (1987). The theory of superconductivity in high-T_c cuprates super-conductors. **Science** 235:1,196.

Anderson, P. W. and Schrieffer, R. (1991). A dialogue on the theory of high T_c. **Physics Today** 44:54.

Ashkenazi, J., Kuper, C. G. and Tyk, R. (1987). Soft-plasmon theory of the new high-temperature superconductors. **Solid State Commun** 63(12):1145.

Bardeen, J., Cooper, L. N. and Schrieffer, J. R. (1957). Theory of superconductivity. **Physical Review** 108(5):1,175.

Bednorz, J. G. and Müller , K. A. (1986). Electronic band properties and supercon-ductivity in $La_{2-y}X_yCuO_4$. **Journal of Physics B** 64:189.

Bill, A., Morawitz, H. and Kresin, V. Z. (2000). Low-energy electronic collective modes and superconductivity in layered systems. **Journal of Superconducti-vity** 13(6):907.

Bill, A., Morawitz, H. and Kresin, V. Z. (2000). Plasmons in layered superconduc-tors. **Elsevier Science Physica B** 284-288(2000):433-434.

Bill, A., Morawitz, H. and Kresin, V. Z. (2002). Dynamical screening and supercon-ducting state in intercalated layered metallochronitrides**. Physical Review B** 66:100,501.

Bill, A., Morawitz, H. and Kresin, V. Z. (2003). Electronic collective modes and superconductivity in layered conductors. **Physical Review B** 68:144,519.

Bose, S. M. and Longe, P. (1990). An explanation for the rise in T_c in the Tl- and Bi-based high-temperature superconductors. **Journal of Physics: Condensed Matter** 2:2,491.

Bose, S. M. and Longe, P. (1992a). Acoustic plasmon exchange in multilayered systems: I. The effective interaction potential. **Journal of Physics: Condensed Matter** 4:1,799.

Bose, S. M., and Gayen, S. (2004). **Plasmon exchange model for superconductivity in carbon nanotubes**. ArXiv: cond-mat/0402531 v1 20 Feb 2004.

Burns, G. (1992). **High-temperature superconductivity : an introduction**. London, Academic Press Limited, pp. 3-5.

Cohen, M. L. *et al.* (1987). Observation of an oxygen isotope shift in the superconducting transition temperature of $La_{1.85}Sr_{0.15}CuO_4$. **Physical Review Letters** 59(8): 915.

Chu, C. W. *et al.* (1987). Superconductivity at 93K in a new mixed- phase Yb-Ba-Cu-O compound system at ambient pressure. **Physical Review Letters** 58(9):908.

Chu, C. W. (2004). **Oxides for high temperature superconductivity and beyond** [On-line]. Available: http://www. tsinghua.edu.cn/docsn/ghdxxb/myweb/ English/98n1/980105.html.

Fetter, A. L. (1974a). **Electrodynamics of a layered electron gas. II.** Periodic array, **Annual Physics** (New York) 88, 1-25.

Fetter, A. L. (1974b). Electrodynamics and thermodynamics of a classical electron surface layer. **Physical Review B** 10(9):3,739.

Fetter, A. L. and Walecka, J. D. (1971). **Quantum theory of many-particle systems.** McGraw-Hill Book Company, New York, pp. 180-182.

Fröhlich, H. (1968). Superconductivity in metals with incomplete inner shells. **Journal of Physics C** 1:544.

Griffin, A. (1988). Response functions of a superlattice with a basis: A model of oxide superconductors. **Physical Review B** 38(13):8,900.

Grosso, G. and Parravicini, G. P. (2000). **Solid state physics.** London, Academic Press Limited, pp. 263-266.

Haddon, R. C. *et al*. (1991). Superconductivity at 28K in Rb_xC_{60}. **Physical Review Letters** 66(21):2,830.

Hwang, E. H. and Sarma, S. D. (2001). Plasmon dispersion in dilute two-dimensional electron systems: Quantum-classical and Wigner crystal-electron liquid cross-over. **Physical Review B** 64(16):165,409.

Jorgensen, J. D. *et al*. (1987). Lattice instability and high-T_c superconductivity in $La_{2-x}Ba_xCuO_4$. **Physical Review Letters** 58(10):1,024.

Kim, D. J., Long, M. W. and Yeung, W. (1987). Equivalence of the dynamical and total-energy approaches in the calculation of elastic constants of magnetic metals. **Physical Review B** 36(1):429.

Kresin, V. Z. (1987a). Critical temperatures of superconductors with low dimensionality. **Physical Review B** 35(16):8,716.

Kresin, V. Z. (1987b). On the critical temperature for any strength of electron-phonon coupling. **Physics Letters A** 122(8):434.

Kresin, V. Z. and Morawitz, H. (1988). Layer plasmons and high-T_c superconductivity. **Physical Review B** 37(13):7,854.

Landau, L. and Lifshitz, E. (1976). **Statistical physics.** Addison-Wesley, Reading, Massachusetts, p.10.

Longe, P. and Bose, S. M. (1992b). Acoustic plasmon exchange in multilayered **sys**tems: II. Application to high-T_c superconductors. **Journal of Physics: Condensed Matter** 4:1,811.

Maldague, P. F. (1978). Many–body corrections to the polarizability of the two-dimensional electron gas. **Surface Science**. 73:269-302.

Malozovsky, Y. M., Bose, S. M. and Longe, P. (1993a). Calculation of the self-energy in a layered two-dimensional electron gas. **Physical Review B** 47(22):15,242.

Malozovsky, Y. M., Bose, S. M., Longe, P. and Fan, J. D. (1993b). Eliashberg equation and superconductivity in a layered two-dimensional metal. **Physical Review B** 48(14):10,504.

Morawitz, H., Bozovic, I., Kresin, V. Z., Rietveld, G. and van der Marel, D. (1993). The plasmon density of states of a layered electron gas. **Journal of Physics B** 90: 277.

Morelli, D. T., Heremans, J. and Swets, D. E. (1987). Thermal conductivity of superconductive Y-Ba-CuO**. Physical Review B** 36(7):3,917.

Nagamatsu, J., Nakagawa, N., Muranaka, T. and Akimitsu, J. (2001). Superconductivity at 39K in magnesium diboride. **Nature** 410(6,824):63.

Nücker, N., Romberg, H., Nakai, S., Sheerer, B. and Fink, J. (1989). Plasmons and interband transition in $Bi_2Sr_2CaCu_2O_8$. **Physical Review B** 39(16):12,379.

Pines, D. (1956). Theory of acoustic surface plasmons. **Canadian Journal of Physics** 34:1,379.

Pines, D. (1990). **High-temperature superconductivity.** Addison-Wesley, Redwood City, CA, pp. 240-245.

Rajagopal, A.K. (1977). Longitudinal transverse dielectric functions of a two-dimensional electron system: Inclusion of exchange correlations. **Physical Review B** 15(9):4,264.

Ruvalds, J. (1987). Plasmons and high-temperature superconductivity in alloys of copper oxides. **Physical Review B** 35(16):8,869.

Scalapino, D. J., Loh, E. Jr. and Hirsch, J. E. (1987). Fermi-surface instabilities and superconducting d-wave pairing. **Physical Review B** 35(13):6,694.

Stern, F. (1967). Polarizability of a two-dimensional electron gas. **Physical Review Letters** 18(14):546.

Stöckli, T., Bonard, J. M. and Châtelain, A. (2000). Plasmon excitations in graphitic carbon spheres measured by EELS. **Physical Review B** 61(8):5,751.

Sulewski, P. E., Noh, T. W., McWhirter, J. T. and Sievers, A. J. (1987). Far-infrared composite-medium study of sintered La_2NiO_4 and $La_{1.85}Sr_{0.15}CuO_{4-y}$. **Physical Review B** 36(10):5,735.

Varshney, D. and Singh, R. K. (1995). Superconductivity in lanthanum cuprates: A layered-electron-gas model. **Physical Review B** 52(10):7,629.

Visscher, P. B. and Falicov, L. M. (1971). Dielectric screening in layered electron gas. **Physical Review B** 3(8):2,541.

Voelker, K., Animisov, V.I. and Rice, T.M. (2004). **Acoustic plasmons in MgB₂** (May 26, 2004), arXiv: cond-mat/0103082 v1 5 March 2001.

Zhou, J., Sinha, S. and Goodenough, J. B. (1989). Comment on"Identification of a su-
peroxide in superconducting $La_2CuO_{4+\delta}$ by x-ray photoelectron spectroscopy".
Physical Review B 39(16):12,331.

Ziman, J. M. (1964). **Principles of the theory of solids.** Cambridge, pp. 155.

APPENDIX

SOMMERFELD METHOD

Integrals of the Fermi-Dirac form

$$I(\alpha) = \int_0^\infty dz \; \frac{g(z)}{e^{z-\alpha}+1} \tag{A-1}$$

occur throughout the many topics in theoretical physics. For $\alpha < 0$, integrals of this type can usually be evaluated by elementary methods. In case with high degeneracy $(\alpha \gg 0)$ and with g (z) slowly varying near $z = \alpha$ and having a Taylor series expansion with a reasonable radius of convergence about that point, it is frequently possible to use the Sommerfeld method to obtain an asymptotic expansion in ascending powers of temperature.

The Fermi function $f(z) = 1/(e^{z-\alpha}+1)$ can be rewritten as

$$\frac{1}{e^{z-\alpha}+1} = \frac{e^{\alpha-z}}{e^{\alpha-z}+1} = 1 - \frac{1}{e^{\alpha-z}+1} \tag{A-2}$$

then Eq. (A-1) becomes

$$I(\alpha) = \int_0^\alpha dz \; \frac{g(z)}{e^{z-\alpha}+1} + \int_\alpha^\infty dz \; \frac{g(z)}{e^{z-\alpha}+1}$$

$$= \int_0^\alpha g(z)dz - \int_0^\alpha dz \; \frac{g(z)}{e^{\alpha-z}+1} + \int_\alpha^\infty dz \; \frac{g(z)}{e^{z-\alpha}+1} \tag{A-3}$$

For the second term in (A-3), let $z' = \alpha - z$, then

$$\int_0^\alpha dz \; \frac{g(z)}{e^{\alpha-z}+1} = -\int_\alpha^0 dz' \; \frac{g(\alpha-z')}{e^{z'}+1} = \int_0^\alpha dz' \; \frac{g(\alpha-z')}{e^{z'}+1}$$

$$= \int_0^\infty dz' \, \frac{g(\alpha - z')}{e^{z'} + 1} - \int_\alpha^\infty dz' \, \frac{g(\alpha - z')}{e^{z'} + 1}$$

For the third term in (A-3), let $z'' = z - \alpha$, then

$$\int_\alpha^\infty dz \, \frac{g(z)}{e^{z-\alpha} + 1} = \int_0^\infty dz'' \, \frac{g(\alpha + z'')}{e^{z''} + 1}$$

Using these terms then Eq. (A-3) becomes

$$I(\alpha) = \int_0^\alpha g(z) dz + \int_0^\infty dz'' \, \frac{g(\alpha + z'')}{e^{z''} + 1} - \int_0^\infty dz' \, \frac{g(\alpha - z')}{e^{z'} + 1} + \int_\alpha^\infty dz' \, \frac{g(\alpha - z')}{e^{z'} + 1}$$

$$\approx \int_0^\alpha g(z) dz + \int_0^\infty dz \big[g(\alpha + z) - g(\alpha - z) \big] \sum_{n=1}^\infty (-1)^{n+1} e^{-nz}$$

where the last integral can be neglected since $\alpha \gg 0$.

Expanding $g(\alpha + z) - g(\alpha - z)$ in Taylor series, then

$$I(\alpha) = \int_0^\alpha g(z) dz + 2 \sum_{m=0} \frac{g^{(2m+1)}(\alpha)}{(2m+1)!} \sum_{n=1}^\infty (-1)^{n+1} \int_0^\infty dz \, z^{2m+1} e^{-nz}$$

$$= \int_0^\alpha g(z) dz + 2 \sum_{m=0} \frac{g^{(2m+1)}(\alpha)}{(2m+1)!} (2m+1)! \sum_{n=1} \frac{(-1)^{n+1}}{n^{2m+2}}$$

or

$$I(\alpha) = \int_0^\alpha g(z) dz + 2 \sum_{m=0}^\infty g^{(2m+1)}(\alpha) \frac{\left(2^{2m+1} - 1\right) \pi^{2m+2}}{(2m+2)!} B_{m+1} \tag{A-4}$$

where B_{m+1} is Bernoulli number; $B_1 = 1/6$, $B_2 = 1/30$.

Equation (A-4) may be rewritten as

$$I(\alpha) = (\pi \csc \pi D) g(z) \tag{A-5}$$

where the operator $\pi \csc \pi D$ indicates the Laurent expansion of the cosecant about zero

with

$$D = \left.\frac{d}{dz}\right|_{z=\alpha} \qquad \text{and} \qquad \frac{1}{D} = \int_0^\alpha dz \qquad (A\text{-}6)$$

Suppose that $g(z) = z^{3/2}$, using Eq. (A-4) we have

$$\int_0^\infty \frac{z^{3/2}dz}{e^{z-\alpha}+1} = \int_0^\alpha z^{3/2}dz + \frac{3}{2}\alpha^{1/2}\frac{\pi^2}{6} - \frac{7\pi^4}{960}\alpha^{-3/2} - \frac{31\pi^6}{10752}\alpha^{-7/2} - \cdots$$

Occasionally, a calculation at non-zero temperature requires the evaluation of a Fermi-Dirac integral, for which the integrand does not satisfy the two conditions mentioned above. For example, g (z) may oscillate rapidly or may have an inopportunely situated branch point. In such circumstances, ordinary methods may fail. A useful technique involves converting the real integral into a complex integral by substituting the representation for the Fermi function,

$$f(z) = \frac{1}{e^{z-\alpha}+1} = \frac{1}{2\pi i}\int_{b-i\infty}^{b+i\infty}(\pi\csc\pi t)e^{t(\alpha-z)}dt \qquad (A\text{-}7)$$

where $0 < b < 1$.

This representation possesses enough algebraic flexibility to permit the reduction of Fermi integral to tabulated Laplace transforms and their inverses, or at worst, to a tractable exercise in residue theory. In some cases exact evaluation in terms of tabulated mathematical functions is possible. For example, the familiar integral

$$I_\nu(\alpha) = \frac{1}{\Gamma(\nu+1)}\int_0^\infty \frac{z^\nu dz}{e^{z-\alpha}+1} \qquad (A\text{-}8)$$

can be expressed in terms of confluent hypergeometric functions. However, this common integral satisfies the second condition above and can be evaluated in the high degeneracy limit by Eq. (A-5).

CURRICULUM VITEA

Mr. Nouphy Hompanya was born on 03 January 1956 in Vientiane Province, Laos. He completed his primary school course in his village natal (Vangvieng) in 1970. He studied in primary normal school for four years and continued to study in secondary normal school for three years in the science section. After that, in 1977-1985 he worked as a teacher in the secondary school in the north province of Laos.

In 1985-1991 he continued his study in Daghestan University (Russia). After finished his Master of Science in Physics from Daghestan University in 1991, he retuned to Laos and worked as a lecturer at Vientiane Pedagogical University in 1991-1996, and became head of Physics department, National University of Laos in 1996-2000.

In 2000-2005 he continues his graduate study in School of Physics, Institute of Science, Suranaree University of Technology, Thailand.